

Condition Monitoring of Misaligned Rotor System and Remaining Useful Life Prediction of Rolling Element Bearing

THESIS

Submitted in partial fulfilment of the requirements for the degree of

DOCTOR OF PHILOSOPHY

by

SHITAL PATIL
ID NO. 2018PHXF0029P

Under the Supervision of

Dr. Amol Marathe

&

Co-Supervision of

Prof. Arun Kumar Jalan



BITS Pilani
Pilani Campus

BIRLA INSTITUTE OF TECHNOLOGY & SCIENCE, PILANI

PILANI-333031, RAJASTHAN, INDIA

2023

*This thesis is dedicated to my parents,
Shri. Mahavir Patil and Sou. Ujwala Patil
For their endless love, support, and encouragement.*

BIRLA INSTITUTE OF TECHNOLOGY AND SCIENCE, PILANI

CERTIFICATE

This is to certify that the thesis titled “**Condition Monitoring of Misaligned Rotor System and Remaining Useful Life Prediction of Rolling Element Bearing**” submitted by **Shital Patil** ID No **2018PHXF0029P** for award of Ph.D. of the institute embodies original work done by him under our supervision.

Signature of Co- Supervisor

Prof. Arun Kumar Jalan

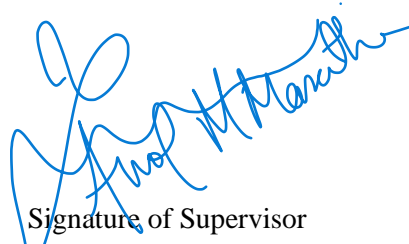
Associate Professor,

Mechanical Engineering Department,

Birla Institute of Technology and Science, Pilani,

Rajasthan-333031, India

Date:



Signature of Supervisor

Dr. Amol M. Marathe

Assistant Professor,

Mechanical Engineering Department,

Birla Institute of Technology and Science, Pilani,

Rajasthan-333031, India

Date

Dr. Amitava Roy
Scientist "G",
Tel.: 011-26512215, 26590208, 40000302
Email: amitava@nic.in

SERB/PM Fellow/CII-FICCI/Meeting/2019

Dated: 30-01-2020

D. O .No.

Subject: Award of Prime Minister's Fellowship for Doctoral Research Scheme

Dear Mr. Shital Patil,

I am happy to inform you that you have been selected to receive the prestigious scholarship 'Prime Minister Fellowship for Doctoral Research', with industry partner National Engineering Industries Limited. This is a unique scholarship scheme of Science and Engineering Research Board, Department of Science and Technology, Government of India, coordinated by The Federation of Indian Chambers of Commerce and Industry (FICCI). Your application has gone through a rigorous selection process and has been scrutinized by high level Apex Council Comprising expert from academia and industry.

I congratulate you on being selection to receive this scholarship and wish you the best in your academic and personal endeavours.

You will receive further instruction and information in this regard soon from Dr. Nirankar Saxena, Deputy Secretary General, FICCI. You may please contact directly to him for all fellowship related matter in future.

With best regards



(AMITAVA ROY)

To
Mr. Shital Patil
Department of Mechanical Engineering
Birla Institute of Technology & Science, Pilani, Vidya
Vihar, Pilani, Rajasthan - 333031

Copy To
Dr. Lokesh Agarwal
Vice President & Head R&D
National Engineering Industries Ltd.
Khatipura Road, Jaipur Rajasthan - 302006

Acknowledgement

My heartfelt and foremost gratitude is expressed to my supervisors, Dr. Amol M. Marathe and Prof. Arun Kumar Jalan. They have welcomed me into this stimulating research journey and have proven to be the best mentors I could have ever wished for. I extend my sincere thanks to Prof. Arun Kumar Jalan for introducing me to the fascinating world of machinery condition monitoring. I humbly offer my respectful obeisance to my supervisor's feet for providing invaluable guidance, excellent direction, unwavering encouragement, and constant inspiration. Without their support, the completion of this work would not have been possible. Working under the supervision of both esteemed intellectuals has been a privilege, and their expertise in presenting scientific work has added significant scientific value to my thesis.

I am immensely thankful to Prof. V. Ramgopal Rao, the Vice-Chancellor of BITS Pilani, and Prof. Sudhir Kumar Barai, the Director of BITS Pilani, Pilani Campus, for their support and blessings. I express my gratitude to Prof. S. K. Verma, the Dean of Administration at BITS Pilani, Pilani Campus, for his kind support. Additionally, I extend my sincere thanks to Prof. Shamik Chakraborty, the Associate Dean of the Academic-Graduate Studies & Research Division (AGSRD), for his motivation and encouragement. I also acknowledge the valuable support and guidance provided by Prof. Srikanta Routroy, the Head of the Department of Mechanical Engineering. I am deeply indebted to Prof. Rajesh Prasad Mishra, The Chief Warden, and Prof. Navin Singh, The Associate Dean of the Student Welfare Division, for their encouragement and insightful suggestions.

I express sincere thanks to Prof. Arun Kumar Jalan, the convener of the Department Research Committee (DRC) in the Department of Mechanical Engineering. I offer my heartfelt gratitude to my Dissertation Advisory Committee (DAC) members, Prof. B. K. Rout and Dr. Venkatesh K. P., for their invaluable suggestions and for sparing their precious time to evaluate this thesis. I would also like to acknowledge the entire faculty and non-academic staff of the Department of Mechanical Engineering for their unwavering support, encouragement, and cooperation. It is with great pleasure that I acknowledge the contributions made by individuals who have played a role in the evolution of this work.

I feel proud to be the first BITSian to receive the prestigious Prime Minister Fellowship award. I would also like to express my gratitude to SERB-DST, FICCI, and NBC Bearing for their financial assistance under the Prime Minister Fellowship Program. I am deeply grateful and would like to express my sincere thanks to my industry mentor, Dr. Lokesh Agrawal, CTO, NBC Bearing Jaipur and Mr. Arendra Singh, Manager, NBC Bearing Jaipur for their firm support throughout my research journey. Their guidance and assistance during the data acquisition phase and while conducting tests at NBC Bearing have been invaluable contributions to the success of my project. Dr. Lokesh Agrawal, in particular, has played a pivotal role in providing me with a remarkable opportunity to work on RUL (Remaining Useful Life) prediction. His belief in my abilities and trust in my potential have been catalysts in my research endeavors. I am immensely

grateful for his continuous support and for making all the necessary facilities available to me. His guidance and mentorship have been instrumental in shaping my understanding of predictive maintenance and have allowed me to develop a robust predictive maintenance scheme specifically tailored for taper roller bearings. Mr. Arendra Singh's support and assistance throughout the data acquisition process have been invaluable. His expertise and experience in the field have greatly contributed to the successful implementation of the tests at NBC Bearing. I am thankful for his collaboration and the knowledge he shared, which have significantly enhanced the quality and accuracy of my research outcomes.

The overwhelming depth of the support, love, and affection bestowed upon me by my cherished family is beyond words. Throughout my journey, my beloved parents, Shri Mahavir Patil and Sou. Ujwala Patil has been an unwavering pillar of strength, providing me with invaluable guidance, encouragement, and blessings. Their love and belief in me have been a constant source of strength.

I am immensely grateful to my wife, Priyanka, who has been my rock and my source of inspiration. Her unwavering support, understanding, and sacrifices have been instrumental in my pursuit of this research endeavor. Her love and encouragement have given me the confidence to overcome challenges and reach my goals.

I would like to take this opportunity to express my profound gratitude and heartfelt thanks to my dear brother, Mr. Shrenik Patil, for his continuous support and encouragement, which was a constant source of motivation throughout my journey. His belief in my abilities has been instrumental in pushing me beyond my limits and instilling confidence in my own potential.

I also would like to express my sincere gratitude to my brother-in-law, Dr. Sheetalnath Rooge, for his invaluable support and wise counsel. His vast knowledge and experience have been invaluable assets that have enriched my journey. His guidance and advice have helped me navigate through complex situations, providing clarity and perspective when I needed it most.

I would like to acknowledge the support of my brother-in-law Sagar Hukkeri. His willingness to lend an ear, offer guidance, and share his insights has been instrumental in helping me navigate through challenges and make informed decisions. He has consistently gone above and beyond to provide assistance and share his wealth of knowledge, enabling me to excel in my research.

In addition, I would like to express my deep gratitude to my loving sisters, Swati and Vaishali, for their boundless love and care, who have been a source of motivation throughout my journey. Their belief in my abilities and their confidence in my potential has been instrumental in shaping my self-belief and pushing me to strive for excellence. Words cannot adequately capture the depth of my appreciation for Swati and Vaishali. I am truly grateful for their support, love, care, and encouragement.

I express my sincere thanks to my father-in-law, Justice P.N. Desai, and my mother-in-law, Sou. Anupama P. Desai, for their blessings, support, and guidance. Their belief in my abilities has provided me with the strength and motivation to persevere.

I would like to extend my thanks and appreciation to my dearest friends Ayush Owhal, Anish Kumar, Nitish Gokhale, Ajay Pingle, and Aayushi Agrawal for their support during my research journey. Finally, I offer my prayers and heartfelt thanks to the almighty for bestowing divine blessings upon me. The inner strength and patience I have acquired throughout this journey are a testament to the power of faith and the grace of a higher power. I am eternally grateful for the guidance and support that have been bestowed upon me, enabling me to overcome challenges and achieve my goals.

Shital Patil

Date: 24th July 2023

Abstract

In industrial applications, rotating machinery is widely employed and plays a significant role. Rotating machinery in modern industry is growing larger and more precise as science and technology advance. Improving the availability, reliability, and security of rotating equipment has become a challenging task. PHM (Prognostics and Health Management) is a useful tool for doing this work. As a result, it has garnered considerable attention over the past few decades. The rotor–bearing system of modern rotating machinery is complex and needs accurate and reliable prediction of its dynamic characteristics. In condition monitoring, accurate fault identification is an essential task for designing a proper maintenance strategy. Vibration in rotating machinery is mostly caused by unbalance, misalignment, bearing faults, mechanical looseness, shaft cracks, and other malfunctions. Even if the perfect alignment was achieved initially, it could not be maintained over an extended period of time due to various effects, such as improper machine assembly, heat generated in casings from bearings, lubrication systems, compression of gases, and foundation movement, resulting in abnormal rotating preload.

Though many researchers have worked on model-based and vibration analysis-based techniques for misalignment fault identification, none of the studies clearly classified the different types of misalignment faults. Also, the interaction among speed, load, and misalignment, and its combined effect on system vibration was not reported. The present work focuses on interactions between speed, load, and defect severity (parallel and angular misalignment) by investigating their effect on the system vibration. Response Surface Methodology (RSM) with Root Mean Square (RMS) as a response factor is used to understand the influence of such interactions on the system performance. Experiments are planned using the design of experiments (DoE) and analysis is carried out using Analysis of Variance (ANOVA). These observations will help to understand the misalignment defect and its effect in a better way. One of the significant challenges associated with misalignment study is the mounting of the sensor. Misalignment is introduced at the coupling between the drive and driven shaft, most of the studies reported that with the mounting of the accelerometer on the bearing housing, there is a possibility that the sensor is too far from the coupling. In industrial applications, the complex machinery may or may not have provision to mount sensors near coupling. To overcome this limitation, the present investigation is also focused on a non-contact type sensor, which can be placed in closed proximity to coupling and the useful signal can be acquired using a microphone. This is one of the primary attempts to examine the impact of interactions among speed, load, and fault severity on system vibrations using a non-contact

type sensor. So, the current study also aims to implement an acoustic sensor with RSM using RMS as a response factor to see how defect type, defect severity, load, and speed affect rotor system efficiency. Using the DoE methodology, experiments were designed and evaluated to determine the effect of operating conditions on RMS. The results described are consistent with the results obtained using a vibration signal.

Conventionally, the diagnosis of misalignment is carried out through vibration measurements. Especially, the presence of a strong 2x vibration peak is generally accepted. Both angular and parallel misalignment shows a peak at 2x, therefore, distinguishing misalignment type by using vibration signals alone is a difficult activity. This research work discusses the classification of misalignment i.e., angular, parallel, and combined misalignment by using a diagnostic medium such as the acoustic emission and the rotor vibration signal. Vibro-acoustic sensors are used to collect data from the misaligned rotor system at two different loading, three different speeds, and three defect severity conditions. Time domain features are extracted and ranked according to their significance to classification using the t-test technique. Extracted features are used to train different algorithms. SVM and Ensemble subspace discriminant algorithms give 100% accurate results for binary and multi-class fault classification respectively. This work also intended to explore using a small amount of training data using different algorithms. The proposed method outperforms fault classification using vibration signal and acoustic signal separately.

Close to 70% of bearing failure occurs due to misalignment. Every rotary system will have some inherent misalignment and most of the time to avoid shaft bending due to severe accelerated tests there needs to be some clearance in the form of misalignment. Establishing a diagnosis and prognostic strategy for a misaligned rotor system is crucial for increasing the reliability of PHM plans. There needs to be a prognostic scheme that can consider the preset misalignment and predict the remaining useful life of bearing. By using standard empirical formulae for ball pass frequency outer raceway, ball pass frequency inner raceway, and ball spin frequency, industries have developed robust bearing fault diagnosis schemes, but now predictive maintenance is gaining much attention. Apart from fault diagnosis, the industries are more focused on the correct prediction of the RUL of bearings to use the optimum life of bearings and plan maintenance activity on time.

Two methods are proposed for the prediction of RUL of taper roller bearings. The data was collected at NBC bearing Jaipur. The proposed methodology includes extraction of time-

frequency domain features and then by using wavelet scattering transform, scattering coefficients are determined. These zeroth and first-order scattering coefficients along with bearing age are used as an input vector for RUL prediction. The R^2 error is used as the performance measure of the xgboost regression method. In another approach time domain feature-based HI is developed, and prediction is carried out using a nonlinear autoregressive network with exogenous inputs (NARX) neural network.

In the present research work, a systematic approach has been followed towards the development of a reliable fault diagnosis and prognosis scheme for the rotor-bearing system by considering different forms of misalignment, bearing defect, and the actual problem in industrial settings regarding the noisy data and residual life assessment of bearings.

Keywords: Misalignment, Condition monitoring, Fault Diagnosis, Prognostics, Predictive maintenance, Rotor-bearing system, Remaining useful life estimation, Classification, regression, Design of experiments, One-way ANOVA, NARX.

Table of Contents

	CONTENTS	Page No.
<i>Acknowledgement</i>		i-iii
<i>Abstract</i>		iv-vi
<i>Table of Contents</i>		vii-ix
<i>List of Figures</i>		x-xii
<i>List of Tables</i>		xiii
<i>Nomenclature</i>		xiv-xv
Chapter 1. Introduction		1-8
1.1 Background and Motivation		1
1.1.1 Introduction to Rotor System		1
1.1.2 Importance of Study on Misalignment		1
1.1.3 Importance of RUL Study of Rolling Element Bearing		2
1.2 Fault Diagnosis and Prognosis		3
1.2.1 Importance of Condition-Based Monitoring (CBM)		3
1.2.1.1 Data Acquisition		4
1.2.1.2 Signal Processing		4
1.2.2 Importance of Machine Learning Techniques		6
1.3 Scope of Work		7
1.4 Organization of Thesis		8
Chapter 2. Literature Review		9-29
2.1 Introduction		9
2.2 Fault Diagnosis and Prognosis of Mechanical Systems		9
2.2.1 Model Based Techniques		10
2.2.2 Signal Based Techniques		11
2.2.2.1 Vibration Analysis		11
2.2.2.1.1 Fast Fourier Transform (FFT)		11
2.2.2.1.2 Orbit Analysis		12
2.2.2.1.3 Discrete Wavelet Transforms (DWT)		12
2.2.2.1.4 Continuous Wavelet Transform (CWT)		12
2.2.2.1.5 Hilbert Huang Transform (HHT)		13
2.2.2.2 Non-Vibration Based Techniques		14
2.2.2.2.1 Acoustic Emission (AE) Technique		14
2.2.2.2.2 Motor Current Signature Analysis (MCSA)		14
2.2.3 Artificial Intelligence Techniques		15
2.3 Research Gaps		20
2.4 Objective of the Present Work		21
References		21

Chapter 3. Experimental Investigation Using RSM for Condition Monitoring of Misaligned Rotor System	30-54
3.1 Introduction	30
3.2 Introduction to Response Surface Methodology	31
3.3 Experimental Test Rig	32
3.4 Experimental Investigation Using RSM for Vibration Data	34
3.4.1 Results and Discussion	34
3.4.1.1 ANOVA Results in Horizontal, Vertical, and Axial Directions for Parallel Misalignment	34
3.4.1.2 ANOVA Result in Horizontal, Vertical, and Axial Direction for Angular Misalignment	41
3.5 Condition Monitoring of Misaligned Rotor System Using Acoustic Sensor by Response Surface Methodology	46
3.5.1 Results and Discussion	46
3.5.1.1 ANOVA Results for Parallel Misalignment	46
3.5.1.2 ANOVA Result for Angular Misalignment	48
3.6 Conclusion	51
<i>References</i>	52
Chapter 4. Machine Learning Techniques for Misalignment Fault Classification	55-86
4.1 Introduction	55
4.2 Experimental Test Rig and Loading Conditions	57
4.3 Binary Fault Classification (Angular and Parallel)	57
4.3.1 Data Acquisition and Signal Processing	58
4.3.2 One-way ANOVA	61
4.3.3 Results and Discussion	62
4.3.3.1 Case 1: No Load Condition	62
4.3.3.2 Case 2: With Load Condition (13.4 N)	68
4.3.3.3 Case 3: With Load Condition (6.7 N)	74
4.4 Parallel, Angular, and Combined Misalignment Fault Classification	75
4.4.1 Data Acquisition and Signal Processing	76
4.4.2 Results and Discussion	78
4.5 Conclusion and Future Scope	83
<i>References</i>	84
Chapter 5. RUL Prediction of Taper Roller Bearing under Industrial Settings	87-111
5.1 Introduction	87
5.2 Theoretical Background	88
5.2.1 Wavelet Scattering Transform (WST)	88
5.2.2 Theory of NARX Network	91
5.3 Experimental setup	92
5.4 Proposed Methodology	94
5.5 Results and Discussion	96

5.5.1	Wavelet Scattering- xgboost Approach	96
5.5.2	Time Domain Feature-based HI-NARX Approach	101
5.6	Conclusion	108
	<i>References</i>	109

Chapter 6. Overall Conclusions and Future Scope **112-115**

6.1	Overall Conclusions	112
6.2	Novelty of work	113
6.3	Future scope	114

List of Publications

Brief Biography of the Candidate

Brief Biography of the Supervisor

Brief Biography of the Co-supervisor

List of Figures

S. No	Figure No	Caption	Page No
1	Figure 1.1	Shaft misalignment: (a) parallel, (b) angular.	2
2	Figure 3.1	Spectra Quest machinery fault simulator	33
3	Figure 3.2	Performance prediction of model in (a) horizontal, (b) vertical, and (c) axial directions	37
4	Figure 3.3	Response surface plot for interaction between speed and load for (a) horizontal, (b) vertical, and (c) axial direction	38
5	Figure 3.4	Response surface plot for interaction between speed and defeat for (a) horizontal, (b) vertical, and (c) axial direction	39
6	Figure 3.5	Response surface plot for interaction between load and defeat for (a) horizontal, (b) vertical, and (c) axial direction	41
7	Figure 3.6	Performance prediction of model for angular misalignment in (a) horizontal, (b) vertical, and (c) axial directions	43
8	Figure 3.7	Response surface plot for interaction between speed and load for (a) horizontal, (b) vertical, and (c) axial direction	44
9	Figure 3.8	Response surface plot for interaction between speed and defect for (a) horizontal, (b) vertical, and (c) axial direction	45
10	Figure 3.9	Response surface plot for interaction between load and defect for (a) horizontal, (b) vertical, and (c) axial direction	45
11	Figure 3.10	Performance prediction of the model	47
12	Figure 3.11	Response surface plot for parallel misalignment for interaction between (a) speed and load, (b) speed and defect, and (c) load and defect	48
13	Figure 3.12	Performance prediction of model for angular misalignment	49
14	Figure 3.13	Response surface plot for angular misalignment for interaction between (a) speed and load, (b) speed and defect, and (c) load and defect	50
15	Figure 4.1	Signal trace (a) vibrational signal in Z-direction (b) acoustic signal	61
16	Figure 4.2	Flowchart of the proposed method	61
17	Figure 4.3	Result of Naive Bays (a) confusion matrix (b) positive predictive value & false discovery rate plot	65
18	Figure 4.4	Result of Ensemble boosted trees (a) confusion matrix (b) positive predictive value & false discovery rate plot	65

19	Figure 4.5	Result of logistic regression (a) confusion matrix (b) positive predictive value & false discovery rate plot	66
20	Figure 4.6	Result of KNN (a) confusion matrix (b) positive predictive value & false discovery rate plot	66
21	Figure 4.7	Result of SVM (a) confusion matrix (b) positive predictive value & false discovery rate plot	67
22	Figure 4.8	Feature Vs Testing accuracy plot for No load conditions	68
23	Figure 4.9	Result of Naive Bays (a) confusion matrix (b) positive predictive value & false discovery rate plot	69
24	Figure 4.10	Result of Ensemble boosted trees (a) confusion matrix (b) positive predictive value & false discovery rate plot	70
25	Figure 4.11	Result of Logistic regression (a) confusion matrix (b) positive predictive value & false discovery rate plot	70
26	Figure 4.12	Result of KNN (a) confusion matrix (b) positive predictive value & false discovery rate plot	71
27	Figure 4.13	Result of SVM (a) confusion matrix (b) positive predictive value & false discovery rate plot	71
28	Figure 4.14	Feature Vs Testing accuracy plot for case II	73
29	Figure 4.15	Predictions model for SVM	74
30	Figure 4.16	Confusion matrix result with a load of 6.7N for a) Naive Bayes b) Ensemble boosted trees c) Logistic regression d) KNN e) SVM	75
31	Figure 4.17	Reverse Dial Indicator	76
32	Figure 4.18	Result of KNN (a) Confusion matrix (b) True Positive Rates and False Negative Rates graph (c) Positive Predictive Values and False Discovery Rates graph (d) ROC curve.	79
33	Figure 4.19	Result of SVM (a) confusion matrix (b) True Positive Rates and False Negative Rates graph (c) Positive Predictive Values and False Discovery Rates graph (d) ROC curve	80
34	Figure 4.20	Result of Ensemble sub space discriminant (a) confusion matrix (b) True Positive Rates and False Negative Rates (c) Positive Predictive Values and False Discovery Rates graph (d) ROC curve.	81
35	Figure 4.21	Feature Vs Testing accuracy plot	82
36	Figure 5.1	The schematic diagram of the feature extraction procedure with the second-order WST	90
37	Figure 5.2	The architecture of NARX neural network	91
38	Figure 5.3	Experimental Setup	92

39	Figure 5.4	Sensor Mounting and Bearing Housing	93
40	Figure 5.5	Set-up	93
41	Figure 5.6	Test bearing: Taper roller bearing (NBC make)	94
42	Figure 5.7	Flowchart of the proposed method for case I: wavelet scattering xgboost approach	95
43	Figure 5.8	Flowchart of the proposed method for case II time domain-based HI and NARX	95
44	Figure 5.9	RSSI repartition	97
45	Figure 5.10	Time series bearing data, (a) 0th and (b) 1st order scattering coefficients of the outer race faulty conditions	97
46	Figure 5.11	Frequency response of the first and second filter banks with eight and one wavelets per octave respectively	98
47	Figure 5.12	(a) Scattering coefficients scattergram for filter bank 1 (b) Scattering coefficients scattergram for filter bank 2	98
48	Figure 5.13	Case I RUL prediction of NBC bearing (a) Bearing 1 (b) Bearing 2 (c) Bearing	100
49	Figure 5.14	NARX net view	102
50	Figure 5.15	Training summary	103
51	Figure 5.16	Training state information	103
52	Figure 5.17	Performance of the network	104
53	Figure 5.18	NARX performance for vibrational data	105
54	Figure 5.19	RUL prediction result	106
55	Figure 5.20	Error histogram	106
56	Figure 5.21	Combined performance plot for training, validation, and testing set	107
57	Figure 5.22	Autocorrelation error plot	107
58	Figure 5.23	(a, b) Validation and testing results for bearing 2 (c, d) validation and testing results for bearing 3	108

List of Tables

S. No	Table No	Caption	Page No
1	Table 3.1	Defects (Parallel and Angular Misalignments)	34
2	Table 3.2	Experimental Load and Speed Conditions	34
3	Table 3.3	ANOVA Table for Quadratic Model	35
3	Table 3.4	Fit Statistics for Parallel Misalignment	35
5	Table 3.5	ANOVA for Quadratic Model	42
6	Table 3.6	Fit Statistics for Angular Misalignment	42
7	Table 3.7	ANOVA Table for Parallel Misalignment	46
8	Table 3.8	Fit Statistics for Parallel Misalignment	46
9	Table 3.9	ANOVA Table for Angular Misalignment	48
10	Table 3.10	Fit Statistics for Angular Misalignment	49
11	Table 3.11	Comparison of Vibration and Acoustic Sensor	50
12	Table 4.1	Feature Ranking For 13.4 N Load	59
13	Table 4.2	Summary Table for Case I: No Load Condition	67
14	Table 4.3	Summary Table for case II	72
15	Table 4.4	Result Summary with a Load of 6.7 N	75
16	Table 4.5	Defects Dimension	76
17	Table 4.6	Feature Ranking	77
18	Table 4.7	Summary Table	82
19	Table 5.1	Specifications of the Test Bearing	94
20	Table 5.2	MSEs Between the Actual and Predicted Life Percentage	101

Nomenclature

k_r - Rotational stiffness

C_r - Rotational damping

f_r - Motor rotational speed in Hz

Re - Reynolds number

Nu - Nusselt number

T_i - initial temperature

f - response function

E_u - experimental error

ANOVA- analysis of variance

HP- horsepower

MFS - Machinery Fault Simulator

ΣD - Sum of the differences

ΣD^2 - Sum of the squared differences

$(\Sigma D)^2$ - Sum of the differences, squared

α_j - population mean for the j th group

ε_{ij} - the random error, with zero mean and constant variance

SINAD- signal to noise and distortion ratio

SNR - signal to noise ratio

RMS- root mean square

THD - Total harmonic distortion

ROC- receiver operating characteristic curve

AUC- Area under curve

IMS- Intelligent Maintenance Systems

AI- Artificial intelligence

AWGN -additive white gaussian noise

N - normal distribution

SVM- support vector machine

KNN- K nearest neighbor

ANN- Artificial neural network

WST- wavelet scattering transform.

CNN- convolution neural network

LSTM- long short-term memory

RSM- response surface methodology

XGBOOST- extreme gradient boosting

ANOVA- analysis of variance

2x – 2 times of rotation speed

SVR- support vector regression

ML- machine learning

DL-deep learning

Xgboost- extreme gradient boosting

NARX - nonlinear autoregressive network with exogenous inputs

1.1 Background and Motivation

1.1.1 Introduction to Rotor System

In any mechanical system, rotating machinery is one of the most essential parts. It is usually susceptible to faults since its functions in a harsh working environment. Any defect in the rotating equipment could cause the overall degradation of mechanical systems and tends to fail, reducing the machinery's reliability, stability, and availability. Rotating machine parts nowadays is more advanced and complex, due to this, detecting potential faults has become more challenging. Rotating machinery vibration is mostly caused by disc unbalance and shaft misalignment. The vibration caused by these sources damages important system components such as bearings, gears, motors, seals, couplings, etc.

1.1.2 Importance of Study on Misalignment

The driveshaft of the prime mover and the shaft of the driven unit, which are both supported on bearings, must usually be in a straight line with the same elevations from the ground levels. A mechanical coupling is used to connect the two shafts. The shafts, however, are not concentric due to the unequal foundation level, and they are displaced either by the same lateral amount or by an angle. This situation causes shaft misalignment, which can be parallel, angular, or combined. There is an axial push and pull on the shafts because of this condition, and a high axial vibration is observed. To avoid shaft misalignments, essential shaft alignments are performed during machine installation by introducing metal shims or modifying jack bolts at the machine foundation. Flexible couplings are frequently utilized to accommodate minor misalignments. However, due to shim corrosion, uneven thermal expansion between the driven and driving ends, and other factors, the misalignment may worsen over time. This misalignment causes an increase in frictional forces within the coupling's flexural parts, as well as an increase in the coupling's temperature. Because of the increase in axial vibration levels at a frequency twice the rotating speeds of the shaft, misalignments in shafts can be identified rather simply by vibration monitoring. This is because when the misalignment increases, the torque on the shaft increases twice as fast as the rotational speed. The phase difference between bearings across the connection is 180 degrees during misalignment. A strong push in one

direction causes misalignment, which produces an elliptical orbit. The figure 1.1 indicates the types of shaft misalignment. Failure of rolling bearings frequently results from misalignment. It can result in cage fracture, which will cause the bearing to seize up, and causes for expensive downtime. Additionally, misalignment may lead to edge loading, which may speed up the failure of the bearing. So, the study of prediction of remaining useful life of rolling element bearing is important.

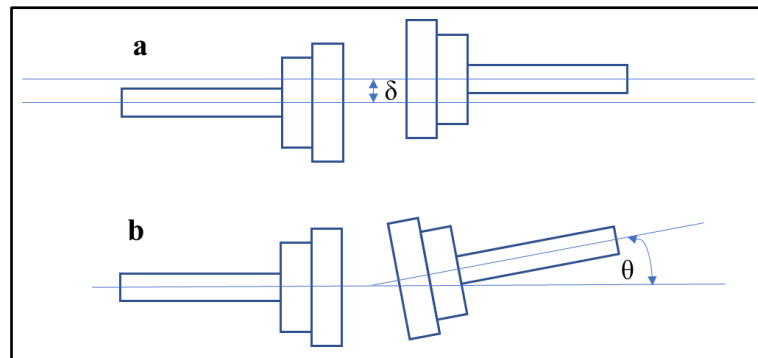


Figure 1.1 Shaft misalignment: (a) parallel, (b) angular.[1]

1.1.3 Importance of RUL Study of Rolling Element Bearings

Prognostics is the process of predicting the future performance of machinery using prediction methods and calculating the remaining time before the machinery loses its capacity to operate, also known as the remaining useful life (RUL). Predictive maintenance is possible with an accurate RUL prediction of machinery, reducing costly unplanned maintenance. As a result, RUL prediction appears to be a trendy topic that has gotten much interest in recent years. Prognostics are far more efficient than diagnostics in achieving zero-downtime performance because they can schedule maintenance strategies before faults occur. The three main steps in the machinery prognostic process are state estimate, state prediction, and RUL prediction. State estimation is based on the output of diagnostics' fault detection, which determines the fault pattern and severity. Condition estimation is used to quantify the severity of a malfunction and forecast the state of machine deterioration. Predicting the state's degradation trend and pace, based on historical degradation curve data is known as state prediction. The time duration of the deterioration curve from the present state to the final failure is calculated based on a chosen failure threshold in the RUL prediction stage. Data-driven methods, model-based methods, and data-model fusion approaches are the three basic types of machinery prognostic methods. Instead of constructing models based on comprehensive system physics and human skill, data-driven techniques aim to identify machinery degradation processes from measurement signals.

These methods are based on the idea that, unless a fault arises, the statistical features of data are reasonably consistent. Based on historical measurement signals, they generate RUL forecast findings. As a result, the precision of data-driven approaches is determined by the quantity and quality of past measurements. However, in most circumstances, gathering enough qualifying measurements is challenging. Model-based methods aim to create mathematical or physical models that characterize equipment degradation processes, and then update model parameters with measurable data. Expert knowledge and real-time data from machinery could both be included in model-based solutions. As a result, they may be helpful in the RUL prediction of machinery. They also require less information than data-driven techniques. Markov-based models, Wiener process models, and inverse Gaussian process models are some of the most often utilized models. Model-based methods, on the other hand, may not be appropriate for dealing with rotating machinery prognostics in the following scenarios: (1) Machinery fault patterns vary depending on operation; (2) The mechanical system is so complex that understanding the principles of the system operation is difficult and developing an accurate model is prohibitively expensive.

1.2 Fault Diagnosis and Prognosis

Shaft misalignment, unbalance, and bearing defects are some of the critical faults which may lead to catastrophic failure of the whole mechanical system and leads to unavoidable downtime which intern causes productivity loss. To avoid such unplanned downtime due to machinery breakdown, a proper maintenance activity needs to be conducted. Greater quality and higher reliability are needed because of the technological advancement and increasing complexity of items. As a result, preventive maintenance becomes increasingly more expensive. Eventually, many industry sectors began to incur high costs for preventive maintenance. Nowadays, condition-based monitoring (CBM), among other more effective maintenance techniques, is being used to deal with the problem.

1.2.1 Importance of Condition-Based Monitoring (CBM)

Based on the data gathered through condition monitoring, CBM suggests maintenance steps, by lowering the amount of unneeded scheduled preventive maintenance activities. If the CBM study is correctly established and successfully performed, can significantly save maintenance costs. In this study, diagnostics and prognostics are crucial components. Diagnostics focuses on locating, isolating, and identifying faults as they happen. When anything goes wrong in the monitored system, fault detection is the task that let us know; fault isolation is the task that

helps us to identify the critical component; and fault identification is the task that helps us to figure out what the fault is when it is discovered. The goal of prognostics is to identify faults before they manifest. The goal of prognosis is to identify impending faults and predict when and how probable they are to occur. Prior event analysis is used in prognostics, while posterior event analysis is used in diagnostics. To achieve zero-downtime performance, prognostics is far more effective than diagnostics. The CBM consists of two main stages, i.e., data acquisition and signal processing.

1.2.1.1 Data Acquisition

The method of obtaining measurement signals from monitored devices using various types of sensors and storing the data in a computer is known as data acquisition. The health conditions of the monitored machines are meant to be linked to the measurement signals. These measurement signals contain certain valuable information about the device's health. Vibration signals, acoustic signals, temperatures, and electric currents are only few of the different forms of measurement signals. Different sorts of sensors have been built to collect different types of signals, such as accelerometers, acoustic emission sensors, infrared thermometers, ultrasonic sensors, and so on. The signals are recorded and sent to a computer via data acquisition (DAQ) devices, where they are stored in memory for later processing.

1.2.1.2 Signal Processing

Time-domain, frequency-domain, and time-frequency-domain signal processing methods are the three types of traditional signal processing methods. Fault features in vibration signals recorded from rotating machinery are very weak, especially for early defects, because they are embedded in a lot of background noise. As a result, vibration signals should be preprocessed to eliminate background noise and measuring system errors, allowing for the acquisition of more meaningful information and an improvement in SNR. When a fault develops, the stiffness of the structural components surrounding the defect must change, causing an impulse or shock to develop. The gathered vibration signals may also vary because of this impulse. These time-domain signals' amplitudes and distributions can be altered. As a result, time-domain statistical features that reflect mechanical flaws can be retrieved from their time-domain features. Table 1 from appendix shows common statistical properties in the time domain. In general, mechanical vibration can be induced by a fault, which raises the mean value, root amplitude, root mean square, and peak. When a fault becomes more severe, the above four characteristics can clearly show the fault's severity. The kurtosis value, crest factor, impulse factor, and

clearance factor can all be used to determine how much impulse is present in vibration signals. The kurtosis value and crest factor are good indications for incipient defects because they are resistant to changing operating conditions. The spikiness of the sharp impulses generated by the contact of a defect with the bearing mating surfaces can also be determined by the impulse and clearance factors. It's worth noting that the kurtosis value is quite sensitive to early defects. The kurtosis value might steadily grow as the severity level rises. However, it drops unexpectedly for more serious flaws. As a result, the kurtosis value is inappropriate for more severe problems. Table 1 from appendix shows the time domain features. They will be able to compensate for each other. Each indicator contains fault information differently at different fault levels. Many indicators can only represent fault changes to a certain extent. As a result, additional features should be retrieved to properly identify rotating equipment defects, and sensitive features should be further screened out.

Signal processing in the frequency domain compensates for the deficiency of signal processing in the time domain, which only reflects the fluctuation in a signal's waveform and does not reveal the signal's intrinsic character. As the most extensively used analytical tool, the frequency spectrum can reflect the frequency components and distribution of a signal. By using the Fourier series, a periodic signal is first split into a sum of many sinusoidal components. The periodic signal's frequency spectrum can then be obtained by projecting these sine and cosine signals in the frequency axis. The magnitude of the corresponding sine or cosine signal determines the amplitude of each frequency. As a result, the Fourier integral transform is offered as a method for converting a continuous periodic signal into a frequency spectrum. The Fourier integral transform, on the other hand, can only process continuous signals, not discrete ones. Computer processing of signals is not appropriate, based on this reasoning, the Discrete Fourier Transform (DFT) is offered as a method for computers to get the frequency spectrum of discrete signals. Traditional DFT takes longer to compute the DFT of a long enough signal as the data length increases. As a result, FFT is presented as a method for quickly calculating the DFT of a signal. Extracting some indicators in the frequency domain is critical for defect identification. Additionally, certain fault-related information may be available in these frequency-domain features or indications that is not present in the time domain. To put it another way, these frequency-domain properties effectively compensate for the time-domain features alone. When a malfunction occurs in the machinery, irregular frequencies appear in the vibration signal's frequency spectra, which can reveal the machinery's health status. Furthermore, because an undetectable change would form a spectrum line in the corresponding frequency spectrum, frequency spectra are more sensitive to incipient flaws.

Frequency domain can only process stationary signals, it is unable to process nonstationary signals. Furthermore, the frequency spectrum acquired by FT cannot indicate how each frequency changes over time. To circumvent these drawbacks, time–frequency analysis approaches for analyzing a nonstationary signal from a time–frequency distribution has been developed. Short Term Fourier Transform (STFT), Wigner Ville Distribution (WVD), wavelet transform (WT), even Wavelet Packet Transform (WPT), and Hilbert Huang Transform (HHT) are examples of classical time–frequency analysis approaches. These approaches can reflect a signal’s shift in both the time and frequency domains. With the introduction of time–frequency analysis techniques such as the standard wavelet transform and empirical mode decomposition (EMD), different signal processing algorithms can extract certain useful aspects from a signal’s time–frequency distribution.

The primary goal of fault diagnosis is to assess relevant external data to evaluate the state of the inaccessible interior components and determine whether the machine has to be disassembled. Vibration analysis is one of the methods for identifying faults in rotary machinery. The vibration analysis allows for the extraction of crucial diagnostic data from the vibration signals by analyzing in time domain, frequency domain and time-frequency domain. The results of conventional fault diagnosis techniques are filtered signals and their spectra with signal processing techniques, which require a visual inspection of the diagnosis results to compare them with the healthy ones and find the fault characteristics, depending on the diagnosticians' expertise and their capacity to analyze the results. To use these diagnosis techniques properly, diagnosticians must thoroughly understand each monitored signal that they must examine one at a time. Traditional diagnosis may not be suited for dealing with huge data captured using sensors in the modern day because data are typically collected faster than diagnosticians can interpret them. Conversely, artificial intelligence can substitute conventional signal processing techniques for diagnosis experts to interpret collected signals quickly and effectively and produce reliable diagnosis results. Fault diagnosis using machine learning and deep learning has the potential to be a useful tool for handling large amounts of machinery fault data in the Big Data Era without the requirement for a diagnosis expert to evaluate data and identify issues.

1.2.2 Importance of Machine Learning Techniques

Data acquisition system is used to collect data from rotating machinery in real-time, and the volume of data collected by various sensors after the long-term operation has increased

massively. The potential of mechanical big data not only promises to improve conventional approaches to mechanical problem detection, but also opens new processing and information-discovery possibilities for this discipline. Therefore, employing cutting-edge algorithms to successfully extract characteristics from huge data and precisely diagnose the machinery health problems becomes a new research area.

Machine learning and deep learning is a framework for information processing that takes clues from how the human brain interprets data. These techniques offer a versatile mechanism for learning and identifying system flaws because of their capacity for extrapolating nonlinear correlations between input and output data. They are well-known as effective intelligence tool for rotating machinery defect diagnostics. The different machine learning techniques are Linear regression, logistic regression, decision trees, support vector machine (SVM), K-Nearest neighbor (KNN), and ensemble subspace discriminant algorithms are used for machinery fault diagnosis. Machine learning techniques are used in data-driven methodologies to extract the trend of degradation processes from the measured data. The interference of noise is always present in the raw measured data. Health indicators, which are meant to provide relevant information about degradation, are typically taken from the raw measured data to show the degradation trend of machinery. Various deep learning techniques such as convolutional neural networks, long short-term memory (LSTM) are also employed to track the degradation of machinery. These deep learning algorithms can automatically extract the functional features and can be used for fault diagnosis and prognosis by analyzing large datasets.

1.3 Scope of Work

In the present investigation, the combined effect of speed, load, and misalignment defects on system vibration is carried out. Both vibrational data and acoustic data is used separately for the response surface methodology study and a comparative study is performed. Results obtained using acoustic sensors were found in line with the result obtained using vibrational data. Conventional vibration analysis techniques can diagnose misalignment as reported by researchers, but it is challenging to classify the different forms of misalignment. This study uses vibro-acoustic sensor data fusion along with machine learning techniques to classify different forms of misalignment. As misalignment is one of the major reasons for bearing failure. Deterioration of bearing caused by misalignment and other malfunctions is studied using prognostics methodology. A remaining useful life of bearing is estimated by considering the degradation of bearing. The effect of noise is also considered during the analysis. The data is collected at NBC Bearing, Jaipur under actual industrial settings.

1.4 Organization of Thesis

This thesis is divided into the following chapters to address the issues of misalignment fault classification, the effect of speed, load, and defect severity on system vibration, misalignment fault classification, and bearing residual life assessment.

Chapter Two gives a detailed literature review of the misalignment fault diagnosis using model-based, and signal-based techniques, the effect of misalignment on bearing life, and the prediction of remaining useful life of bearing using statistical data-driven techniques are carried out. The development of various fault diagnosis schemes is discussed.

Chapter Three discusses the relation between speed, load, and the presence of various types of misalignment defects with varied degrees of severity and their impact on system vibration. To comprehend the impact of such interactions on system performance, Response Surface Methodology (RSM) is utilized.

Chapter Four covers the classification of misalignment, such as angular, parallel, and combined, employing a diagnostic tool such as the rotor vibration signal and acoustic emission. Time domain features are retrieved and using the t-test technique, they are ranked in order of significance. Different algorithms are trained using the extracted features and classification is performed.

Chapter Five discusses 2 approaches for the estimation of the RUL of taper roller bearing (TRB). In the first approach the data fusion, wavelet scattering in combination with xgboost regression is proposed, while in the second approach, time domain feature-based HI along with NARX neural network is proposed. The own dataset, collected at NBC bearing Jaipur is used in the study.

Chapter Six presents the thesis's general conclusion. This chapter also discusses the novelties of the research and its potential application in the future.

Reference

[1] O. A. Omitaomu, M. K. Jeong, A. B. Badiru and J. W. Hines, "Online Support Vector Regression Approach for the Monitoring of Motor Shaft Misalignment and Feedwater Flow Rate," in *IEEE Transactions on Systems, Man, and Cybernetics, Part C (Applications and Reviews)*, vol. 37, no. 5, pp. 962-970, Sept. 2007, doi: 10.1109/TSMCC.2007.900648.

2.1 Introduction

Rotary machines are significant resources in most industrial applications. The applications include motors, generators, gas turbines, the transmission system of vehicles, helicopters, etc. The rotor-bearing coupling system of advanced rotary machinery is very complicated, it needs a precise and reliable estimation of its dynamic behavior. Unbalance, looseness of machine parts, misalignment, cracks, and other malfunctions are the main reasons for vibration in rotary systems. Misalignment and bearings are the most frequent and critical faults among them. In general, machines assembled with zero misalignment cannot retain their alignment over a long period due to foundation vibration, lubricating systems, compression of gases and heat generation in casings. In any rotating machinery, the basic cause of misalignment is improper assembly, excessive or unequal load, thermal distortion, bolt loosening, unequal foundation, and force transmission to supporting elements [1], [2]. Jesse et al. [3] in their experimental analysis classified the effects of misalignment on the rotor system separately. He suggested that offset misalignment degrades the bearing and angular misalignment degrades the coupling. Misalignment increases vibration amplitude (radially and axially)[4], which causes wear of bearings, bending and deformation of the shaft, deformation of the rotor, excessive temperature rise, shaft crack, bearing house damage, etc.[5]. Sanjiv Kumar [6] conducted an experiment in support of context to show how drastically the vibration amplitude of misalignment varies. Few researchers found that 2x running speed is an indication of a misalignment fault in the system [7]. Vibrational signals also consider external disturbances and unwanted noise from sensors and machine, which creates the need to filter these signals.

2.2 Fault Diagnosis and Prognosis of Mechanical Systems

Fault diagnosis of rotating machinery has become increasingly important in industrial applications to avoid economic losses and improve machine availability. The fault characteristic frequency and its harmonics are referred to as the main characteristics. The diagnosticians then identify faults based on the presence of these characteristics in signals. These traditional methods are effective and widely used in the diagnosis of rotating machinery faults. However, as modern industry has advanced, condition monitoring systems are being used to collect real-time data from machines to fully inspect the health conditions of rotating

machinery, and massive data are being collected after long periods of machine operation. Because data is generally collected faster than diagnosticians can analyze it, there is a demand for methods that can replace vibration analyst to automatically make decisions on the running health of the machines.

A detailed literature review is carried out majorly focused on fault diagnosis of misaligned rotor system. The state-of-art has been discussed in 3 sections, Model based techniques, Signal based techniques and artificial intelligence (AI) techniques. AI techniques are further extended for addressing data driven methodologies for the prediction of remaining useful life of rolling element bearing.

2.2.1 Model Based Techniques

Model-based method that employs theoretical and residual values to pinpoint the system's flaws. When incorporated into a rotor bearing coupling system, the coupling is modelled as a rigid body and treated as a rigid disc model. The model, however, ignores the coupling's flexibility.

The Kramer [8] and Nelson and Crandall's [9] model considered the inherent coupling flexibility. The basic model recommended by Kramer considers mechanical coupling flexibility and describes it as radially stiff non-friction coupling. Classical FEM is used to model the coupled shaft as the 8-degree beam element at each node. In the revised model recommended by Kramer, while maintaining the constraints used in the first model, he also considered coupling's rotational stiffness (k_r) and damping (C_r). Nelson & Mcvaugh [10] presented a procedure for mathematical modelling of the rotor-bearing system by considering the effect of rotatory inertia, axial load and gyroscopic moments of developed finite element model. Consistent matrix approach was used for this study.

Sekhar and Prabhu [11] considered the deflection, shear forces, slope and bending moment to model the rotor system with higher-order finite element method and derived moments and reaction forces developed owing to the flexibility of coupling misalignment. Lee and Lee [12] derived a dynamic model for a misaligned system by considering deformations and reaction forces. They verified experimental results with simulation results, they found that increase in natural frequency in the direction of misalignment. Axial vibration is also considered in this model, which is a key indicator of the existence of misalignment. Isermann [13] elaborately described methodology for machine and other processes by using some measurement, dynamic process and signal parameter to generate analytical assumptions. Jalan and Mohanty [14],

considered equivalent loads as a sign of a fault in the rotary system and by using experimental time response method for both faulty as well as the healthy system, they successfully detected the amount, type, and location of a mechanical fault in the rotor-bearing system.

Jalan and Mohanty [14] used a residual generation method for misalignment and unbalance identification in the system. Pennacchi and Vania [15] suggested that combining model-based analysis with other techniques of fault diagnosis would provide better health information than a single diagnostic technique.

2.2.2 Signal based techniques

In a rotating system, shaft misalignment can be identified by using the signal-based technique. These signal-based techniques can be classified into two types, vibrational and non-vibrational signal analysis.

2.2.2.1 Vibration Analysis

Vibration analysis uses the vibrational signal for detecting any mechanical asymmetry by studying frequency harmonics of varying peak amplitude in a system. Such vibrational techniques are discussed in the following sections.

2.2.2.1.1 Fast Fourier Transform (FFT)

FFT works on converting the time domain into the frequency domain using a Fourier transform. It represents the vibration signal as peaks at various frequencies in the spectrum where the repetition of the signal occurs. This allows early detection of fault present in the system.

Motor shaft misalignment was predicted online using spectra information produced by FFT and supporting vector regression[16]. The 2x and 4x reaction elements of the vibrational scheme have been proved experimentally by Dewell and Mitchell [17] for the evaluation of anticipated vibration frequencies for a misaligned coupling. Kumar et al. [18] used a full spectrum analysis for signal processing of complex vibration signals and revealed fault-specific whirl signatures and related fault. As per their conclusion, FFT loses the orbital information (both backward and forward whirling), which is preserved by full spectrum.

FFT is replaced by other technical tools because it is inefficient in disclosing information for non-stationary signals, fault identification and separation. It also loses its time-domain signal information[19].

2.2.2.1.2 Orbit Analysis

Orbit analysis uses orbit plots which show the shaft rotation under the given loading conditions [20]. It captures accelerometer data in time-domain itself, eliminating the need for the frequency-domain study. Analysis of the orbit is useful when the system simultaneously suffers from several failures. Orbit plot is almost circular in shape for healthy and distorted and asymmetrical for the unhealthy faulty system [21].

Monte et al. [20] extended the analysis to three dimensions, where axial direction helped in detecting system asymmetry. Orbit plot was constructed based on data captured by vibration measurement using accelerometers (2 in radial and 1 in the axial direction) and load imbalance, to detect parallel and angular misalignment. Costa et al. [22] deduced that the ellipticity of the orbit plot profile obtained from proximity sensors is used to detect rotary system misalignment.

2.2.2.1.3 Discrete Wavelet Transforms (DWT)

Wavelet transform is used for non-stationary signal analysis for early fault detection, which is otherwise a limitation for FFT [23]. Wavelet representation is more sensitive to misalignment fault diagnosis than FFT. It offers energy distribution over frequencies that change at all times [24]. It overcomes the problem of low-resolution and time information faced by other techniques. The correct choice of the mother wavelet function is very essential, as it helps to detect the error in the system accurately [25]. Umbrajkaar and Krishnamoorthy [19] analysed signal using DWT, helping in proper identification and fault wise separation of signals by proper selection and application of mother wavelet. The minimum, maximum, mode, median, mean values of detailed coefficients help in the correct selection of mother wavelet. By using DB2 as a mother wavelet, they combined DWT with FIS (Fuzzy inference system) for predicting the degree of misalignment [26]. The result obtained had the least deviation. It covered information in both time and frequency domain, making it a multilevel analysis.

2.2.2.1.4 Continuous Wavelet Transform (CWT)

CWT is useful for transient signal analysis and time-frequency localization [27]. It provides time-frequency information of signals of the misaligned motor system unlike Fourier analysis. It is preferred for more noisy data analysis. CWT for energy-limited signals is given by equation (2.1),

$$Wf(a, b) = \int_{-\infty}^{\infty} f(t) \frac{1}{\sqrt{a}} \psi * \left(\frac{t-b}{a}\right) dt \quad (2.1)$$

Where ψ^* is complex conjugation of $\psi(t)$ (mother wavelet function), and a, b are the dilation and translation and $1/\sqrt{a}$ is used for energy preservation. In CWT, the wavelet function spans the entire frequency band, making it an inefficient way to analyse the data. CWT analyses the transient signal, by decomposing it into a series of time-domain components with each component covering a certain range, thus providing a finer resolution than Orthogonal wavelet transformation (OWT) to extract mechanical error information. By analysing non-stationary signals, Al-Badour et al. [25] worked on a combination of both Wavelet transform and Continuous Wavelet transform to detect impulsive faults by considering 2 non-stationary signal producing cases (i) stator to blade rubbing (ii) fast start-up and coast down of the motor. Wavelet transform when combined with acoustic analysis can also detect underwater faulty objects with a neural network.

2.2.2.1.5 Hilbert Huang Transform (HHT)

It is a time-domain and frequency independent which does not affect the non-stationary modulating signal [23]. By removing carrier signals carrying irrelevant information, it helps in early detection of the fault via visual inspection in time-domain. The computational time of HHT is less as compared to CWT. It is used for multiple fault diagnosis in a rotary system and detection of a lower case of misalignment, which is otherwise difficult in other techniques. HHT is a two-step procedure: (1) Empirical mode decomposition (EMD) for obtaining intrinsic mode functions (IMF's) (2) processing of IMFs with Hilbert transform for obtaining frequency corresponding to IMF[27].

The Hilbert Transform $h(t)$ of a function $x(t)$ is given by equation (2.2)

$$h(t) = H\{x(t)\} = \frac{1}{\pi} \int_{-\infty}^{\infty} \frac{x(\tau)}{t-\tau} d\tau \quad (2.2)$$

Chandra and Sekhar [27] compared HHT with CWT and Fourier transform to experimentally detect the least possible misalignment. They corrupted the signals with instantaneous Gaussian noise with different SNR to check HHT performance, but Hilbert transforms effectively distinguished the error. Wu and Chung [28] utilized the combined method of EEMD and EMD, which decomposed non-stationary and non-linear signals in intrinsic mode functions (IMFs) to examine misaligned shaft characteristics in time-frequency Hilbert spectrum using intrawave frequency modulation (FM) phenomenon. Misalignment level was proportional to level to amplitude modulation (AM) in IMF. Fan and Zuo [23] proposed early fault detection methods that combine both HHT and Wavelet packet transform (WPT) for a multistage gearbox

containing close or identical frequency components and proved its efficiency and accuracy to handle non-stationary signals. HHT loses its performance while handling a low SNR.

2.2.2.2 Non-Vibration Based Techniques

2.2.2.2.1 Acoustic Emission (AE) Technique

Tandon et al. [29] concluded AE to be more reliable than MCSA and Vibrational analysis after the study of peak amplitudes which increased proportionally to defect. Chacon et al.[30] carried out an experimental analysis to demonstrate enhancement of AE over vibrational analysis for detecting shaft angular misalignment. Chacon et al.[30] studied AE signal analysis for misalignment detection by linking shaft displacement with AE sensor and accelerometer analysed signals. He proposed a shaft angular misalignment (SAM) detection method which begins with signal acquisition using an AE sensor. The acquired signal is filtered from undesirable frequencies and amplified in the AE envelope spectrum to distinguish the signals of different frequencies and converted from analog to digital (ADC) signal. Fast Fourier transformation (FFT) comes into play after the envelope extraction to obtain the AE envelope frequency spectrum where the signals obtained at different frequencies are compared based on their amplitudes, thus defining the peak for misalignment detection. Le and Hi [31] used EMD based acoustic feature where de noised AE signals are compressed into a single AE signal and by providing a threshold for separating healthy and damaged states, these compressed signals help in fault detection.

2.2.2.2.2 Motor Current Signature Analysis (MCSA)

It is the most popular and widely used tool for diagnosing mechanical and electrical problems related to AC motors. It is a non-contact type method for fault detection, where the motor works under its normal condition without any disturbance[32]. MCSA implementation does not require expensive sensors thus making it very economical[33]. It is widely used in induction machine's fault diagnosis[34]. It focuses on analysing spectral information of stator current and uses FFT to extract the current features and signal processing. FFT of current samples can be generated by NV gate software packages where small misalignment can be detected by using FFT plot of current samples. MCSA provides an algorithm for diagnosing faults but fails to determine failure thresholds.

Bossio et al. [35] inspected the misaligned motors by using current, flux as diagnostic medium and experimentally concluded that frequency components ($f \pm nfr$) produce sidebands of

different amplitude in the frequency spectrum that help to distinguish faulty and healthy systems.

Verma et al. [36] considered vibration and current as a diagnostic medium, concluded misalignment as a cause of instability in the healthy system. Experimentally, Sivarao et al.[32] revealed that the current increases with the load value and considering misalignment as a type of load on a healthy rotating system, the current value is proportional to the level of misalignment. Current spectrum can also be generated by current and frequency values drawn from both healthy and faulty system using MATLAB with current spectrum showing a rise in amplitude for sideband frequency and reduction in peak amplitude for the faulty motor.

Dewell and Mitchell [37] also investigated the presence of misalignment by using 2x and 4x frequency components. There are many harmonics at different frequencies in the motor current signature, and we need to perform signal conditioning to analyse the system's defects.

2.2.3 Artificial Intelligence Techniques

It is standard practice to diagnose misalignment when a strong peak appears at double the running speed. It is challenging to determine the type of misalignment by analyzing vibrational signal alone since both angular and parallel misalignment type display peak at 2x running speed. Also, to handle the big data from continuous data acquisition from machinery there is need of artificial intelligence (AI) techniques like machine learning and deep learning techniques. These AI techniques can help to classify the different misalignment fault types. Although a lot of work had been reported on model based and signal-based approaches towards misalignment fault diagnosis, but very limited work was reported to classify these faults using machine learning techniques. The subsequent sub-section discusses the use of machine learning techniques for the machinery fault diagnosis and prognosis.

For misalignment fault detection, Haroun et al. [38] used the Autoregressive (AR) torque signal model. Firstly, the torque signal obtained from the experimental setup and coefficients of the AR model were extracted as features under various operating conditions. To pick the best features for fault classification, Min Redundancy Max Relevance (mRMR) was used. The features extracted from acoustic signal contributing significantly to the fault diagnosis and segregation of different faults.

A full spectrum analysis was conducted for both signals to reveal the fault-specific whirl patterns. For fault detection, Alok Kumar et al. [39] used stator current and vibration samples. Feature extraction is carried out using multiscale entropy (MSE), and for fault classification by

using SVM. Vibration analysis was used by Umbrajkaar et al. [40] to perform misalignment fault classification using the machine learning method, SVM and ANN. For fault classification, they extracted time-frequency domain features. Feature ranking was carried out using the ReliefF algorithm, the accuracy of fault classification using ANN was 94.17 percent and using SVM was 97.72 percent. Yong et al. [41] carried out misalignment fault classification using vibrational data alone, they used power spectrum features to classify the faults using SVM, they reported an accuracy of 98%. Some researchers [40], [41] have already obtained near-perfect results in misalignment fault classification for only angular and parallel cases, but there is need to attempts to establish an even higher accuracy than the 98% percent accuracy reported with considering combined misaligned case.

Even though data-driven strategies for bearing fault diagnosis have been very well proposed and implemented[42]. Diagnosing and classifying the bearing faults is still a challenge based on the knowledge obtained from a single transducer. Gryllias et al. [43] suggested two stage hybrid approaches for the bearing fault diagnosis. Based on an envelope study to diagnose ball bearings with inner race, outer race, and ball faults. Safizadeh et al.[44] employed the K-nearest neighbour (KNN) classifier to determine the state of the ball bearing based on vibration and load signal data. With data from a single transducer, the functionality of these machine learning classifiers was tested. The overall device dependability is improved by combining data from various diagnostic transducers into a classifier. The sensor fusion technique provides precise decision-making capabilities to obtain defect-related data. Moslem et al. [45] carried out the multi sensor data level fusion for the diagnosis of gear box faults using motor current signature analysis. They presented a comparative study of sensor data fusion with other machine learning algorithms. The result of multi sensor data fusion were better. Praveen Kumar et al.[46] performed accelerometer, microphone, and acoustic emission data fusion for fault diagnosis in case of centrifugal pump. They extracted wavelet features for the analysis. Glowacz [47] carried out fault diagnosis of single-phase induction motor based on acoustic signals alone. Shan et al. [48] carried out multi sensor data fusion for ball fault screw diagnosis using CNN. Abdullah et al. [49] performed vibro-acoustic sensor data fusion for identification of bearing defect and estimation of defect size. Gunerkar et al. [50] performed a bearing fault classification using an accelerometer and microphone sensor data fusion. The fault classification is carried out using KNN. Anil Kumar et al. [51] carried out bearing fault diagnosis using novel convolutional neural network for small training samples. They achieved a fault classification accuracy of 91%. The cost function of a CNN is adjusted by adding additional sparsity costs to the original cost function for effective feature learning from small training data. The sparsity

cost is calculated using a unique trigonometric cross-entropy function. Sugumaran et al.[52] investigated the effect of number of features on fault classification using SVM. Fatima et al. [53] used multi class SVM for faults classification in a rotor-bearing device due to bearings and unbalance by considering SVM generated by the various combinations of the two most sensitive features for each category of fault. They found that as more transducers are included, the classification accuracy improves. To obtain certain features in both the time-frequency domain, Singh et al.[54] applied the stockwell transformation to the stator current signals. They applied SVM to the experimental data of defective bearings collected from the industry with 91.66% success. Based on the principal component analysis process, the feature selection has been made. Using both supervised and unsupervised defect classification methods, the efficacy of the scheme was experimentally tested on a bearing test bed [55]. Once the features are retrieved, the dimensionality of the feature vectors must be minimized since there is no guarantee that most of these features are equally valuable in characterizing machine health. Misalignment is one of the major reasons for bearing degradation. Sometimes misalignment is provided in the experimental setup to avoid jamming due to severe accelerated test under high speed and loading conditions. So there need to be attention on predicting the possible failure when the system has inherent misalignment.

A lot of emphasis has been paid to evaluating bearing reliability and predicting remaining useful life (RUL) because of the system's increasingly harsh operating circumstances. A large number of life data samples can be used to infer a specific statistical distribution for bearing life. However, in reality, bearing life is highly random due to the influence of manufacturing defects, misalignment, material flaws, and load changes[56], [57]. In engineering practice, research attention has turned to the evaluation of a single bearing's RUL while considering its real working circumstances. By creating a weibull proportional regression model based on the PRONOSTIA platform's monitored data, Kundu [58] estimated the bearing RUL. Liu[59] presented a new network to predict the bearing RUL employing the datasets made available by NASA and FEMTO-ST by combining the advantages of long- and short-term memory (LSTM) and statistical process analysis. Huang [60] described the transfer learning approach and built a transfer depth-wise separable convolution recurrent network to forecast the bearing RUL using the same public datasets while considering various working situations. To forecast the health state of a ball bearing, Xu [61] developed a novel health indicator termed moving average cross-correlation of the power spectral density (MACPSD). The issue with these health indicators, though, is that in reality, their computed values do not correspond to the degree of actual bearing deterioration. Model-driven approaches, like the Paris-Erdogan approach [62],

can precisely forecast the bearing RUL under various working circumstances. Still, developing a useful model based on the physical system is necessary for accuracy. The statistical model, which is frequently referred to as an empirical model-based method, is used by the data-driven method to forecast the RUL. For instance, Kumar [63] coupled the Gaussian process regression with Kullback-Leibler divergence to forecast the RUL. To anticipate the RUL, Li [64] and Qiu [65] suggested a stochastic approach. To estimate the RUL of wind turbine bearings, Xing[66] and Li[67] suggested a mixed Gauss model-hidden Markov model (GM-HMM).

Other approaches include artificial intelligence (AI) mathematical models like the support vector machine [68] and artificial neural network[69], which have the ability to solve complex systems issues without the need for prior knowledge. However, data-driven approaches lack universal adaptability and can only handle the specific work environment. On the other hand, a hybrid method combines the benefits of a model-driven method and a data-driven method; examples of this sort of methodology include the Kalman filter [70] and particle filter [71]. Although numerous studies about bearing RUL prediction have been offered, only a small number of pertinent studies have focused on accurately determining when damage would develop and when it will reach its end of life two factors that are essential for accurate prediction results. Entropic evidence was utilized by Antoni [72] to identify the early flaws in rotary equipment. To identify the first flaws in rotating equipment, Chegini [73] employed ensemble empirical model decomposition and wavelet packet decomposition, and Nirwan [74] used acoustic emission. Even though the detection findings from the aforementioned investigations were quite precise, the detection models or the extracted features were the result of extensive calculations. Implementing such techniques when real-time responses are required is challenging, particularly when the process of predicting bearing RUL is ongoing.

ANNs mimic the functioning of human brains by connecting many nodes in a complex layer structure. They are the most widely used AI techniques in the field of RUL prediction in machinery. Feed-forward neural networks (FFNNs) are the most widely used. Most of publications [75]–[82] used an FFNN to learn the relationship between HIs and lifetime. To estimate the RUL of fatigue cracks, barufatti et al. [83] used FFNNs with sequential Monte-Carlo sampling. A FFNN was utilized by Pan et al. [84]. To forecast future HIs, Wang et al.[85] utilized a three-layer FFNN. They then entered the anticipated HIs into a PH model to calculate the hazard rate and survival probability. The ability of recurrent neural networks (RNNs) to handle explicit time-series data makes them a popular choice for RUL prediction. To anticipate the RUL of machinery, Zemouri et al. [86] presented a recurrent radial basis function network. To improve the long-term prediction accuracy, Malhi et al. [87] developed a competitive

learning-based methodology to change the training method of RNNs. A predictive method based on an RNN that was trained using time gradient computations and extended KF was proposed by Heimes et al.[88]. By replacing the hidden layer with a sizable sparse reservoir, Peng et al. [89] improved the RNN and created a novel RUL prediction method. By enhancing RNNs' memory property, Liu et al.[90] presented an improved RNN for RUL prediction.

For predictive RUL estimate, Li et al. [91] developed a new deep learning architecture. To improve CNN feature extraction, a temporal window approach was employed for sample preparation. In the proposed method, the raw sensor measurements were directly employed as model inputs. They asserted that because their method required no prior understanding of prognostics or signal processing, it was more suitable for industrial usage. The suggested approach's prognostic performance was validated using experiments on the prominent C-MAPSS dataset. The experimental findings of the proposed technique were compared to those of LSTM. Many sequential applications have embraced the RNN and its variation, the LSTM networks. In recent years, RUL prediction researchers have begun to examine the use of RNN, particularly LSTM. The RNN training approach consists of a Truncated Back Propagation via Time Gradient Calculation, an Extended Kalman Filter training method, and evolutionary algorithms. Wu et al. [92] used vanilla LSTM networks to obtain excellent RUL prediction accuracy in the context of demanding operations, working conditions, and model degradations. To detect the onset of decline, the RUL was generated using vanilla LSTM and a Relevance Vector Machines (RVM). The downside of this technique is that the RUL necessitates labelling at each time step for each sample, and some previous knowledge is necessary to identify an appropriate threshold before the SVM can be employed. Inspired by the Vanilla LSTM networks, Wu et al. [93] built another LSTM network focusing on fault forecasting with machinery degradation process, in which the RUL may be predicted without any pre-defined threshold.

In a practical industrial setting, noise from the surrounding environment is inescapable, causing machinery performance to deteriorate. In many instances, it has been claimed that the added noise degrades diagnosis performance. Lower testing accuracies are the result of increased noise. For defect diagnosis, Zhang et al.[94] introduced a deep learning-based approach called Convolution Neural Networks with Training Interference (TICNN). They discovered that in a noisy environment, fault diagnosis performance suffers rapidly. The impact of noise on diagnosis is significant. Some researchers have performed a study on effect of noise on remaining useful life estimation of different rotating machinery. In the first step, degradation features were extracted from both the training and testing data sets by Xiao et al. [95]

employing probabilistic principal component analysis. In the second stage, the degradation characteristics were infused using additive white Gaussian noise (AWGN), which was then coupled with manually introduced noise before being imported into a bidirectional LSTM network. The AWGN increased the robustness of the RUL prediction approach and achieved machine prediction in a variety of settings. They proved the usefulness of the suggested strategy by using the C-MAPSS lifetime data set for aeroengines.

2.3 Research Gaps

Misalignment occurs most frequently and an important rotor problem. However, this rotor fault is not completely understood. Despite its importance and frequent occurrence in practice and unlike other malfunctions, only a few researchers have paid attention to misalignment due to the complexity in developing mathematical model.

The above literature survey summarizes the different studies on coupling misalignment modelling, identification, and condition monitoring techniques in rotor systems. In addition to studies using vibration analysis, the literature highlights the misalignment identification by various techniques based on FFT, CWT etc. The state-of-art research on misalignment focuses the need for further work on this very important rotor fault. It causes for bearing failure. The prognosis of bearing is also one of the important aspects. The following are few key areas where still need a lot of research.

- 1) Misalignment is one of the key reasons for vibrations in most of the rotating system. These rotary systems are associated with varied operating conditions. Speed and load are the most common parameters, which frequently change. There was NO investigation carried out on interactions among speed, load, and defect (misalignment) severity by investigating their effect on the system vibration.
- 2) Conventionally, the diagnosis of misalignment is carried out through vibration measurements. Especially, the presence of strong 2x vibration peak is generally accepted. Both angular and parallel misalignment shows peak at 2x, therefore, distinguishing misalignment type based by vibration analysis alone is a difficult activity. No article mentioned about combined fault class, which also appears frequency in case of misalignment.
- 3) Acoustic emission (AE) is playing an important role in the fault diagnosis of ball bearings, but such technology is very rarely used in misalignment fault diagnosis. The very first attempt of AE in Shaft angular misalignment is reported by Ferrando [30]. Now a days, the focus is on non-contact type sensors. From the literature, it had been

observed imperatively, that early detection of the fault has not been attempted effectively along with vibration study alone. The role of AE in case of misalignment fault detection and classification needs to be investigated.

- 4) Misalignment causes the degradation of bearings. Machineries fail well before its stated life. So, there is a need to understand this degradation of machinery and predict the possible failure well in advance. Prediction of remaining useful life is important to avoid such unplanned downtimes. A significant amount work has been reported on prediction of remaining useful life of ball bearing but in actual industrial settings, the acquired data will have lot of noise. This noise can affect the performance of algorithms but there was scanty literature found on RUL prediction of bearings in actual industrial settings.

The present works aims at addressing these gaps and develop a hybrid model which classify the different types of misalignment faults. In its extension of understanding the characteristics of multiple fault types, there will be the establishment of study for the dynamics of interaction between multiple parameters and its effect on system vibrations. The study will not only improve the diagnosis of defective system but also results in reliable prognosis of defects, which will result in estimating the remaining useful life of taper roller bearings.

2.4 Objective of the Present Work

- a) Experimental investigation of condition monitoring of misaligned rotor system using response surface methodology.
- b) Misalignment fault classification under different loading conditions.
- c) Investigate the role of acoustic data for misalignment fault classification.
- d) Estimation of remaining useful life of taper roller bearing with inherent misalignment in the setup.

References

- [1] D. Singh and J. Srinivas, *Dynamic Modeling and Analysis of Propeller Shaft Supported on Rolling Element Bearings*. 2021.
- [2] Ludeca, "A Practical Guide to Shaft Alignment," *Prüftechnik*, p. 63, 2002.
- [3] J. W. Hines, S. Jesse, A. Edmondson, and D. Nower, "Motor Shaft Misalignment Bearing Load Analysis," *Proc. Maint. Reliab. Conf. (MARCON 99)*, no. February, 1999.
- [4] G. N. D. S. Sudhakar and A. S. Sekhar, "Coupling Misalignment in Rotating Machines: Modelling, Effects and Monitoring," *Noise Vib. Worldw.*, vol. 40, no. 1, pp. 17–39, Jan.

- 2009.
- [5] D. P. Behera, R. Behera, and V. N. A. Naikan, "Virtual fault simulation for diagnosis of shaft misalignment of rotating machine," in *2014 International Conference on Advances in Computing, Communications and Informatics (ICACCI)*, 2014, pp. 2476–2480.
- [6] S. Kumar, "Vibration Signature Analysis of 4 Jaw Flexible Coupling Considering Misalignment in Two Planes .," *Int. Res. J. Eng. Technol.*, vol. 2, no. 1, pp. 73–84, 2015.
- [7] M. Chandra Sekhar Reddy and A. S. Sekhar, "Detection and monitoring of coupling misalignment in rotors using torque measurements," *Measurement*, vol. 61, pp. 111–122, Feb. 2015.
- [8] Erwin Krämer, *Dynamics of Rotors and Foundations*, 1993rd ed. Springer, 1993.
- [9] F. F. Ehrich, *Handbook of Rotordynamics*. Krieger Publishing Company; 3rd UK ed. edition (31 August 2004), 2004.
- [10] H. D. Nelson and J. M. McVaugh, "The Dynamics of Rotor-Bearing Systems Using Finite Elements," *J. Eng. Ind.*, vol. 98, no. 2, pp. 593–600, May 1976.
- [11] A. S. Sekhar and B. S. Prabhu, "Effects of coupling misalignment on vibrations of rotating machinery," *J. Sound Vib.*, vol. 185, no. 4, pp. 655–671, Aug. 1995.
- [12] Y.-S. Lee and C.-W. Lee, "Modelling and Vibration Analysis of Misaligned Rotor-Ball Bearing Systems," *J. Sound Vib.*, vol. 224, no. 1, pp. 17–32, Jul. 1999.
- [13] R. Isermann, "Fault diagnosis of machines via parameter estimation and knowledge processing—Tutorial paper," *Automatica*, vol. 29, no. 4, pp. 815–835, Jul. 1993.
- [14] A. K. Jalan and A. R. Mohanty, "Model based fault diagnosis of a rotor–bearing system for misalignment and unbalance under steady-state condition," *J. Sound Vib.*, vol. 327, no. 3–5, pp. 604–622, Nov. 2009.
- [15] P. Pennacchi and A. Vania, "Diagnosis and Model Based Identification of a Coupling Misalignment," *Shock Vib.*, vol. 12, no. 4, pp. 293–308, 2005.
- [16] O. A. Omitaomu, M. K. Jeong, A. B. Badiru, and J. W. Hines, "On-Line Prediction of Motor Shaft Misalignment Using Fast Fourier Transform Generated Spectra Data and Support Vector Regression," *J. Manuf. Sci. Eng.*, vol. 128, no. 4, pp. 1019–1024, Nov. 2006.
- [17] D. L. Dewell and L. D. Mitchell, "Detection of a misaligned disk coupling using spectrum analysis," *J. Vib. Acoust. Trans. ASME*, vol. 106, no. 1, pp. 9–16, 1984.
- [18] C. Kumar, G. Krishnan, and S. Sarangi, "Experimental investigation on misalignment fault detection in induction motors using current and vibration signature analysis," in *2015 International Conference on Futuristic Trends on Computational Analysis and*

-
- Knowledge Management (ABLAZE)*, 2015, pp. 61–66.
- [19] A. Umbrajkaar and A. Krishnamoorthy, “Shaft misalignment prediction on basis of discrete wavelet transform,” *Int. J. Mech. Eng. Technol.*, vol. 9, no. 7, pp. 336–344, 2018.
- [20] M. Monte, F. Verbelen, and B. Vervisch, “Detection of coupling misalignment by extended orbits,” *Conf. Proc. Soc. Exp. Mech. Ser.*, vol. 8, pp. 243–250, 2015.
- [21] L. Arebi, F. Gu, N. Hu, and A. Ball, “Misalignment Detection using a Wireless Sensor Mounted on a Rotating Shaft - University of Huddersfield Repository,” *Proc. 24th Int. Congr. Cond. Monit. Diagnostics Eng. Manag. COMADEM*, no. January, pp. 1289–1299, 2011.
- [22] C. da Costa, R. S. Da Gama, C. E. Nascimento, I. M. Randão, E. C. De Medeiros, and M. H. Mathias, “Orbit Analysis For Imbalance Fault Detection In Rotating Machinery,” *IOSR J. Electr. Electron. Eng.*, vol. 13, no. 1, pp. 43–53, 2018.
- [23] X. Fan and M. J. Zuo, “Gearbox fault detection using Hilbert and wavelet packet transform,” *Mech. Syst. Signal Process.*, vol. 20, no. 4, pp. 966–982, May 2006.
- [24] P. Jayaswal, S. N. Verma, and A. K. Wadhvani, “Application of ANN, Fuzzy Logic and Wavelet Transform in machine fault diagnosis using vibration signal analysis,” *J. Qual. Maint. Eng.*, vol. 16, no. 2, pp. 190–213, 2010.
- [25] F. Al-Badour, M. Sunar, and L. Cheded, “Vibration analysis of rotating machinery using time–frequency analysis and wavelet techniques,” *Mech. Syst. Signal Process.*, vol. 25, no. 6, pp. 2083–2101, Aug. 2011.
- [26] A. Umbrajkaar and A. Krishnamoorthy, “Vibration analysis using wavelet transform and fuzzy logic for shaft misalignment,” *J. Vibroengineering*, vol. 20, no. 8, pp. 2855–2865, Dec. 2018.
- [27] N. H. Chandra and A. S. Sekhar, “Detection and Monitoring of Shaft Misalignment in Rotors Using Hilbert Huang Transform,” in *Volume 7A: Structures and Dynamics*, 2014.
- [28] T. Y. Wu and Y. L. Chung, “Misalignment diagnosis of rotating machinery through vibration analysis via the hybrid EEMD and EMD approach,” *Smart Mater. Struct.*, vol. 18, no. 9, p. 095004, Sep. 2009.
- [29] N. Tandon, G. S. Yadava, and K. M. Ramakrishna, “A comparison of some condition monitoring techniques for the detection of defect in induction motor ball bearings,” *Mech. Syst. Signal Process.*, vol. 21, no. 1, pp. 244–256, Jan. 2007.
- [30] J. L. Ferrando Chacon, E. Artigao Andicoberry, V. Kappatos, G. Asfis, T.-H. Gan, and W. Balachandran, “Shaft angular misalignment detection using acoustic emission,”

-
- Appl. Acoust.*, vol. 85, pp. 12–22, Nov. 2014.
- [31] R. Li and D. He, “Rotational Machine Health Monitoring and Fault Detection Using EMD-Based Acoustic Emission Feature Quantification,” *IEEE Trans. Instrum. Meas.*, vol. 61, no. 4, pp. 990–1001, Apr. 2012.
- [32] K. V. Sivarao, G. Diwakar, and M. R. S. Satynarayana, “Determination Of Misalignment Using Motor Current Signature Analysis In Rotating Machine,” vol. 1, no. 8, pp. 1–11, 2012.
- [33] C. Verucchi, J. Bossio, G. Bossio, and G. Acosta, “Misalignment detection in induction motors with flexible coupling by means of estimated torque analysis and MCSA,” *Mech. Syst. Signal Process.*, vol. 80, pp. 570–581, Dec. 2016.
- [34] A. Bouzida, O. Touhami, R. Ibtouen, A. Belouchrani, M. Fadel, and A. Rezzoug, “Fault Diagnosis in Industrial Induction Machines Through Discrete Wavelet Transform,” *IEEE Trans. Ind. Electron.*, vol. 58, no. 9, pp. 4385–4395, Sep. 2011.
- [35] J. M. Bossio, G. R. Bossio, and C. H. De Angelo, “Angular misalignment in induction motors with flexible coupling,” in *2009 35th Annual Conference of IEEE Industrial Electronics*, 2009, pp. 1033–1038.
- [36] A. Verma, S. Sarangi, and M. Kolekar, “Shaft Misalignment Detection using Stator Current Monitoring,” *Int. J.*, no. 1, pp. 305–309, 2013.
- [37] D. L. Dewell and L. D. Mitchell, “Detection of a Misaligned Disk Coupling Using Spectrum Analysis,” *J. Vib. Acoust.*, vol. 106, no. 1, pp. 9–16, Jan. 1984.
- [38] S. Haroun, A. N. Seghir, S. Touati, and S. Hamdani, “Misalignment fault detection and diagnosis using AR model of torque signal,” *Proc. - SDEMPED 2015 IEEE 10th Int. Symp. Diagnostics Electr. Mach. Power Electron. Drives*, pp. 322–326, 2015.
- [39] E.-S. M. El-Alfy, S. M. Thampi, H. Takagi, S. Piramuthu, and T. Hanne, Eds., *Advances in Intelligent Informatics*, vol. 320. Cham: Springer International Publishing, 2015.
- [40] A. M. Umbrajkaar, A. Krishnamoorthy, and R. B. Dhumale, “Vibration Analysis of Shaft Misalignment Using Machine Learning Approach under Variable Load Conditions,” *Shock Vib.*, vol. 2020, pp. 1–12, Jul. 2020.
- [41] Y. E. Lee, B.-K. Kim, J.-H. Bae, and K. C. Kim, “Misalignment Detection of a Rotating Machine Shaft Using a Support Vector Machine Learning Algorithm,” *Int. J. Precis. Eng. Manuf.*, vol. 22, no. 3, pp. 409–416, Mar. 2021.
- [42] M. Seera, M. L. D. Wong, and A. K. Nandi, “Classification of ball bearing faults using a hybrid intelligent model,” *Appl. Soft Comput.*, vol. 57, pp. 427–435, Aug. 2017.
- [43] K. C. Gryllias and I. A. Antoniadis, “A Support Vector Machine approach based on

- physical model training for rolling element bearing fault detection in industrial environments,” *Eng. Appl. Artif. Intell.*, vol. 25, no. 2, pp. 326–344, Mar. 2012.
- [44] M. S. Safizadeh and S. K. Latifi, “Using multi-sensor data fusion for vibration fault diagnosis of rolling element bearings by accelerometer and load cell,” *Inf. Fusion*, vol. 18, pp. 1–8, Jul. 2014.
- [45] M. Azamfar, J. Singh, I. Bravo-Imaz, and J. Lee, “Multisensor data fusion for gearbox fault diagnosis using 2-D convolutional neural network and motor current signature analysis,” *Mech. Syst. Signal Process.*, vol. 144, p. 106861, Oct. 2020.
- [46] T. Praveen Kumar, M. Saimurugan, R. B. Hari Haran, S. Siddharth, and K. I. Ramachandran, “A multi-sensor information fusion for fault diagnosis of a gearbox utilizing discrete wavelet features,” *Meas. Sci. Technol.*, vol. 30, no. 8, 2019.
- [47] A. Glowacz, “Fault diagnosis of single-phase induction motor based on acoustic signals,” *Mech. Syst. Signal Process.*, vol. 117, pp. 65–80, Feb. 2019.
- [48] P. Shan, H. Lv, L. Yu, H. Ge, Y. Li, and L. Gu, “A Multisensor Data Fusion Method for Ball Screw Fault Diagnosis Based on Convolutional Neural Network With Selected Channels,” *IEEE Sens. J.*, vol. 20, no. 14, pp. 7896–7905, Jul. 2020.
- [49] A. M. Al-Ghamd and D. Mba, “A comparative experimental study on the use of acoustic emission and vibration analysis for bearing defect identification and estimation of defect size,” *Mech. Syst. Signal Process.*, vol. 20, no. 7, pp. 1537–1571, Oct. 2006.
- [50] R. S. Gunerker and A. K. Jalan, “Classification of Ball Bearing Faults Using Vibro-Acoustic Sensor Data Fusion,” *Exp. Tech.*, vol. 43, no. 5, pp. 635–643, Oct. 2019.
- [51] A. Kumar, G. Vashishtha, C. P. Gandhi, Y. Zhou, A. Glowacz, and J. Xiang, “Novel Convolutional Neural Network (NCNN) for the Diagnosis of Bearing Defects in Rotary Machinery,” *IEEE Trans. Instrum. Meas.*, vol. 70, pp. 1–10, 2021.
- [52] V. Sugumaran and K. I. Ramachandran, “Effect of number of features on classification of roller bearing faults using SVM and PSVM,” *Expert Syst. Appl.*, vol. 38, no. 4, pp. 4088–4096, Apr. 2011.
- [53] S. Fatima, B. Guduri, A. R. Mohanty, and V. N. A. Naikan, “Transducer invariant multi-class fault classification in a rotor-bearing system using support vector machines,” *Measurement*, vol. 58, pp. 363–374, Dec. 2014.
- [54] M. Singh and A. G. Shaik, “Faulty bearing detection, classification and location in a three-phase induction motor based on Stockwell transform and support vector machine,” *Measurement*, vol. 131, pp. 524–533, Jan. 2019.
- [55] A. Malhi and R. X. Gao, “PCA-Based Feature Selection Scheme for Machine Defect

- Classification,” *IEEE Trans. Instrum. Meas.*, vol. 53, no. 6, pp. 1517–1525, Dec. 2004.
- [56] H. D. M. de Azevedo, A. M. Araújo, and N. Bouchonneau, “A review of wind turbine bearing condition monitoring: State of the art and challenges,” *Renew. Sustain. Energy Rev.*, vol. 56, pp. 368–379, Apr. 2016.
- [57] Y. Lei, N. Li, L. Guo, N. Li, T. Yan, and J. Lin, “Machinery health prognostics: A systematic review from data acquisition to RUL prediction,” *Mech. Syst. Signal Process.*, vol. 104, pp. 799–834, May 2018.
- [58] P. Kundu, A. K. Darpe, and M. S. Kulkarni, “Weibull accelerated failure time regression model for remaining useful life prediction of bearing working under multiple operating conditions,” *Mech. Syst. Signal Process.*, vol. 134, p. 106302, Dec. 2019.
- [59] L. Liu, X. Song, K. Chen, B. Hou, X. Chai, and H. Ning, “An enhanced encoder–decoder framework for bearing remaining useful life prediction,” *Measurement*, vol. 170, p. 108753, Jan. 2021.
- [60] G. Huang, Y. Zhang, and J. Ou, “Transfer remaining useful life estimation of bearing using depth-wise separable convolution recurrent network,” *Measurement*, vol. 176, p. 109090, May 2021.
- [61] L. Xu, P. Pennacchi, and S. Chatterton, “A new method for the estimation of bearing health state and remaining useful life based on the moving average cross-correlation of power spectral density,” *Mech. Syst. Signal Process.*, vol. 139, p. 106617, May 2020.
- [62] P. Paris and F. Erdogan, “A Critical Analysis of Crack Propagation Laws,” *J. Basic Eng.*, vol. 85, no. 4, pp. 528–533, Dec. 1963.
- [63] prem shankar kumar, L. A. Kumaraswamidhas, and S. K. Laha, “Bearing degradation assessment and remaining useful life estimation based on Kullback-Leibler divergence and Gaussian processes regression,” *Measurement*, vol. 174, p. 108948, Apr. 2021.
- [64] N. Li, Y. Lei, J. Lin, and S. X. Ding, “An Improved Exponential Model for Predicting Remaining Useful Life of Rolling Element Bearings,” *IEEE Trans. Ind. Electron.*, vol. 62, no. 12, pp. 7762–7773, Dec. 2015.
- [65] G. Qiu, Y. Gu, and J. Chen, “Selective health indicator for bearings ensemble remaining useful life prediction with genetic algorithm and Weibull proportional hazards model,” *Measurement*, vol. 150, p. 107097, Jan. 2020.
- [66] J. Xing, Z. Zeng, and E. Zio, “A framework for dynamic risk assessment with condition monitoring data and inspection data,” *Reliab. Eng. Syst. Saf.*, vol. 191, p. 106552, Nov. 2019.
- [67] J. Li, X. Zhang, X. Zhou, and L. Lu, “Reliability assessment of wind turbine bearing

- based on the degradation-Hidden-Markov model,” *Renew. Energy*, vol. 132, pp. 1076–1087, Mar. 2019.
- [68] M. Yan, X. Wang, B. Wang, M. Chang, and I. Muhammad, “Bearing remaining useful life prediction using support vector machine and hybrid degradation tracking model,” *ISA Trans.*, vol. 98, pp. 471–482, Mar. 2020.
- [69] Z. Pan, Z. Meng, Z. Chen, W. Gao, and Y. Shi, “A two-stage method based on extreme learning machine for predicting the remaining useful life of rolling-element bearings,” *Mech. Syst. Signal Process.*, vol. 144, p. 106899, Oct. 2020.
- [70] Chaochao Chen, Bin Zhang, G. Vachtsevanos, and M. Orchard, “Machine Condition Prediction Based on Adaptive Neuro-Fuzzy and High-Order Particle Filtering,” *IEEE Trans. Ind. Electron.*, vol. 58, no. 9, pp. 4353–4364, Sep. 2011.
- [71] R. K. Singleton, E. G. Strangas, and S. Aviyente, “Extended Kalman Filtering for Remaining-Useful-Life Estimation of Bearings,” *IEEE Trans. Ind. Electron.*, vol. 62, no. 3, pp. 1781–1790, Mar. 2015.
- [72] J. Antoni, “The infogram: Entropic evidence of the signature of repetitive transients,” *Mech. Syst. Signal Process.*, vol. 74, pp. 73–94, Jun. 2016.
- [73] S. Nezamivand Chegini, M. J. Haghdoost Manjili, B. Ahmadi, I. Amirmostofian, and A. Bagheri, “New bearing slight degradation detection approach based on the periodicity intensity factor and signal processing methods,” *Measurement*, vol. 170, p. 108696, Jan. 2021.
- [74] N. W. Nirwan and H. B. Ramani, “Condition monitoring and fault detection in roller bearing used in rolling mill by acoustic emission and vibration analysis,” *Mater. Today Proc.*, vol. 51, pp. 344–354, 2022.
- [75] N. Z. Gebraeel and M. A. Lawley, “A Neural Network Degradation Model for Computing and Updating Residual Life Distributions,” *IEEE Trans. Autom. Sci. Eng.*, vol. 5, no. 1, pp. 154–163, Jan. 2008.
- [76] S. Wu, N. Gebraeel, M. A. Lawley, and Y. Yih, “A Neural Network Integrated Decision Support System for Condition-Based Optimal Predictive Maintenance Policy,” *IEEE Trans. Syst. Man, Cybern. - Part A Syst. Humans*, vol. 37, no. 2, pp. 226–236, Mar. 2007.
- [77] Z. Tian, “An artificial neural network method for remaining useful life prediction of equipment subject to condition monitoring,” *J. Intell. Manuf.*, vol. 23, no. 2, pp. 227–237, Apr. 2012.
- [78] Z. Tian, “A neural network approach for remaining useful life prediction utilizing both

- failure and suspension data,” in *2010 Proceedings - Annual Reliability and Maintainability Symposium (RAMS)*, 2010, pp. 1–6.
- [79] M. Elforjani, “Estimation of Remaining Useful Life of Slow Speed Bearings Using Acoustic Emission Signals,” *J. Nondestruct. Eval.*, vol. 35, no. 4, p. 62, Dec. 2016.
- [80] C. Lu, L. Tao, and H. Fan, “An intelligent approach to machine component health prognostics by utilizing only truncated histories,” *Mech. Syst. Signal Process.*, vol. 42, no. 1–2, pp. 300–313, Jan. 2014.
- [81] F. Yang, M. S. Habibullah, T. Zhang, Z. Xu, P. Lim, and S. Nadarajan, “Health Index-Based Prognostics for Remaining Useful Life Predictions in Electrical Machines,” *IEEE Trans. Ind. Electron.*, vol. 63, no. 4, pp. 2633–2644, Apr. 2016.
- [82] R. Huang, L. Xi, X. Li, C. Richard Liu, H. Qiu, and J. Lee, “Residual life predictions for ball bearings based on self-organizing map and back propagation neural network methods,” *Mech. Syst. Signal Process.*, vol. 21, no. 1, pp. 193–207, Jan. 2007.
- [83] C. Sbarufatti, M. Corbetta, A. Manes, and M. Giglio, “Sequential Monte-Carlo sampling based on a committee of artificial neural networks for posterior state estimation and residual lifetime prediction,” *Int. J. Fatigue*, vol. 83, pp. 10–23, Feb. 2016.
- [84] Y. Pan, M. J. Er, X. Li, H. Yu, and R. Gouriveau, “Machine health condition prediction via online dynamic fuzzy neural networks,” *Eng. Appl. Artif. Intell.*, vol. 35, pp. 105–113, Oct. 2014.
- [85] L. Wang, L. Zhang, and X. Wang, “Reliability estimation and remaining useful lifetime prediction for bearing based on proportional hazard model,” *J. Cent. South Univ.*, vol. 22, no. 12, pp. 4625–4633, Dec. 2015.
- [86] R. Zemouri, D. Racoceanu, and N. Zerhouni, “Recurrent radial basis function network for time-series prediction,” *Eng. Appl. Artif. Intell.*, vol. 16, no. 5–6, pp. 453–463, Aug. 2003.
- [87] A. Malhi, R. Yan, and R. X. Gao, “Prognosis of Defect Propagation Based on Recurrent Neural Networks,” *IEEE Trans. Instrum. Meas.*, vol. 60, no. 3, pp. 703–711, Mar. 2011.
- [88] F. O. Heimes, “Recurrent neural networks for remaining useful life estimation,” in *2008 International Conference on Prognostics and Health Management*, 2008, pp. 1–6.
- [89] Y. Peng, H. Wang, J. Wang, D. Liu, and X. Peng, “A modified echo state network based remaining useful life estimation approach,” in *2012 IEEE Conference on Prognostics and Health Management*, 2012, pp. 1–7.
- [90] Datong Liu, Wei Xie, Haitao Liao, and Yu Peng, “An Integrated Probabilistic Approach to Lithium-Ion Battery Remaining Useful Life Estimation,” *IEEE Trans. Instrum.*

-
- Meas.*, vol. 64, no. 3, pp. 660–670, Mar. 2015.
- [91] R. Li, P. Sapon, and D. He, “Fault features extraction for bearing prognostics,” *J. Intell. Manuf.*, vol. 23, no. 2, pp. 313–321, Apr. 2012.
- [92] Y. Wu, M. Yuan, S. Dong, L. Lin, and Y. Liu, “Remaining useful life estimation of engineered systems using vanilla LSTM neural networks,” *Neurocomputing*, vol. 275, pp. 167–179, Jan. 2018.
- [93] Q. Wu, K. Ding, and B. Huang, “Approach for fault prognosis using recurrent neural network,” *J. Intell. Manuf.*, vol. 31, no. 7, pp. 1621–1633, Oct. 2020.
- [94] W. Zhang, C. Li, G. Peng, Y. Chen, and Z. Zhang, “A deep convolutional neural network with new training methods for bearing fault diagnosis under noisy environment and different working load,” *Mech. Syst. Signal Process.*, vol. 100, pp. 439–453, Feb. 2018.
- [95] L. Xiao, F. Duan, J. Tang, and D. Abbott, “A Noise-Boosted Remaining Useful Life Prediction Method for Rotating Machines Under Different Conditions,” *IEEE Trans. Instrum. Meas.*, vol. 70, pp. 1–12, 2021.

Chapter 3

EXPERIMENTAL INVESTIGATION USING RSM FOR CONDITION MONITORING OF MISALIGNED ROTOR SYSTEM

3.1 Introduction

Rotary machines are major assets in many industries such as aerospace, automobile, chemical, energy, and production of the modern era. A machine could be genuinely imperilled if a defect occurs in its rotor-bearing system. Early discovery of the defect, therefore, is essential for the avoidance of a complete breakdown of related large systems. Various model and signal-based methods are used for the detection of misalignment faults in the rotor-bearing system. Rivin [1] proposed that the couplings be classified as rigid, compensating for misalignment, and torsionally flexible. Misalignment of shafts is the reason to develop reaction forces and moments in the coupling. Gibbons [2] introduced parallel misalignment in the system and studied the effect of force and moment on the different types of coupling. Jalan and Mohanty [3] considered equivalent loads to be an indication of a rotary machine fault. They successfully detected the amount, type, and position of a mechanical fault in the rotor-bearing system by using the experimental time response method for both defective and healthy systems. Jalan and Mohanty [4] used a residual generation method for misalignment and unbalance identification in the system. Dewell and Mitchell [5] focused on a vibration in structure generated due to misalignment, several investigators [6] have developed vibration identification charts, coupling misalignment generally produces 2X frequency component. The study conducted by Xu and Marangoni [7], [8] showed that vibration responses due to coupling misalignment generally indicated at multiples even integer of speed of rotation. Wavelets provide time-scale signal information, allowing for the extraction of time-varying features. This property makes 'wavelets' an effective method for non-stationary signals analysis. Newland [9], [10] introduced orthogonal wavelets and its implementation to signal analysis. Different wavelet techniques presented by Staszewski [11] for the identification of different faults. Prabhakar et al. [12] Used the finite element method to study vibration response, they studied the effect of misalignment and unbalance on rotor system. They modelled two separate flexible couplings. The continuous wavelet transform technique is used to derive the coupling misalignment characteristics from time domain signals in a rotor system.

In their review paper, Jalan et al. [13] provides a brief overview of various model and signal-based techniques for misalignment fault detection. Different machine learning and artificial

intelligent techniques have been used for the fault classification. The algorithms like Artificial Neural Networks (ANN) [14]–[16], Support Vector Machine (SVM) [17]–[19] and Fuzzy Logic Classifier [20], [21], are commonly used methods to identify failures. Darpe et al. [22] conducted an experiment to understand how misalignment causing for system vibrations. To monitor the whirl's direction, they used a Full Spectrum vibration signal. The laser technique is a non-contact method of fault detection that uses a laser set to locate the fault while the unit is under operational condition. It utilizes a laser distance that measures displacement rather than vibration; Simm et al. [23] used laser-based technique for the detection of misalignment. Chacon et al. [24] used acoustic emission technique for the detection of angular misalignment under different speed and loading conditions. Umbrajkaar et al. [25] used vibration analysis to classify misalignment faults using the machine learning techniques SVM and ANN. They used time-frequency domain features to classify the faults.

3.2 Introduction to Response Surface Methodology

The statistical methods assist to draw clear conclusions from the data obtained from experiments. Effective experimentation needs understanding of the main factors affecting the performance. Design of Experiment (DoE) [26] assists to evaluate the factors that are relevant for describing a variation in the process. Interactions between the factors are the main thing in many processes and it can be difficult or impossible to understand the mechanism properly if critical interactions are not detected. These statistical techniques used effectively in many areas. Response Surface Methodology (RSM) is an experimental design technique for designing and optimizing the parameters [27]. In 1951, Box and Wilson [28] developed RSM. Including its mathematical and statistical techniques, RSM is an essential tool for product and process development, enhancement, and refinement. RSM is widely used in process or system performance where many input variables will affect the output. RSM's approach is to estimate approximate model between the response and independent variables and improving it such that the model produces the desired output values. Here, the inputs or variables that affect the system's behaviour are called factors or variables, and the outputs depict the response that the system produces under the factors' causal action. If all the input parameters represent quantitative variables, then it is possible to interpret the responses as a function of levels and variables. The relationship between response Y , and independent variables $X_{1u}, X_{2u}, X_{3u} \dots X_{ku}$ is given by Eq. (3.1). The nonlinear model is considered.

$$Y = f(X_{1u}, X_{2u}, X_{3u} \dots X_{ku}) + E_u \quad (3.1)$$

Where, $u=1,2,3\dots N$. N represents observations in the factorial experiment and X_{iu} represents the level of i^{th} factor in u^{th} observation. The function f is called as response function. The residual E_u measures the experimental error of the u^{th} observation. The implementation of the RSM is crucial when it is necessary to examine the relationship between the factor and dependent variable within the experimental region and not only at the borders, after the significant factors influencing the response have been identified. For these types of factorial designs, response surfaces are recommended for their effectiveness and prompt responses.

Kankar et al. [29], [30] used RSM for bearing fault diagnosis and detailed explanation of operating parameter and interaction among the faults addressed and compared with the analytical dynamic model. Patil et al. [31] used kurtosis as the output vector and defect size, load, and speed as the input vector. Kankar et al. [32] used RSM to explore the reaction of rotor-bearing systems under dynamic conditions. Along with the defects on bearing, rotor defects were also simulated using cracked and un-cracked rotor.

According to the literature review, numerous researchers have worked towards model-based fault diagnosis methods, and the severity of the defect has been evaluated with the help of dynamic modelling, but the interaction between load, speed, and defect, and their combined effect on system vibration has not been explored. This chapter delves into the relationship of speed, load, with the existence of several types of misalignment defects of varying severity and their effect on the system vibration. Response Surface Methodology (RSM) with Root Mean Square (RMS) (refer Table 1.1 from appendix for formulae) as a response factor is used to understand the influence of such interactions on the system performance. One second of data has been captured for each combination of experiments with 25KHz sampling frequency. The time domain features computed from each captured data file. Out of all features few of the features showing unstable trend, such features are not considered. while RMS was consistently showing an incremental trend as fault severity increased. So, RMS is used as a response parameter. Experiments are planned using design of experiments and analysis is carried out using analysis of variance (ANOVA). Machinery fault simulator is used to conduct the tests; misalignment is introduced in the horizontal plane. Described findings are in agreement with the experiments conducted for this study. DoE and RSM are employed to identify a rotor bearing system's dynamic response. Three level full factorial design used for the analysis.

3.3 Experimental Test Rig

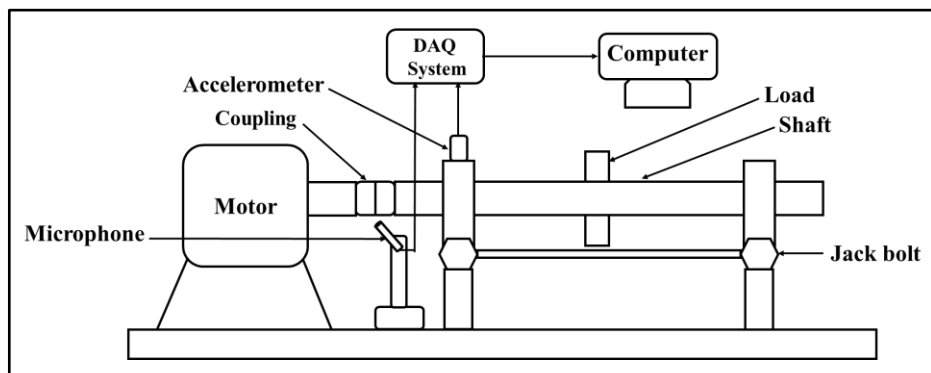
In the present study, experiments are conducted with the machinery fault simulator, as shown in Figure 3.1 (a). It consists of three-phase AC servomotors, one HP motor controlled by one

HP variable-frequency AC drive. The shaft is coupled with a motor using the coupling and is supported on two bearings. A pre-amplified tri-axial accelerometer (Kistler 8076K, sensitivity 102.0 mV/g) is used for the acquisition of vibration signals. The recorded vibration signals are filtered and analyzed using an eight channel multi-analyzer (OROS-OR35 with NVGATE software). Reverse dial indicator is used to check the initial alignment and to remove previously existing misalignment if any.

Both parallel and angular misalignments are considered at three levels of severity. Parallel misalignment is introduced by rotating the jack bolts in clockwise direction by the same amount, while for angular misalignment only one jack bolt is rotated in clockwise direction by predefined amount. The details of the misalignment introduced are presented in Table 3.1, Factors considered in our analysis are speed, load, and defect. The levels of speed and load are given in Table 3.2, For each speed, load, and defect combination, one experiment is performed.



(a)



(b)

Figure 3.1 (a) Spectra Quest machinery fault simulator (1-coupling, 2-microphone, 3-load, 4-shaft, 5- Jack bolt) (b) Schematic of setup

Table 3.1 Defects (Parallel and Angular Misalignments).

Sr.No.	Defect type	Unit	Levels		
			-1	0	1
1	Parallel	mm	0.3	0.5	0.7
2	Angular	degree	0.1	0.2	0.3

Table 3.2 Experimental Load and Speed Conditions.

Sr.No.	Factors	Unit	Levels		
			-1	0	1
1	Speed	rpm	1020	1860	2580
2	Load	N	0	6.7	13.4

3.4 Experimental Investigation Using RSM for Vibration Data

3.4.1 Results and Discussion

Design matrices for parallel and angular misalignments have been presented in Appendix I. For analysing the response parameter RMS, from the collected experimental data, Design Expert statistical software is used. Three-level full factorial design method is used. In which 3 factors, each at three levels (low, intermediate, and high) is considered. A total of 3^3 (27) experiments are performed as the nonlinear model is considered for the study. These levels are coded in digital format of -1, 0, +1 (Refer to Table 3.2).

3.4.1.1 ANOVA Results in Horizontal, Vertical, and Axial Directions for Parallel Misalignment

Quadratic regression model is suggested by the Design Expert, which fits the data better than the linear model. Natural log and inverse square root transforms are used for data in horizontal and vertical directions while no transform function is used in case of axial direction data. To decrease variance variability, data transformations are commonly performed, otherwise the accuracy of the fit will be poor, and predictions might not give better results. Box et al. [28] recommended data transformation prior to process optimization, if needed. Table 3.3 shows the results of ANOVA table for quadratic model of the RMS in horizontal, vertical, and axial directions for parallel misalignment. In the ANOVA analysis the p-value helps to determine which variables and correlations are statistically important. It is observed that the individual effect of speed, load and defect are statistically significant in case of the horizontal direction; only speed in case of vertical direction while in the axial direction, both speed and load are statistically significant. p-values below 0.05 indicates model terms are significant. Model terms

for directions with p -value <0.001 are significant for the analysis, i.e., A, B, C, AB, A^2 , B^2 in horizontal, A, A^2 in vertical and A, B, B^2 are significant model terms in axial direction.

Table 3.3 ANOVA Table for Quadratic Model.

Direction	Horizontal	Vertical	Axial	
Source	p-value	p-value	p-value	
Model	< 0.0001	< 0.0001	< 0.0001	significant
Speed (A)	< 0.0001	< 0.0001	< 0.0001	
Load (B)	< 0.0001	0.5043	< 0.0001	
Defect (C)	0.0001	0.5571	0.2647	
AB	< 0.0001	0.5801	0.2395	
AC	0.3602	0.7027	0.5368	
BC	0.2042	0.9449	0.8427	
A^2	< 0.0001	< 0.0001	0.3288	
B^2	< 0.0001	0.3064	< 0.0001	
C^2	0.6994	0.5762	0.3709	

Table 3.4 Fit Statistics.

Direction	R^2	Adjusted R^2	Predicted R^2	Adequate Precision
Horizontal	0.9992	0.9989	0.9981	129.871
Vertical	0.9925	0.9886	0.9810	37.8585
Axial	0.9735	0.9595	0.9346	26.0293

Fit statistics is indicated in Table 3.4. R^2 is a statistical measure of how close the data fitted to the regression line. It calculates the percentage of variation in the dependent variable that can be explained by all the model's independent variables. Each independent variable in the model is assumed to contribute to the explanation of variance in the dependent variable. R^2 is determined mathematically by dividing the sum of squares of residuals by the total sum of squares, then subtracting it from 1. It ranges from 0 percent to 100 percent. A model with an R^2 value of 100 percent describes all variation in the target variable. A score of 0 percent indicates that the model has no predictive power. Higher R^2 value means the better fit. It is also known as the coefficient of determination. R^2 value is in good agreement with the adjusted R^2 , indicating that variables (predictors) clearly explain the amount of variation observed in the RMS value. Adjusted R^2 calculates the percentage of variation explained by only those independent variables that contribute significantly to the explanation of the dependent

variable. The Predicted R^2 is also in good agreement with the Adjusted R^2 for all three directional data. The predicted R^2 is a measure of how effectively a model predicts new observations' responses. This statistic assists to determine when a model fits the original data but is not capable of making accurate predictions for new data. Adequate Precision is the indication of the signal to noise ratio (desirable ratio > 4). It is observed that the signal is adequate for the analysis from Table 3.4.

The coefficient estimate (refer Table 2 of appendix for horizontal, vertical, and axial directions in case of parallel misalignment) indicates the expected change in response per unit factor value while keeping the remaining factors constant. Standard error is very minimal for all three directional data (refer to Table 2 of appendix).

Equation (3.2) indicates the second-degree polynomial equation for RMS in horizontal direction in terms of coded factors from Design Expert software. Equation (3.3) represents polynomial equation for RMS in vertical direction. and the same for RMS in axial direction is given by Eq. (3.4)

$$\ln(\text{RMS}) = +2.49 + 0.6809 A - 0.0863 B + 0.0232 C - 0.0334 AB + 0.0054 AC - 0.0076 BC - 0.2931 A^2 - 0.0757 B^2 + 0.0032C^2. \quad (3.2)$$

$$\frac{1}{\text{sqrt}(\text{RMS})} = +0.5057 - 0.2227A - 0.0033B - 0.0029C - 0.0033AB - 0.0023AC + 0.0004BC + 0.0730A^2 - 0.0087B^2 + 0.0047C^2. \quad (3.3)$$

$$\text{RMS} = +10.15 + 3.78 A + 0.8617 B - 0.1953 C - 0.2528 AB - 0.1307 AC + 0.0418 BC + 0.2948A^2 + 2.85 B^2 - 0.2696C^2. \quad (3.4)$$

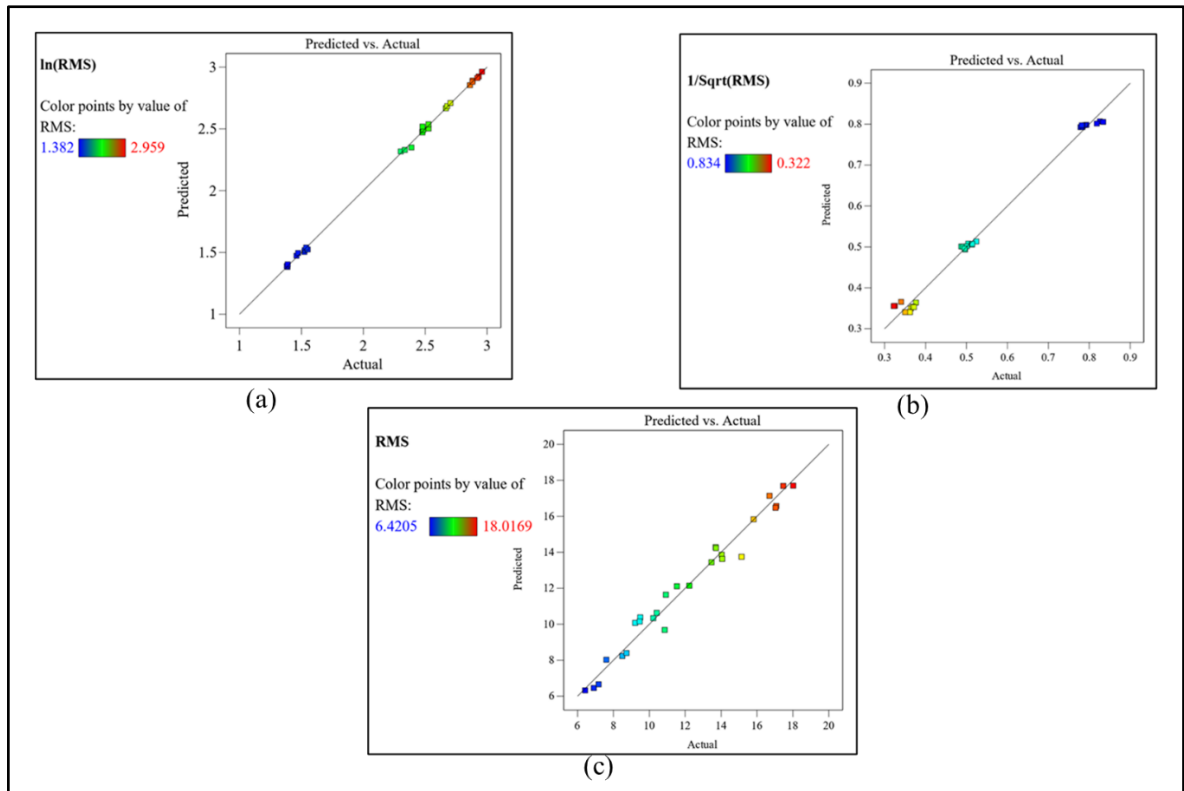
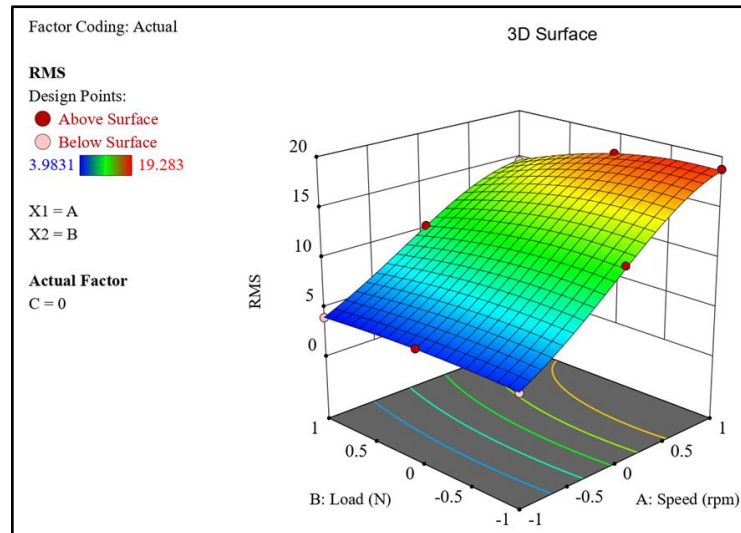


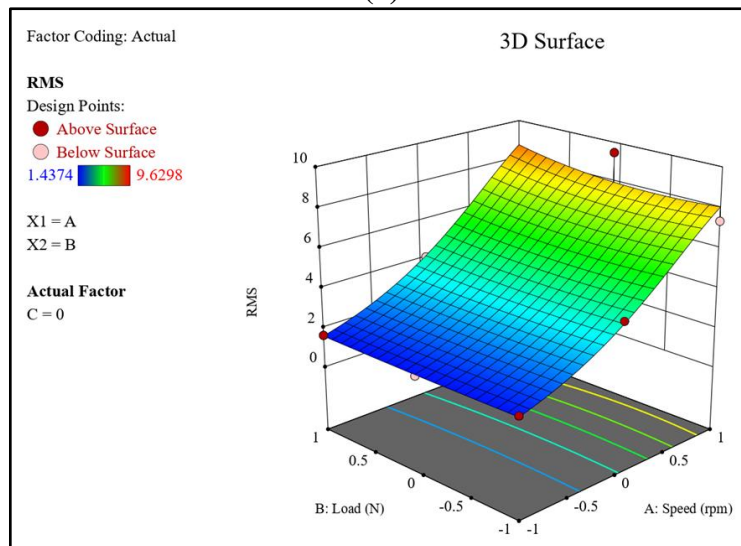
Figure 3.2 Performance prediction of model in (a) horizontal, (b) vertical, and (c) axial directions

Coefficients in the above equations indicate the relative influence of the variables. Figure 3.2 shows predicted Vs actual RMS value comparison for horizontal, vertical, and axial direction. It depicts that the predicted and actual values are close and indicates fitness of the model. It is found that a quadratic model predicts well, and the generated surface response captures the parameter interaction accurately (refer figure 3.3).

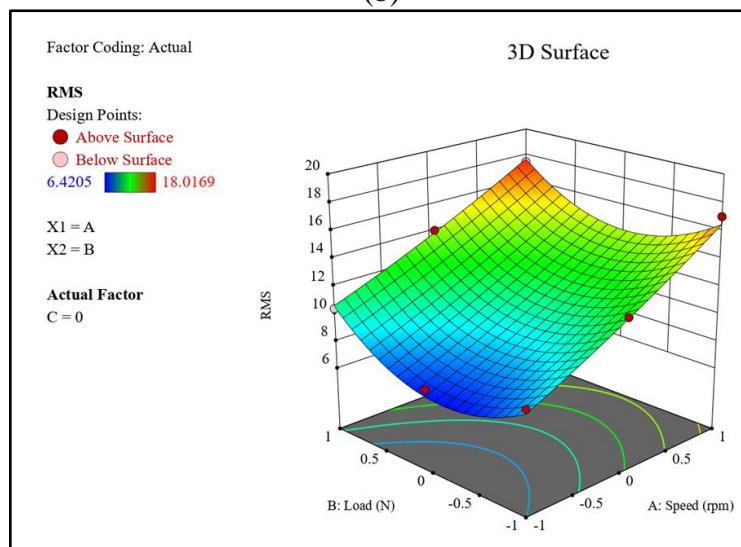
The interaction between the speed and load is shown in figure 3.3 using response surface plot. It shows an increase in the shaft speed results in an increase in the RMS value which results in increase in system vibrations. The curved and deformation in the response surface indicate that there exists a significant interaction between the speed and the load influencing the response. In case of horizontal and vertical directions, it is observed that there is not much change in RMS value with increase in load. In case of axial direction, the initial addition of load decreases the vibration while RMS value keeps on increasing as the load increases. Initial load helps to minimize the misalignment effect up to certain value; further increase in it causes the system to vibrate.



(a)

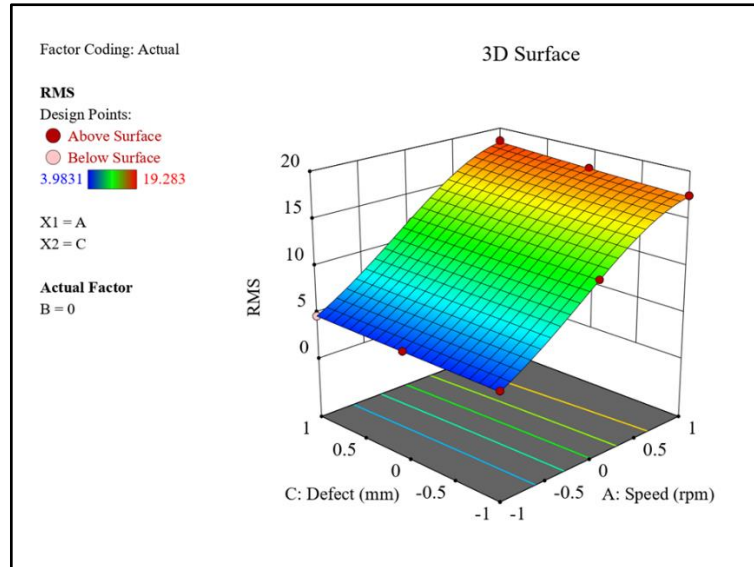


(b)

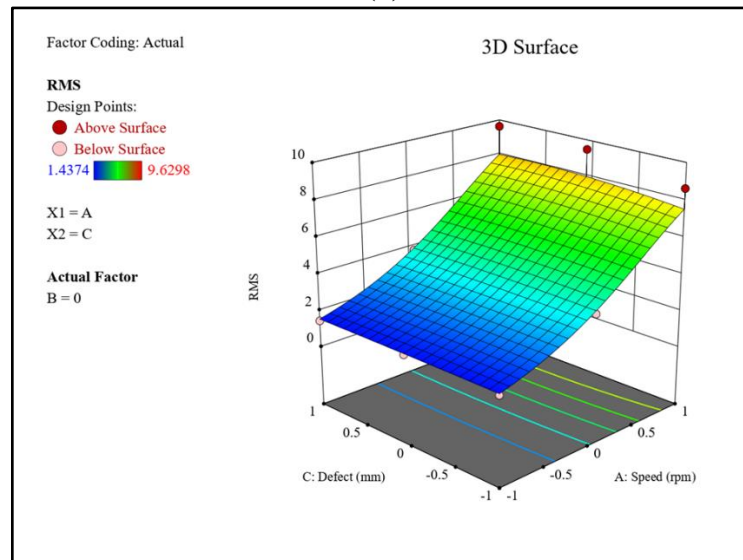


(c)

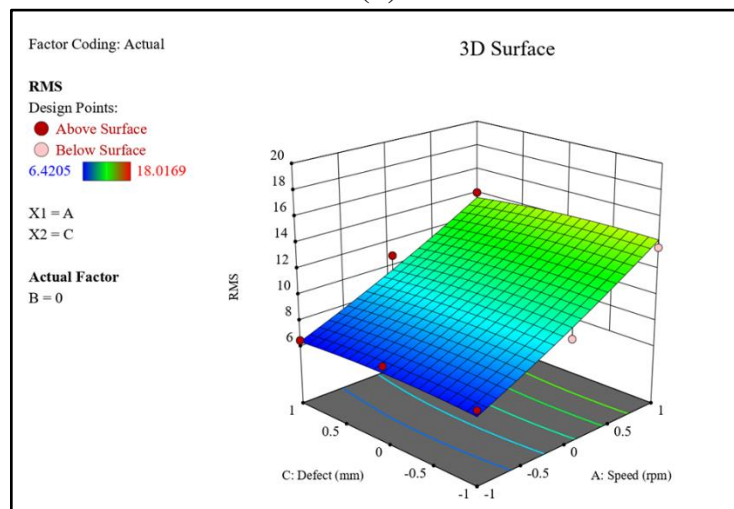
Figure 3.3. Response surface plot for interaction between speed and load for (a) horizontal, (b) vertical and (c) axial direction



(a)



(b)

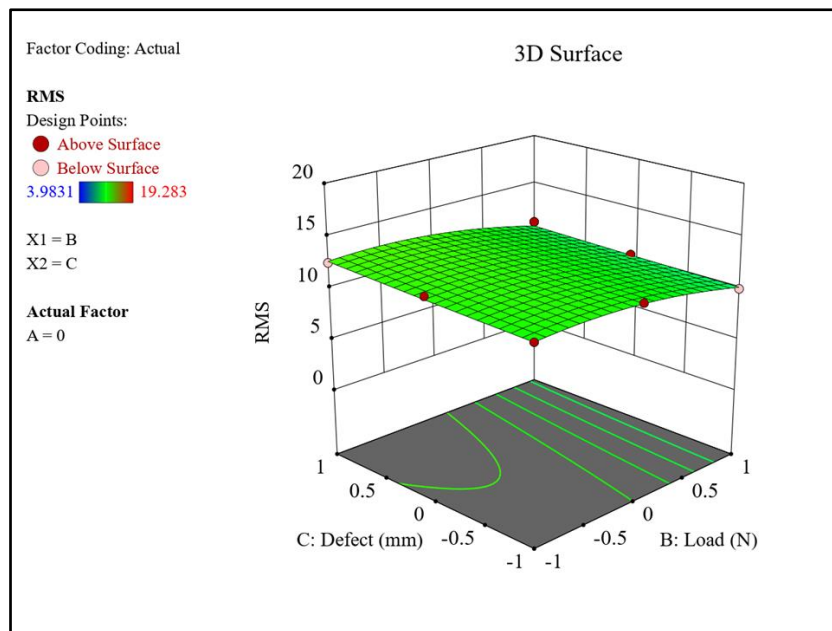


(c)

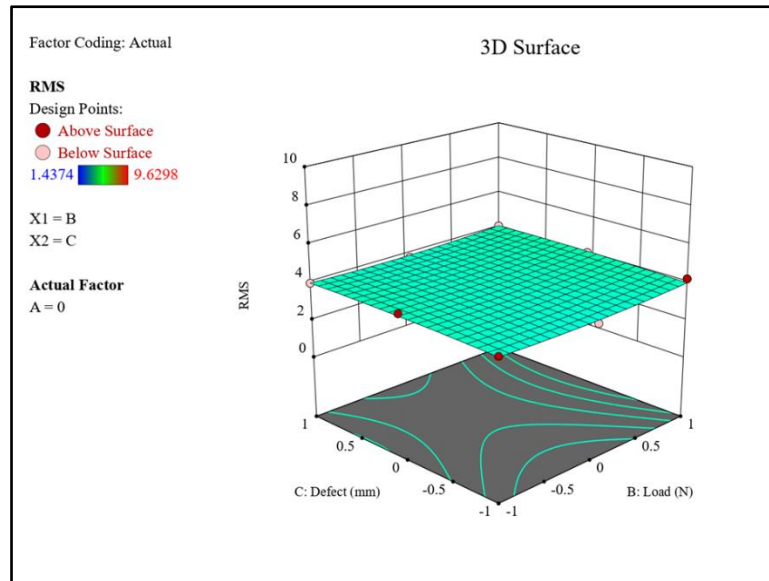
Figure 3.4 Response surface plot for interaction between speed and defect for (a) horizontal, (b) vertical and (c) axial direction

Figure 3.4 shows the interaction between the speed and defect. The p-value > 0.05 for AC (speed-defect) in Tables 3.3 indicates that the interaction effect between speed and defect size is not significant for all three directional data. It is observed that, the increase in the speed results in an increase in the RMS value but RMS value is not affected much with increase in defect severity (refer figure 3.4). The response surface plot depicts that there is no significant interaction between the speed and defect in horizontal and vertical directional data but there is slight increase in RMS value in axial directional vibration data. From response surface plot, it is confirmed that RMS value increasing with the shaft frequency.

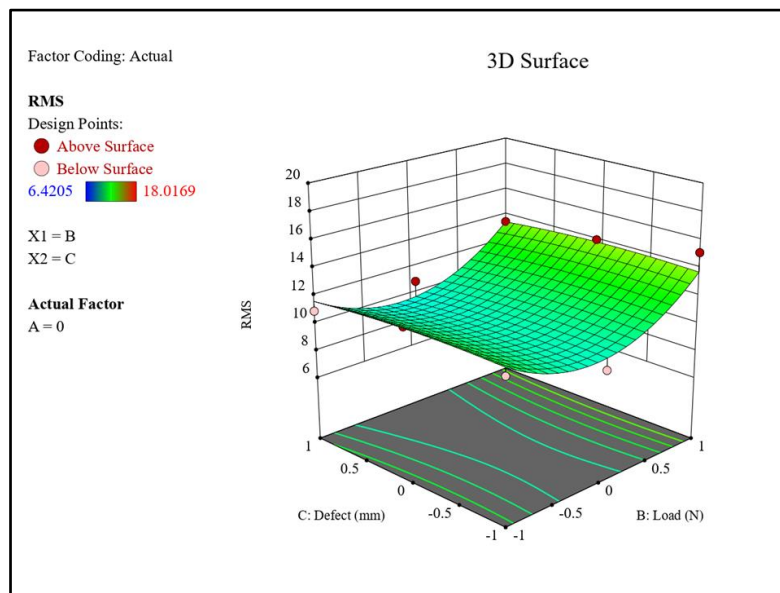
The P value for load and defect interaction is 0.2042 in horizontal, 0.9449 in vertical and 0.8427 in axial direction, indicates that there is no significant interaction between them. Figure 3.5 (a) shows the response surface plot in horizontal direction, it is observed that increase in the load results in a decrease in the vibration and increase in defect severity causes RMS value to increase slightly. In case of vertical direction (refer figure 3.5 (b)) there is slight increase in RMS with increase in load and defect severity, while in case of axial direction (refer figure 3.5 (c)), as the load increases, RMS value is varying. Initially when the shaft is loaded with 6.7N, the RMS value found to be decreasing and when the load is increased to 13.4N, the RMS value started increasing, while slight increase in the RMS value is observed with fault severity.



(a)



(b)



(c)

Figure 3.5. Response surface plot for interaction between load and defect for (a) horizontal, (b) vertical and (c) axial direction

3.4.1.2 ANOVA Result in Horizontal, Vertical, and Axial Direction for Angular Misalignment

Three levels of angular misalignment are considered for this study, the amounts of misalignment introduced are 0.1, 0.2 and 0.3 degrees. The results of angular misalignment in horizontal, vertical, and axial directions are discussed in this section. From Tables 3.5, it is noticed that in case of horizontal A, B, C, AB, A^2 , B^2 , in case of vertical A, A^2 , B^2 and A, B, A^2 , B^2 , C^2 are significant model terms in axial direction. From Table 3.6, it is observed that

there is reasonable agreement between Predicted R² and Adjusted R² and an adequate signal to noise ratio.

Table 3.5 ANOVA for Quadratic Model.

Direction	Horizontal	Vertical	Axial	
Source	p-value	p-value	p-value	
Model	< 0.0001	< 0.0001	< 0.0001	significant
Speed (A)	< 0.0001	< 0.0001	< 0.0001	
Load(B)	< 0.0001	0.1290	0.0001	
Defect(C)	0.0410	0.7995	0.9204	
AB	< 0.0001	0.7407	0.6511	
AC	0.6512	0.6985	0.6700	
BC	0.7426	0.6423	0.7194	
A ²	< 0.0001	< 0.0001	0.0285	
B ²	< 0.0001	0.0111	< 0.0001	
C ²	0.0864	0.8248	0.0461	

Table 3.6 Fit Statistics.

Direction	R ²	Adjusted R ²	Predicted R ²	Adeq Precision
Horizontal	0.9995	0.9993	0.9989	163.9546
Vertical	0.9946	0.9918	0.9863	45.8503
Axial	0.9731	0.9589	0.9393	26.8207

Equations (3.5), (3.6), and (3.7) represent the Second-degree polynomial equation in coded factors for horizontal, vertical, and axial directions, respectively.

$$\ln(\text{RMS}) = +2.48 + 0.6681A - 0.0888B - 0.0080C - 0.0382AB - 0.0020AC + 0.0015BC - 0.3004A^2 - 0.0710 B^2 + 0.0114C^2. \quad (3.5)$$

$$\frac{1}{\text{Sqrt}(\text{RMS})} = +0.5141 - 0.2137A - 0.0062B - 0.0010C - 0.0016AB + 0.0019AC + 0.0023BC + 0.0721A^2 - 0.0192B^2 + 0.0015C^2 \quad (3.6)$$

$$\text{RMS} = +10.73 + 3.74 A + 0.8329 B - 0.0171 C - 0.0952 AB - 0.0897 AC - 0.0756 BC + 0.7001A^2 + 2.79 B^2 - 0.6293C^2 \quad (3.7)$$

Figure 3.6 (a), (b), (c) shows that there is close agreement between predicted Vs actual RMS values.

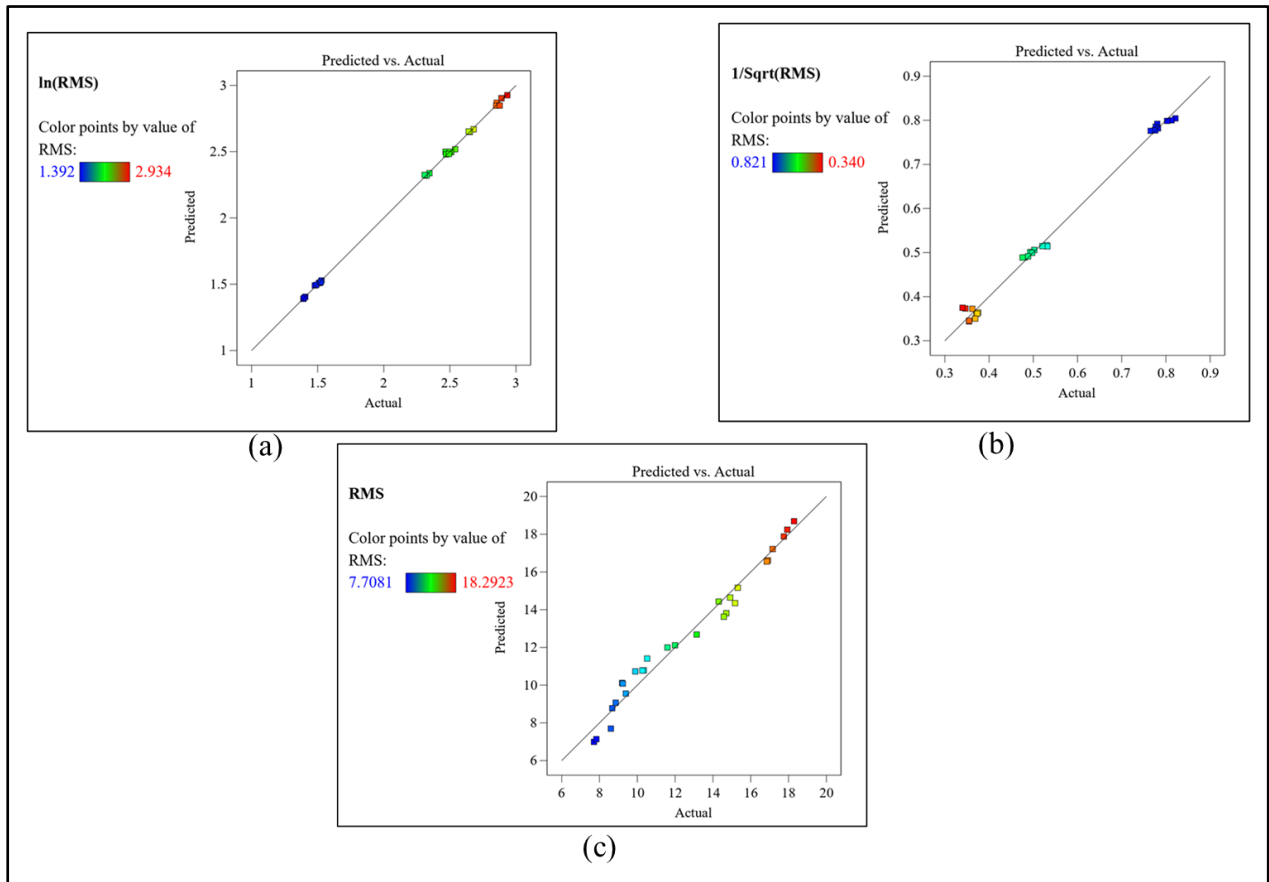


Figure 3.6. Performance prediction of model for angular misalignment in (a) horizontal, (b) vertical, and (c) axial directions

The interaction between speed and load (refer figure 3.7) for angular misalignment is same as parallel misalignment. With the increase in the speed, RMS value is continually increasing. There is no remarkable change observed in RMS value with increase in load in horizontal and vertical directions, while in axial direction the initial addition of load caused to reduce the vibration till some extent but further addition of load causes for system vibration (refer figure 3.7 (c)).

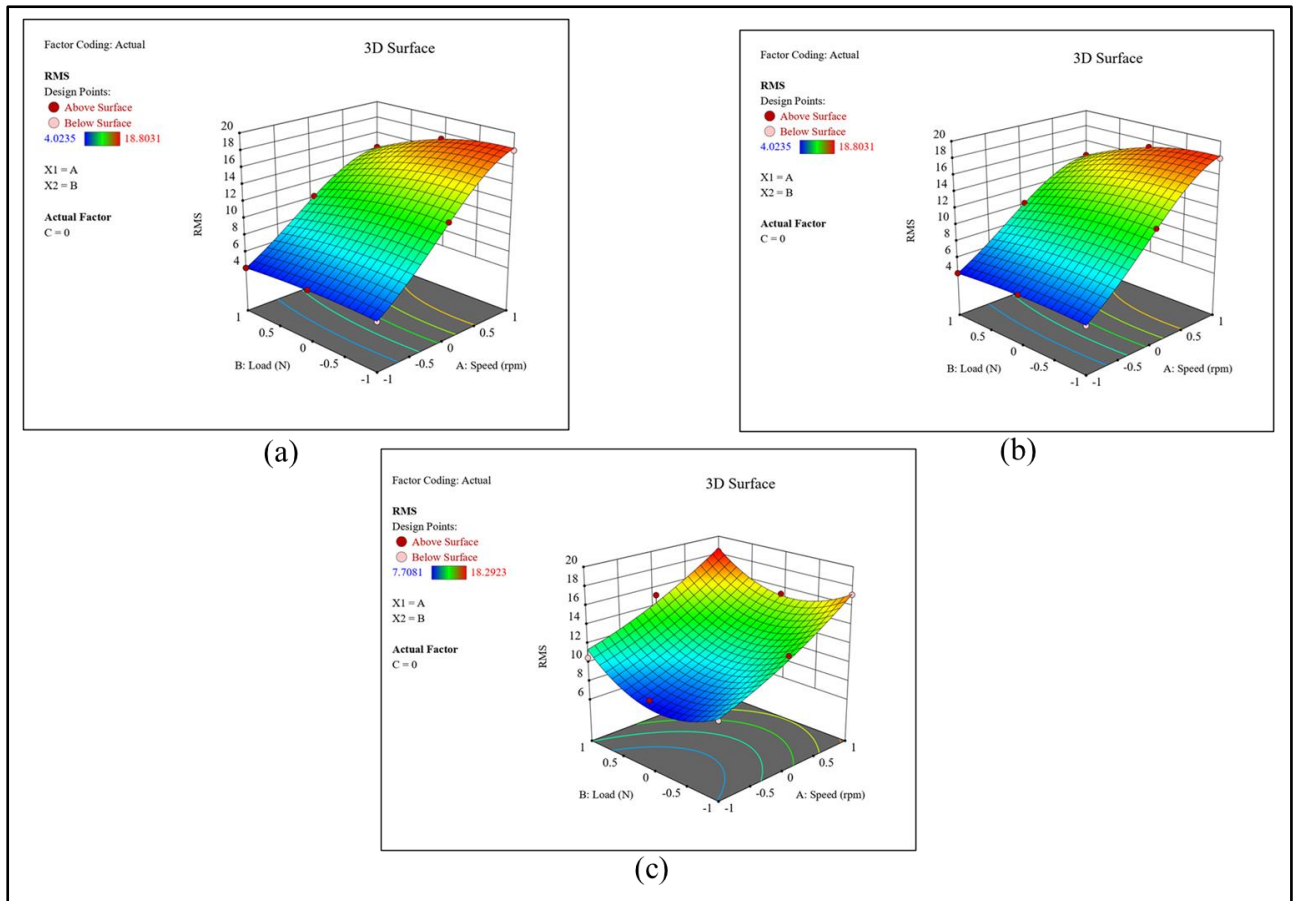


Figure 3.7. Response surface plot for interaction between speed and load for (a) horizontal, (b) vertical and (c) axial direction

From figure 3.8, it is observed that the response for angular misalignment is same as parallel misalignment. In horizontal and vertical directions, with increase in defect severity, RMS values are not affecting much. This may be because of load on the shaft reducing the effect of misalignment, while in case of axial direction there is variation in the RMS value in accordance with defect severity.

From the surface plot as shown in figure 3.9, it is observed that there is slight drop in RMS value with increase in load and the fault severity in horizontal directional vibration data. There is slight increase in RMS value with increase in load and defect severity in vertical direction vibrational data while in case of axial direction as the load increases, RMS value is varying. Initially when the shaft is loaded with 6.7N, the RMS value found to be decreasing and when the load is increased to 13.4N, the RMS value started increasing. The load caused to eliminate the effect of misalignment. Defect severity did not affect the RMS value significantly.

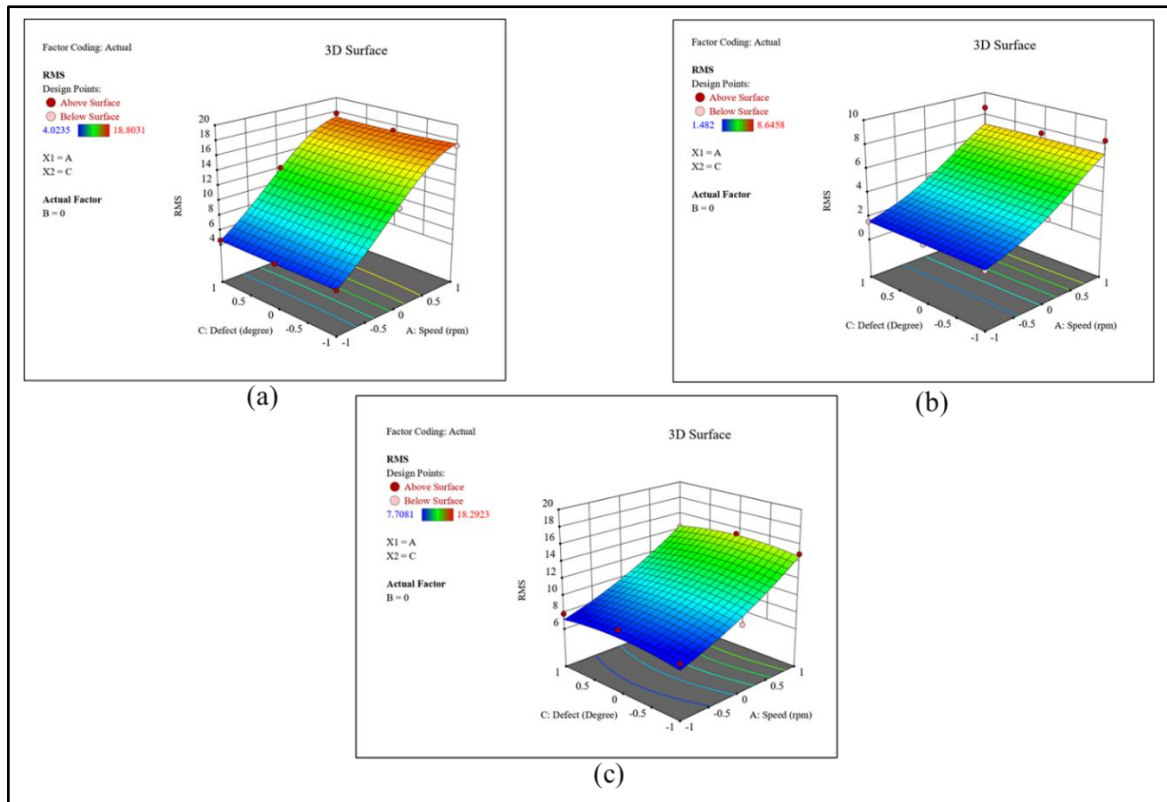


Figure 3.8. Response surface plot for interaction between speed and defect for (a) horizontal, (b) vertical and (c) axial direction

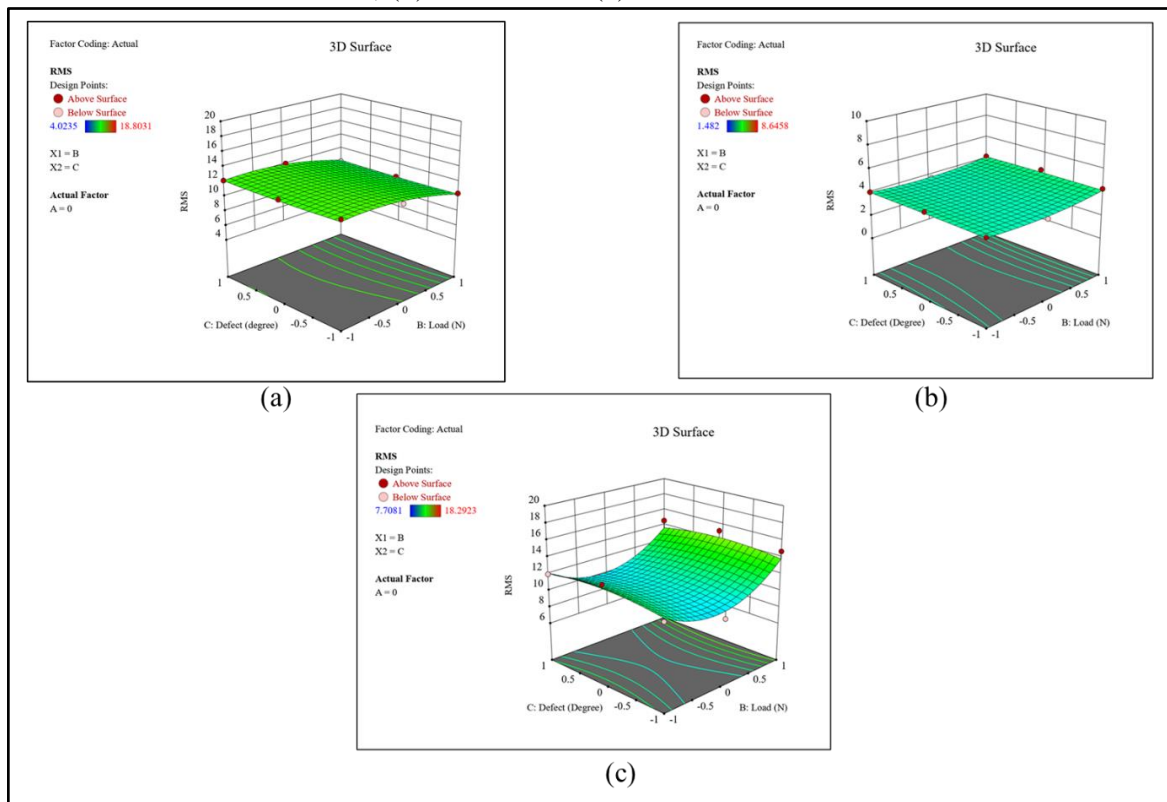


Figure 3.9 Response surface plot for interaction between load and defect for (a) horizontal, (b) vertical and (c) axial direction

3.5 Experimental Instigation Using Response Surface Methodology for Acoustic Sensor Data

3.5.1 Results and Discussion

3.5.1.1 ANOVA Results for Parallel Misalignment

Modern machinery is complicated and installing a sensor might be tricky at times. As a result, non-contact type sensors are critical in such situations. The same experimental setup (Figure 3.1) is used for acoustic study. RMS is taken as a response parameter. For acoustic signal acquisition, a microphone (type 40DD, sensitivity 0.65 mV / Pa) is placed using magnetic stand. The response parameter is calculated from the recorded time domain data using MATLAB same as computed in case of vibrational data. The Design Expert recommends the 2FI (Sequential sum of squares for the two-factor interaction) regression model, which fits the data superior to the linear model. For data transformation, natural log transforms are utilized. Data transformations are widely used to reduce variance variability; otherwise, the fit's accuracy would be low, and predictions may not yield better outcomes. Table 3.7 shows the results of ANOVA. It is observed that the individual effect of speed and load are statistically significant. Model terms with p-values < 0.05 are considered significant, the significant model terms are A, B, and AB. Table 3.8 shows the fit statistics. R² indicates how well the data fits the regression line. The Predicted R² is in good agreement with the Adjusted R². From Table 3.8, it is found that the signal appears to be sufficient for the analysis.

Table 3.7 ANOVA Table for Parallel Misalignment.

Source	Sum of Squares	df	Mean Square	p-value	
Model	12.60	6	2.10	< 0.0001	significant
Speed (A)	11.79	1	11.79	< 0.0001	
Load (B)	0.4582	1	0.4582	0.0017	
Defect (C)	0.0001	1	0.0001	0.9635	
AB	0.3112	1	0.3112	0.0075	
AC	0.0003	1	0.0003	0.9266	
BC	0.0451	1	0.0451	0.2708	
Residual	0.7034	20	0.0352		
Cor Total	13.31	26			

Table 3.8 Fit Statistics for Parallel Misalignment.

R ²	Adjusted R ²	Predicted R ²	Adequate Precision
0.9471	0.9313	0.9131	21.6835

The second-degree polynomial equation for RMS in the form of coded factors is shown in Eq. (3.8).

$$\ln(\text{RMS}) = +0.3421 + 0.8093 A + 0.1595 B - 0.0020 C + 0.1610 AB + 0.0051 AC + 0.0613 BC$$

(3.8)

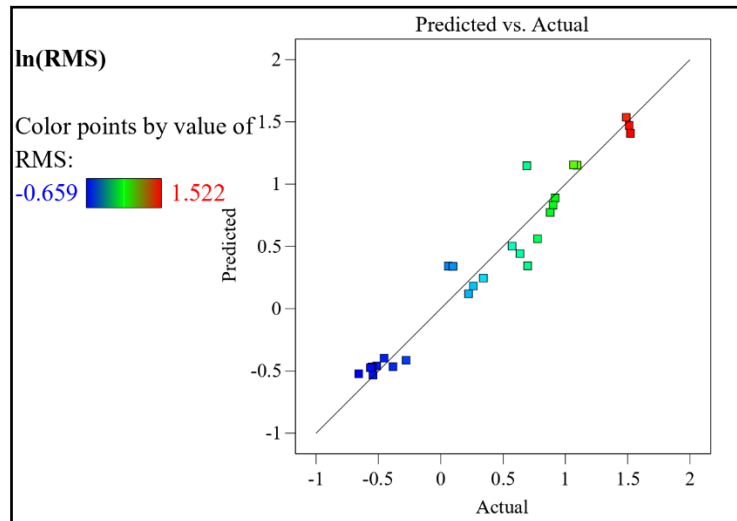


Figure 3.10. Performance prediction of model

Figure 3.10 displays a comparison between predicted and actual RMS values, it shows that the predicted and actual values are in close agreement, indicates that the model is fit. A model is found to forecast well, and the generated surface response accurately depicts the parameter interaction.

In case of parallel misalignment, the association between speed and load is depicted in figure 3.11(a) using response surface plot. It indicates that when the shaft speed increases, the RMS value rises, leading to an increase in system vibrations. The curvature in the response surface represents a substantial interaction between the speed and load, which influences the output. Increased load also contributes to system vibration, and the RMS value continues to rise. The plots clearly show that when system is misaligned, increasing the speed, load, or speed combined with load causes the RMS value to rise, making the system unstable.

Figure 3.11 (b) indicates the interaction between speed and defect. The P-value 0.9266 indicates that they are not significant, increase in defect severity does not contribute towards system vibration but speed has effect on system vibrations, RMS value keeps on increases as speed increases.

Figure 3.11 (c) depicts the interaction between load and defect. Surface response plot indicates the connection between change in load and defect and its effect on system vibrations. It is found

that change in load causing for increase in RMS but change in defect severity did not affect the response parameter.

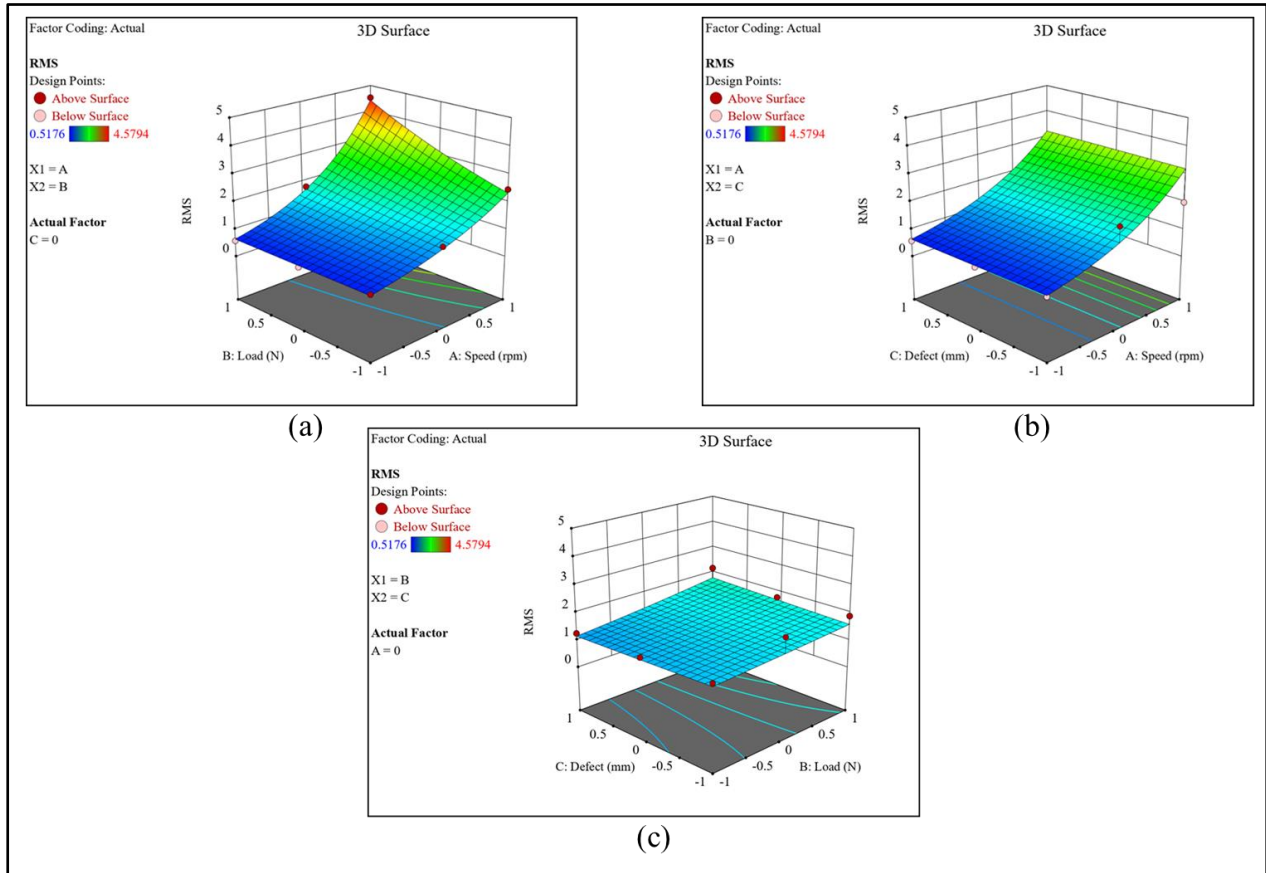


Figure 3.11. Response surface plot for parallel misalignment for interaction between (a) speed and load, (b) speed and defect and (c) load and defect

3.5.1.2 ANOVA Result for Angular Misalignment

Table 3.9 ANOVA Table for Angular Misalignment.

Source	Sum of Squares	Mean Square	df	p-value	
Model	10.82	1.80	6	< 0.0001	significant
Speed (A)	10.54	10.54	1	< 0.0001	
Load (B)	0.0886	0.0886	1	0.0306	
Defect (C)	0.0001	0.0001	1	0.9431	
AB	0.1972	0.1972	1	0.0024	
AC	0.0009	0.0009	1	0.8172	
BC	0.0008	0.0008	1	0.8283	
Residual	0.3273	0.0164	20		
Cor Total	11.15		26		

The model value < 0.001 shows the model is significant, from Table 3.9, it is found that A, B, and AB are significant model terms. Table 3.10 shows that the Predicted R^2 and Adjusted R^2 have a reasonable agreement and an acceptable signal to noise ratio.

Table 3.10 Fit Statistics for Angular Misalignment.

R^2	Adjusted R^2	Predicted R^2	Adequate Precision
0.9707	0.9618	0.9359	27.6937

The Second-degree polynomial equation in coded factors is represented by Eq. (3.9).

$$\ln(\text{RMS}) = +0.3060 + 0.7651A + 0.0702B + 0.0022C + 0.1282AB + 0.0086AC - 0.0081BC \quad (3.9)$$

figure 3.12 illustrates that the predicted and actual RMS values are very similar.

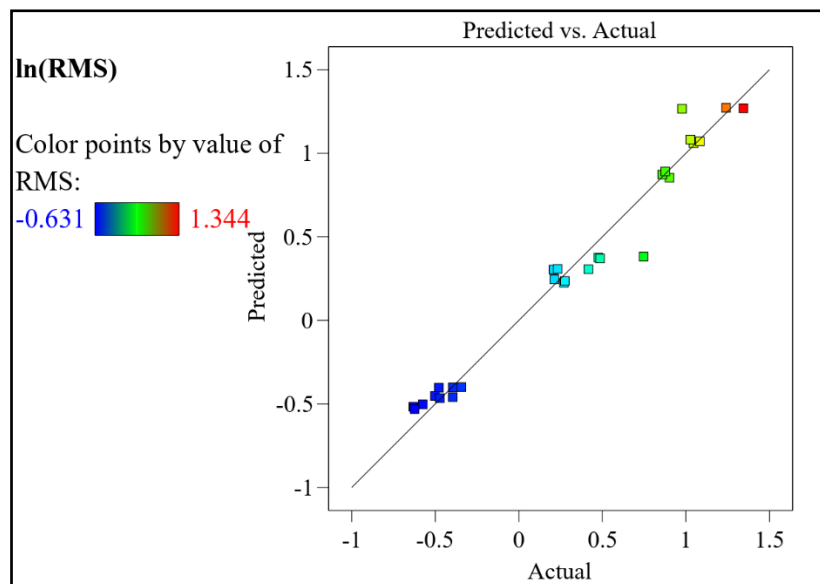


Figure 3.12. Performance prediction of model for angular misalignment

For angular misalignment, the interaction between speed and load (refer figure 3.13 (a)) is same as in case of parallel misalignment. The RMS value rises in lockstep with the speed. When the load is increased, there is slight increment in the RMS value. The contour lines are slightly deformed for change in load intensity. From figure 3.13 (b), it is observed that with increase in defect severity, RMS value is not affected. This may be because of load on the shaft reducing the effect of misalignment, while there is uniform rise in RMS value with the increase in speed. The counter and surface plot in figure 3.13 (c) shows that as the severity of the fault increases, the RMS value decreases slightly. With increasing load, the RMS value increases considerably. The severity of the defect has no effect on the RMS value.

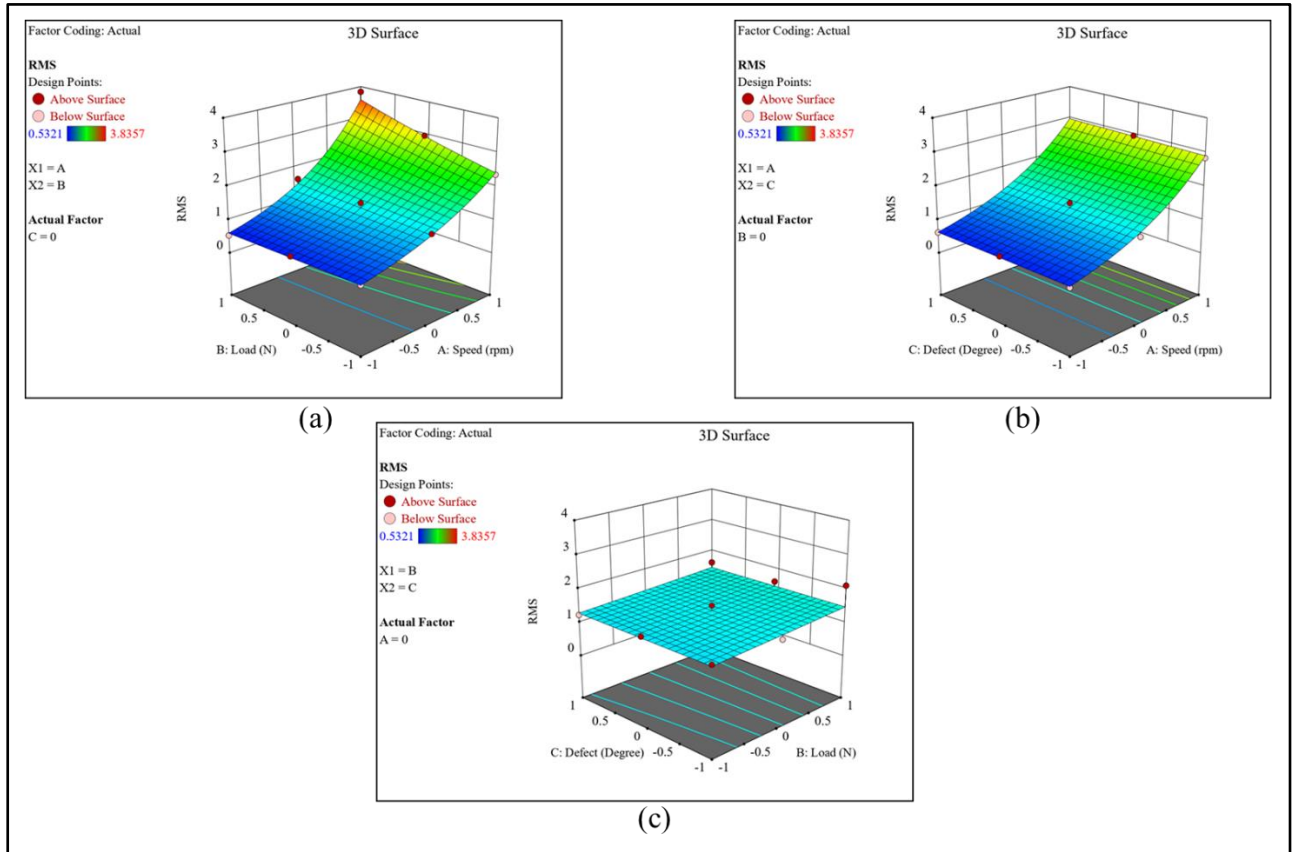


Figure 3.13. Response surface plot for angular misalignment for interaction between (a) speed and load, (b) speed and defect and (c) load and defect

Table 3.11 Comparison of Vibration and Acoustic Sensor

Specification	Vibration sensor	Acoustic sensor
Sensitivity	102.0 mV/g	0.65 mV / Pa
Model	Kistler 8076K	40DD
Type of sensor	Contact	Non-contact

The study has also been extended to combined misalignment fault. Three defect severity are considered for the study (0.3mm+0.1 degree, 0.5mm+0.2 degree and 0.7mm+0.3 degree). The response surface plot shows the same nature as parallel and angular misalignment. The observations in the present study are based on the following unique aspects.

Novelty in Misaligned Rotor System: The present study focuses specifically on a misaligned rotor system, which is distinct from previous studies that concentrate on bearing faults using response surface methodology. In this context, the observations regarding load value and defect size/type are different from those in studies that primarily examine bearing faults.

Radial and Axial Load Interactions: While the radial load in this study may not have a significant impact on vibration amplitudes, there could be notable interactions among the

parameters in the axial direction. This finding is unique and novel. Unlike bearing studies where axial data is often ignored, here it plays a crucial role.

Load Minimization and Defect Impact: It is observed that the effect of defects on vibration response can be minimized when subjected to load. This indicates that the load plays a role in attenuating the impact of defects on the vibration behavior of the system. Such observations align with the specific conditions and characteristics of the misaligned rotor system under investigation.

The unique nature of the misaligned rotor system in this study leads to different observations compared to studies primarily focused on bearing faults or different rotor faults. These observations contribute to the novelty and understanding of the behavior of misaligned rotor systems and highlight the importance of axial data and load interactions in such systems.

3.6 Conclusion

Through the vibration data analysis following conclusions can be made

- A surface response approach using three-level factor design and ANOVA has proven to be an effective technique for determining the significant factors associated with a misalignment. As the literature reported in this area is very scanty, this work will help to understand the misalignment defect and its effect in a better way. It is observed that all model terms are found to be statistically adequate.
- Response surface shows that the change in load value does not affect vibration amplitude significantly in case of Horizontal and vertical directions, while significant variation in RMS value is observed in axial direction in both parallel and angular misalignment. This observation can play a vital role in identifying misalignment when there are multiple faults present in the system. Axial vibrations, which are often overlooked in bearing analysis, play a significant role in locating misalignment faults. This result is consistent with previous research on the function of axial vibration in the detection of misalignment defects. In the same experiment variation in load and its effect on RMS value in horizontal and vertical directions are also recorded but it is observed that there is no significant change in RMS value. These results differentiate the misalignment from other defects.
- Defect size variation has no significant impact on the vibration response in horizontal and vertical directions; the change in RMS value is very small, while in case of axial direction a slight increase in RMS value with respect to defect severity is observed. This observation can help us to identify the misalignment from other faults.

- It is observed that there is a significant increase in RMS value with increase in speed in both types of misalignments.
- Axial vibration plays an important role in the diagnosis of misalignment in the shaft.
The following are some of the conclusions that can be drawn from the data obtained using acoustic signal investigation.
- Response surface shows that the change in load value has significant impact on system vibrations.
- The vibration response is unaffected by change in defect severity. In both types of misalignments, the change in RMS value is quite small as the defect severity increases.
- In both types of misalignments, there is a substantial increase in RMS value with increase in speed.
- Results obtained using acoustic sensor are well aligned with the RSM finding using vibrational data. So, acoustic sensors which is non-contact type can be effectively used at the places where installation of accelerometer is not possible.
- The conditions considered in the present investigation mimic the actual conditions under which such type of fault is generated. So, it helps to understand the important parameters for system vibrations in misaligned rotor system.

References:

- [1] E. I. Rivin, "Design and Application Criteria for Connecting Couplings," *J. Mech. Transm. Autom. Des.*, vol. 108, no. 1, pp. 96–104, Mar. 1986.
- [2] Gibbons C B, "Coupling Misalignment Forces," in *Proceedings of 5th Turbomachinery Symposium, Gas Turbine Laboratories, Houston, TX*, 1976, pp. 111–116.
- [3] A. K. Jalan and A. R. Mohanty, "Model-Based Fault Diagnosis of Rotor System," *Int J Performability Eng*, vol. 7, no. 6, pp. 515–523, 2011.
- [4] A. K. Jalan and A. R. Mohanty, "Model based fault diagnosis of a rotor–bearing system for misalignment and unbalance under steady-state condition," *J. Sound Vib.*, vol. 327, no. 3–5, pp. 604–622, Nov. 2009.
- [5] D. L. Dewell and L. D. Mitchell, "Detection of a Misaligned Disk Coupling Using Spectrum Analysis," *J. Vib. Acoust.*, vol. 106, no. 1, pp. 9–16, Jan. 1984.
- [6] J. Piotrowski, *Shaft Alignment Handbook*. CRC Press, 2006.
- [7] M. Xu and R. D. Marangoni, "Vibration Analysis Of A Motor-Flexible Coupling-Rotor System Subject To Misalignment And Unbalance, Part I: Theoretical Model And Analysis," *J. Sound Vib.*, vol. 176, no. 5, pp. 663–679, Oct. 1994.

- [8] M. Xu and R. D. Marangoni, "Vibration Analysis Of A Motor-flexible Coupling-Rotor System Subject To Misalignment And Unbalance, Part II: Experimental Validation," *J. Sound Vib.*, vol. 176, no. 5, pp. 681–691, Oct. 1994.
- [9] D. E. Newland, "Wavelet Analysis of Vibration: Part 1—Theory," *J. Vib. Acoust.*, vol. 116, no. 4, pp. 409–416, Oct. 1994.
- [10] D. E. Newland, "Wavelet Analysis of Vibration: Part 2—Wavelet Maps," *J. Vib. Acoust.*, vol. 116, no. 4, pp. 417–425, Oct. 1994.
- [11] W. J. Staszewski, "Structural and Mechanical Damage Detection Using Wavelets," *Shock Vib. Dig.*, vol. 30, no. 6, pp. 457–472, Nov. 1998.
- [12] S. Prabhakar, A. S. Sekhar, and A. R. Mohanty, "Vibration analysis of a misaligned rotor—coupling—bearing system passing through the critical speed," *Proc. Inst. Mech. Eng. Part C J. Mech. Eng. Sci.*, vol. 215, no. 12, pp. 1417–1428, Dec. 2001.
- [13] A. K. Jalan, S. Patil, and G. Mittal, "A Review on Fault Diagnosis of Misaligned Rotor Systems," *Int. J. Performability Eng.*, vol. 16, no. 4, p. 499, 2020.
- [14] M. -y. Chow, P. M. Mangum, and S. O. Yee, "A neural network approach to real-time condition monitoring of induction motors," *IEEE Trans. Ind. Electron.*, vol. 38, no. 6, pp. 448–453, 1991.
- [15] I. E. Alguindigue, A. Loskiewicz-Buczak, and R. E. Uhrig, "Monitoring and diagnosis of rolling element bearings using artificial neural networks," *IEEE Trans. Ind. Electron.*, vol. 40, no. 2, pp. 209–217, Apr. 1993.
- [16] B. Samanta and K. R. Al-balushi, "Artificial Neural Network Based Fault Diagnostics Of Rolling Element Bearings Using Time-Domain Features," *Mech. Syst. Signal Process.*, vol. 17, no. 2, pp. 317–328, Mar. 2003.
- [17] B. Samanta, "Gear fault detection using artificial neural networks and support vector machines with genetic algorithms," *Mech. Syst. Signal Process.*, vol. 18, no. 3, pp. 625–644, May 2004.
- [18] L. B. Jack and A. K. Nandi, "Fault Detection Using Support Vector Machines And Artificial Neural Networks, Augmented By Genetic Algorithms," *Mech. Syst. Signal Process.*, vol. 16, no. 2–3, pp. 373–390, Mar. 2002.
- [19] Q. Hu, Z. He, Z. Zhang, and Y. Zi, "Fault diagnosis of rotating machinery based on improved wavelet package transform and SVMs ensemble," *Mech. Syst. Signal Process.*, vol. 21, no. 2, pp. 688–705, Feb. 2007.
- [20] W. Q. Wang, M. F. Golnaraghi, and F. Ismail, "Prognosis of machine health condition using neuro-fuzzy systems," *Mech. Syst. Signal Process.*, vol. 18, no. 4, pp. 813–831,

- Jul. 2004.
- [21] W. Wang, F. Ismail, and F. Golnaraghi, "A Neuro-Fuzzy Approach to Gear System Monitoring," *IEEE Trans. Fuzzy Syst.*, vol. 12, no. 5, pp. 710–723, Oct. 2004.
- [22] T. H. Patel and A. K. Darpe, "Experimental investigations on vibration response of misaligned rotors," *Mech. Syst. Signal Process.*, vol. 23, no. 7, pp. 2236–2252, Oct. 2009.
- [23] A. Simm, Q. Wang, S. Huang, and W. Zhao, "Laser based measurement for the monitoring of shaft misalignment," *Measurement*, vol. 87, pp. 104–116, Jun. 2016.
- [24] J. L. Ferrando Chacon, E. Artigao Andicoberry, V. Kappatos, G. Asfis, T.-H. Gan, and W. Balachandran, "Shaft angular misalignment detection using acoustic emission," *Appl. Acoust.*, vol. 85, pp. 12–22, Nov. 2014.
- [25] A. M. Umbrajkaar, A. Krishnamoorthy, and R. B. Dhumale, "Vibration Analysis of Shaft Misalignment Using Machine Learning Approach under Variable Load Conditions," *Shock Vib.*, vol. 2020, pp. 1–12, Jul. 2020.
- [26] Design Expert, "Version 7.0.0. Stat-Ease." Design Expert Inc., Minneapolis, 2005.
- [27] C. Manoharan and V. P. Arunachalam, "Dynamic analysis of hydrodynamic bearing performance in ic engines by using Taguchi technique and Response Surface Methodology (RSM)," *Int. J. Adv. Manuf. Technol.*, vol. 36, no. 11–12, pp. 1061–1071, Apr. 2008.
- [28] G. E. P. Box and K. B. Wilson, "No Title," *J. R. Stat. Soc.*, vol. 13, no. 1, pp. 1–45, 1951.
- [29] P. K. Kankar, S. P. Harsha, P. Kumar, and S. C. Sharma, "Fault diagnosis of a rotor bearing system using response surface method," *Eur. J. Mech. - A/Solids*, vol. 28, no. 4, pp. 841–857, Jul. 2009.
- [30] P. K. Kankar, S. C. Sharma, and S. P. Harsha, "Fault Diagnosis of High Speed Rolling Element Bearings Due to Localized Defects Using Response Surface Method," *J. Dyn. Syst. Meas. Control*, vol. 133, no. 3, May 2011.
- [31] M. S. Patil, J. Mathew, P. K. Rajendrakumar, and S. Karade, "Experimental Studies Using Response Surface Methodology for Condition Monitoring of Ball Bearings," *J. Tribol.*, vol. 132, no. 4, Oct. 2010.
- [32] P. Kankar, S. C. Sharma, and S. Harsha, "Vibration signature analysis of a high speed rotor supported on ball bearings due to localized defects," *J. Vib. Control*, vol. 19, no. 12, pp. 1833–1853, Sep. 2013.

Chapter 4

MACHINE LEARNING TECHNIQUES FOR MISALIGNMENT FAULT CLASSIFICATION

4.1 Introduction

In the previous chapter interaction effect between speed, load, and misalignment on system vibrations has been studied. In the PHM scheme diagnostics plays a significant role. We need to identify the right type of fault in the system. As we studied, the misalignment in combination with speed and load causes system vibration to increase. It is essential to know what type of misalignment the system is subjected to. The correct diagnosis of fault can reduce unplanned downtime. The model-based technique failed to classify the misalignment fault, and vibration analysis shows a peak at 2x for both angular and parallel misalignment. So there need a study that segregates these faults.

The selection of the appropriate features is essential for correctly identifying the issue of classification and, the choice of features can have a huge effect on the performance of classification. Generally, time-domain features are widely used to get a report on condition of machine. The energy entropy of the empirical mode decomposition is also used to derive features from the vibration signals. Features are then picked using the intrinsic mode functions process, which is then supplied to the Back Propagation, Artificial Neural Network (ANN) to recognize defects in bearings [1]. Two functions extraction methods, Hilbert Transform and fast Fourier transform used for vibration signals. The ANN-based fault estimation algorithm is used for the fault diagnosis of rolling bearings using a genetic algorithm and better classification results are obtained[2]. Delgado et al. [3] stated that classification accuracy for SVM were better than those for ANN. Similarly, Saidi et al. [4] have shown that the important benefit of SVM in fault diagnosis is that it is sufficient even for few sample-based decisions. Initially, the SVM was intended for binary classification[5]. However, more than two classes were needed by most induction motor diagnostic classification systems, such as: multiple fault conditions and/or multiple fault severity classes under different load levels. Samantha et al. [6] found contrast between the neural network (NN) and SVM and they also found that both NN and SVM gave 100 % accurate results in extracting features from the vibration signals of a defective gearbox. For automatic fault diagnosis of bearing, a combination of the decision tree and the fuzzy classifier is used [7]. Gunerkar et al. [8] perform a bearing fault

classification using an accelerometer and microphone sensor data fusion. The fault classification is carried out using K nearest neighbor (KNN).

Haroun et al. [9] used the Autoregressive (AR) torque signal model for misalignment fault detection. Firstly, in different operating conditions, the torque signal obtained from the experimental setup and coefficients of the AR model were extracted as features. Min Redundancy Max Relevance (mRMR) was used to select the optimal features for fault classification. Finally, Self-Organizing Map neural network was used for fault classification. Chandan kumar et al. [10] carried out experimental research to detect rotor misalignment on a three-phase induction motor. To track the vibration and current signals, proximity and current probes were used. FFT was used for signal processing. For both signals to disclose the fault-specific whirl signatures, a full spectrum analysis was presented. Alok kumar et al. [11] used both stator current and vibration samples for fault detection. They used multi-scale entropy (MSE) for feature extraction and SVM for fault classification. Jun lin et al. [12] extracted features using MSE and then signal denoised using wavelet transform, they got better results than frequency related features. For different cases of misalignment at different operating frequencies, experimental findings using a torque sensor were recorded by Chandra shekhar et al. [13]. They used Fourier and wavelet transforms to detect the fault. Alok kumar et al. [14] concluded that misalignment effect can be predicted by the current signature alone without using the vibration signal. Orbit plots were used easily to illustrate the particular existence of the fault of misalignment. During machine operation, shaft displacement and stator current samples were measured and analysed under aligned and misaligned conditions. Chacon et al. [15] carried out detailed experimental investigation using the acoustic emission (AE) technique in order to determine the probability of detecting angular misalignment. The test rig was run under various load and speed conditions.

By considering deformation and reaction forces, for a misaligned structure, Lee and Lee [16] derived a dynamic model. In this model, they considered axial vibration, which is a key indicator of the presence of misalignment. Isermann [17] elaborately defined the process of residual generation for the diagnosis of faults. Jalan and Mohanty [18] considered equal loads as an indication of a rotary system fault and successfully detected the amount, form and position of a mechanical fault in the rotor-bearing system by using the experimental time response method for both the defective and the healthy system. The research was expanded to three dimensions by Monte et al. [19], where axial direction helped to detect system inconsistency. Jalan et al. [20]

presented a review on the diagnosis of rotor system misalignment faults using model based and signal-based techniques.

The minimal sample size available for training and testing is sometimes a constraining element in determining the optimal fault classification features and algorithms. In comparison to those trained with an unlimited sample size, training on a small dataset creates bias and variance in performance [21]. SVM has proven to be one of the most successful algorithms for dealing with few sampled data. Wei Liu et al. [22] used SVM for the detection of the coal-gangue interface during top-coal excavation mining with limited data available. Based on singular value decomposition techniques and SVM, they provided a new vibration signal analysis approach for detecting the coal-gangue interface. Umbrajkaar et al. [23] used vibration analysis to carry out misalignment fault classification using machine learning approach, SVM and ANN was used. They extracted time-frequency domain features for fault classification. The feature ranking was done by using ReliefF algorithm, the accuracy of fault classification using ANN was 94.17% and using SVM was 97.72%. Both angular and parallel misalignment shows peak at $2x$, then it will be difficult to identify the type of misalignment. There are other rotor-bearing faults, which lead to major $2x$ vibrations. Therefore, distinguishing misalignment by using vibration signals alone is a difficult activity [24]. Acoustic signals were used for the detection of shaft angular misalignment [15]. In the present chapter two cases have been discussed, in case (i) Only binary (parallel and angular) fault classification is performed while in case (ii) Angular, parallel, and combined misalignment cases are considered.

4.2 Experimental Test Rig and Loading Conditions

Machinery Fault Simulator (MFS), shown in figure 3.1 is used to conduct the tests. Two loading conditions are considered i.e., zero N and 13.4 N. Two major types of misalignment faults are considered at three levels of defect severity and at three different speed conditions. The defect specifications are listed in Table 3.1, these values are decided based on literature survey and speed levels considered are 1020, 1860 and 2580 rpm.

4.3 Binary Fault Classification (Angular and Parallel)

In the present investigation, vibro-acoustic sensor data fusion technique is used to detect various forms of misalignment under different operating conditions. There are 18 tests performed for each fault case (total 36 experiments for parallel and angular), and 9 tests for each fault mode, for each

case. A pareto rule is applied while splitting the train/test data. Each case data was randomly divided into 80-20 portion, 80% of the data was used for training and 20% of data was used for testing purpose. The data division is done for each case separately. In misalignment fault classification, some researchers [23] had achieved near perfect results already, but this study aims to attempt to create an even higher accuracy approach than the 97.72% accuracy listed.

For the analysis, Matlab R2019b, update cycle 5 with default settings is used. Feature extraction and feature ranking was carried out using diagnostic feature designer app. The ranked features then extracted to classification learner app. Gaussian naive bayes, ensemble boosted trees, logistic regression, fine KNN and Cubic SVM results are discussed for misalignment fault classification by considering two loading conditions. These algorithms perform better for binary fault classification [5-8]. The classification accuracy of these algorithms is discussed using confusion matrix and positive predictive value & false discovery rate plot. Vibro-acoustic sensors are used to capture the data and time domain features are extracted from both sensors and ranked using one-way ANOVA (t test). The selected features are used to train the machine learning algorithms. In the present study limited samples are used, one of the goals of this work is to explore fault classification using a small amount of dataset.

4.3.1 Data Acquisition and Signal Processing

To process and analyse the collected vibration and acoustic signals from MFS, an eight channel multi-analyser (OROS-OR35, NVGATE software) is used. For 10 seconds, the signal acquisition is carried out, the sampling rate during data acquisition was 25.6KHz, the sample times are synchronized between vibration and acoustic sensors while data acquiring from each signal and the obtained signals are passed through the built-in anti-aliasing filters of the analyser. To fetch the useful information from the acquired signal, different time domain features are extracted using MATLAB from vibrational signal in X (Radial), Z (Axial) directions and acoustic signal data.

Table 4.1. Feature Ranking For 13.4 N Load

Feature Ranking	Features	t test-Score (One-way ANOVA)
1	Acoustic Data_Skewness	1.4709
2	Z_Vib.Data_CrestFactor	1.3494
3	Z_Vib.Data_ImpulseFactor	1.3437
4	Z_Vib.Data_ClearanceFactor	1.3426
5	X_Vib.Data_Skewness	1.2714
6	Acoustic Data_ShapeFactor	1.0414
7	Acoustic Data_SINAD	1.0222
8	Acoustic Data_CrestFactor	1.0122
9	Acoustic Data_SNR	1.0065
10	Acoustic Data_ImpulseFactor	0.9945
11	Acoustic Data_ClearanceFactor	0.9842
12	Acoustic Data_Kurtosis	0.9506
13	Z_Vib.Data_THD	0.8431
14	X_Vib.Data_CrestFactor	0.7366
15	X_Vib.Data_ImpulseFactor	0.7269
16	Acoustic Data_Mean	0.7254
17	X_Vib.Data_ClearanceFactor	0.7213
18	Acoustic Data_RMS	0.6743
19	Acoustic Data_Std	0.6742
20	Acoustic Data_THD	0.6384
21	Z_Vib.Data_Kurtosis	0.5444
22	Z_Vib.Data_ShapeFactor	0.5318
23	Z_Vib.Data_PeakValue	0.5239
24	X_Vib.Data_THD	0.5009
25	X_Vib.Data_Mean	0.4392
26	X_Vib.Data_Kurtosis	0.3884
27	X_Vib.Data_ShapeFactor	0.3587
28	Z_Vib.Data_Mean	0.3352
29	Z_Vib.Data_RMS	0.3319
30	Z_Vib.Data_Std	0.3319
31	Acoustic Data_PeakValue	0.2557
32	X_Vib.Data_SNR	0.2370
33	X_Vib.Data_SINAD	0.2365
34	Z_Vib.Data_SINAD	0.1817
35	Z_Vib.Data_SNR	0.1799
36	Z_Vib.Data_Skewness	0.1612
37	X_Vib.Data_Std	0.0772

A slice from the original signal with 2048 points is shown in Figure 4.1. Feature extraction will help to decrease irrelevant variables that would otherwise reduce the accuracy of the classifier. A total of 37-time domain features are derived from vibrational and acoustic sensor data. After extracting the time domain features of the signal, they are ranked as per their importance towards fault classification using t test (One-way ANOVA). The ranking of features based on the one-way ANOVA is shown in Table 4.1 and the values indicates the ANOVA t Scores. The value in the table shows the t score values. The t test tells us how significant the differences between groups are. The t score is a ratio between the difference between two groups to the difference within the groups. The larger is the t score, the more difference between groups. The smaller the t score, the more similarity there is between groups. A large t score tells us that the groups are different, and a small t score indicates the groups are similar. The t score can be calculated using equation (4.1).

$$t = \frac{(\sum D)/N}{\sqrt{\frac{\sum D^2 - \frac{(\sum D)^2}{N}}{(N-1)(N)}}}$$
(4.1)

$\sum D$: Sum of the differences

$\sum D^2$: Sum of the squared differences

$(\sum D)^2$: Sum of the differences, squared.

Features which are more sensitive towards fault classification are selected. We will get an indication of the relative efficacy of classification features if we refer to histograms. Histogram charts clustered by defect code can help decide if certain features are powerful differentiators between types of faults. Their distributions are more isolated from each other if they are strong differentiators. Feature representations appear to overlap and there are no features that can be used explicitly to distinguish faults. Figure 4.2 shows the flowchart of the proposed method.

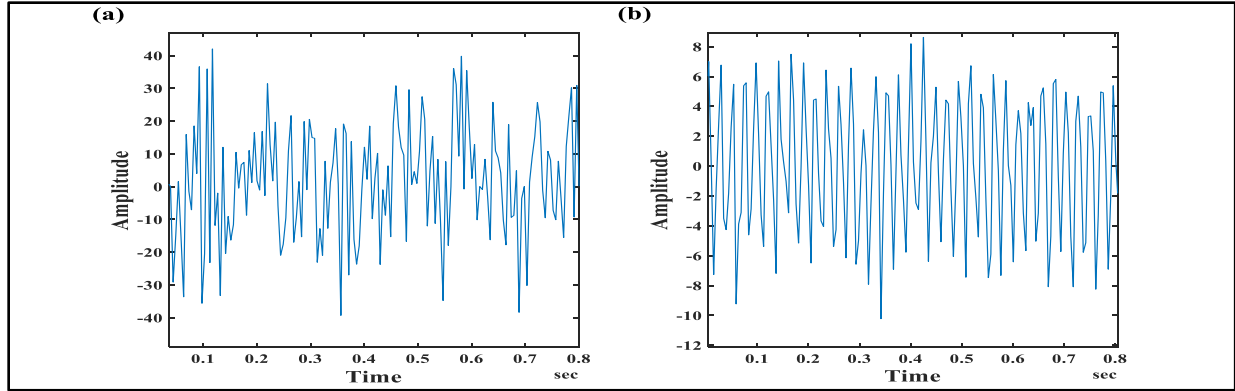


Figure 4.1 Signal trace (a) vibrational signal in Z-direction (b) acoustic signal

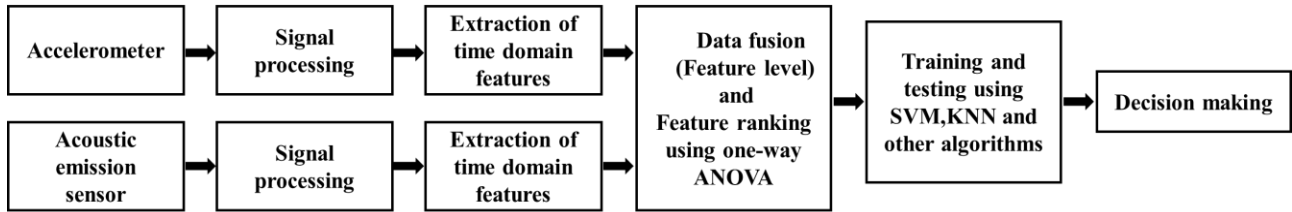


Figure 4.2. flowchart of the proposed method

4.3.2 One-way ANOVA

The objective of a one-way ANOVA is to see if data from different groups (levels) of a factor have the same mean. One-way ANOVA allows us to see if various groups of an independent variable have distinct impacts on the response variable y . One-way ANOVA is a basic variant of the linear model. The model's one-way ANOVA version is,

$$y_{ij} = \alpha_j + \varepsilon_{ij} \tag{4.2}$$

with assumptions

y_{ij} is an observation, in which i represents the observation number, and j represents a different group (level) of the predictor variable y .

α_j represents the population mean for the j th group.

ε_{ij} is the random error, with zero mean and constant variance,

The assumption that all group means are equal is tested using ANOVA, as compared to the alternative theory that at least one group differs from the others. ANOVA divides the entire variation in the data into two parts to test for differences in group means:

- a) Variation of group means from the overall mean, i.e., variation between groups.
- b) Variation of observations in each group from their group mean estimates, variation within group.

4.3.3 Results and Discussion

Using the MATLAB's diagnostic feature designer framework, the extraction and ranking of features is achieved. These ranked features are used to train the algorithms. Results of fault classification using naive bays, ensemble boosted trees, logistic regression, KNN and SVM are discussed in following sections.

Naive Bayes algorithm is a collection of supervised learning algorithms based on Bayes' theorem. The supervised learning classification algorithm logistic regression is used to predict the probability of a target variable. Because the nature of the objective or dependent variable is binary, there are only two classifications. In comparison to individual classifiers, the ensemble classifier combines several classifiers to produce better classification results. Boosting is a method of weighting constructed models based on their results by averaging/voting multiple models. The KNN classifier is a basic yet powerful fault classification tool. When a decision concerning new incoming data is required, the distance between test and training samples is computed. The KNN classifier uses the Euclidean distance method to calculate distances in multidimensional input space. The SVM is the most popular machine learning technique. The SVM algorithm is derived from an optimal separating hyper-plane in the context of linearly separable data. SVM creates a hyper-plane that is separated into two categories (can be extended to multi-class problems). From the literature it is found that SVM works well for binary fault classification and SVM also perform effectively with limited dataset. KNN was effectively used in numerous bearing fault classification and proved to be one of the effective tools.

4.3.3.1 Case 1: No load condition

The ranked features were imported to classification learner platform of matlab. In classification learner platform, the cross-validation model was chosen. The total data was divided into 5 folds. If we choose 5 folds, then the app: Partitions the data into 5 disjoint sets or folds, for each fold: Trains a model using the out-of-fold observations. Assesses model performance using in-fold data and calculates the average test error over all folds. This method gives a good estimate of the predictive accuracy of the final model trained with all the data. It requires multiple fits but makes efficient use of all the data, it is recommended for small data sets. So initially 4 folds (F1, F2, F3 and F4) used for training (80% of data) and 1-fold (F5) was used for testing (20% of data). Then in next step it takes F1, F2, F3 and F5 for training and then use F4 for testing. Same way it uses

all data for training and for testing. In confusion matrix we can see 9 parallel and 9 angular faults cases of test data. This method suits best for small number of datasets. The ranked features are fed to the algorithms for training purpose. The testing accuracy changes with the number of input features, according to the performance measures of the features from large to small, with the number of sensitive features added one by one till all the features are fed to the selected algorithms. Some of them aren't affected by fault classification at all. These features would perplex the classifier, resulting in no discernible improvement in classification accuracy. Observing that the testing accuracy varies with the number of features fed into the algorithms, we may discover that the features have higher sensitivity at first, and that the testing accuracy improves as the number of features fed into the algorithms increases. However, as the number of selected features increases to 12 (of total 37 features), the accuracy begins to decline because the features added beyond that were not sensitive. This could imply that as the number of features increases, the selected features contain too much fault-unrelated information, and the values of these features have a significant degree of overlap.

The confusion matrix and positive predictive value & false discovery rate plot are used to check the accuracy of each algorithm for proper fault classification. Confusion matrix map is used to understand how each class performed with the currently selected classifier. The rows (refer Figure 4.3 a) represent the true class and in the columns the predicted class is shown. The diagonal cell shows the true class and the expected match for the class. The green colour cells show that the classifier categorizes true class findings correctly and well. Figure 4.4 shows the result for Naive Bayes algorithm. From the confusion matrix (refer figure 4.3 a), it is observed that five of nine angular faults are classified accurately while remaining are misclassified as parallel and seven of the parallel faults are classified accurately while two parallel faults are misclassified as angular. Figure 4.3 (b) shows the rows below the table with a summary. For the correctly predicted points in each class, positive predictive values are shown in green and false discovery rates for the incorrectly predicted points in each class are shown in pink colour below. False discovery rate for angular is 29% and for parallel, it is 36%. It depicts that 29% of the parallel fault misclassified as angular while 36% angular faults are misclassified as parallel. The positive predictive values for angular and parallel is 71% and 64% respectively. Figure 4.4 shows the result for ensemble boosted trees. This algorithm failed to distinguish between the parallel and angular fault. It is observed from figure 4.4(a), the confusion matrix, the classifier predicted the angular faults accurately while

failed to classify parallel faults. All the parallel faults are misclassified as angular fault. So, the false discovery rate is 50% and positive prediction is also 50%. The fault classification accuracy obtained using Naive Bays and ensemble boosted trees is 66.7% and 50% respectively. The result for logistic regression is indicated in figure 4.5. The accuracy achieved using logistic regression is quite better than naïve bays and ensemble boosted tress. This classifier was able to segregate the different faults effectively. All angular class faults are classified correctly while two of parallel faults misclassified as angular. From figure 4.5 (b), is it observed that positive prediction accuracy for parallel is 100% because none of angular class is predicted at parallel. The fault classification accuracy is 88.9%.

Figure 4.6 shows the classification accuracy for KNN. KNN classifies the angular and parallel faults effectively. Two faults from each class are misclassified. The positive predictive value for each case is 78%, and false discovery rate is 22% for each class. The accuracy achieved using this classifier is 77.8%. Figure 4.7 shows result for SVM algorithm. The precision of fault classification is 100%. The faults are accurately classified by this algorithm. Green diagonal entries imply that each fault is grouped into an exact category. The false discovery rate is zero for the predicted class; it indicates that no fault is misclassified.

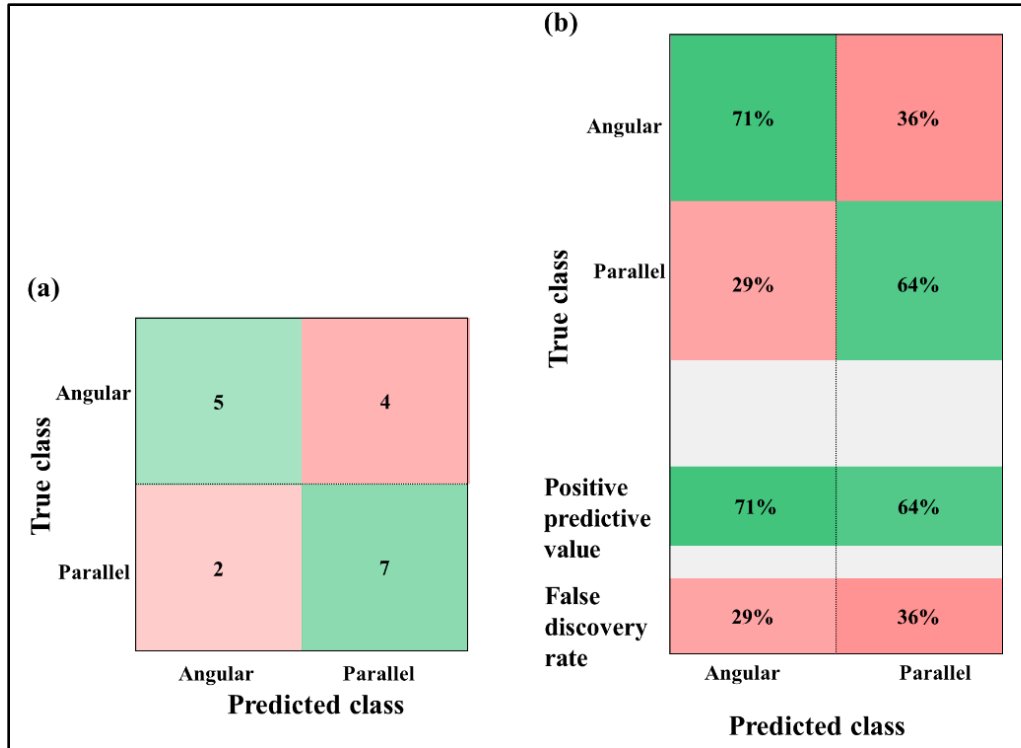


Figure 4.3. Result of Naive Bays (a) confusion matrix (b) positive predictive value & false discovery rate plot

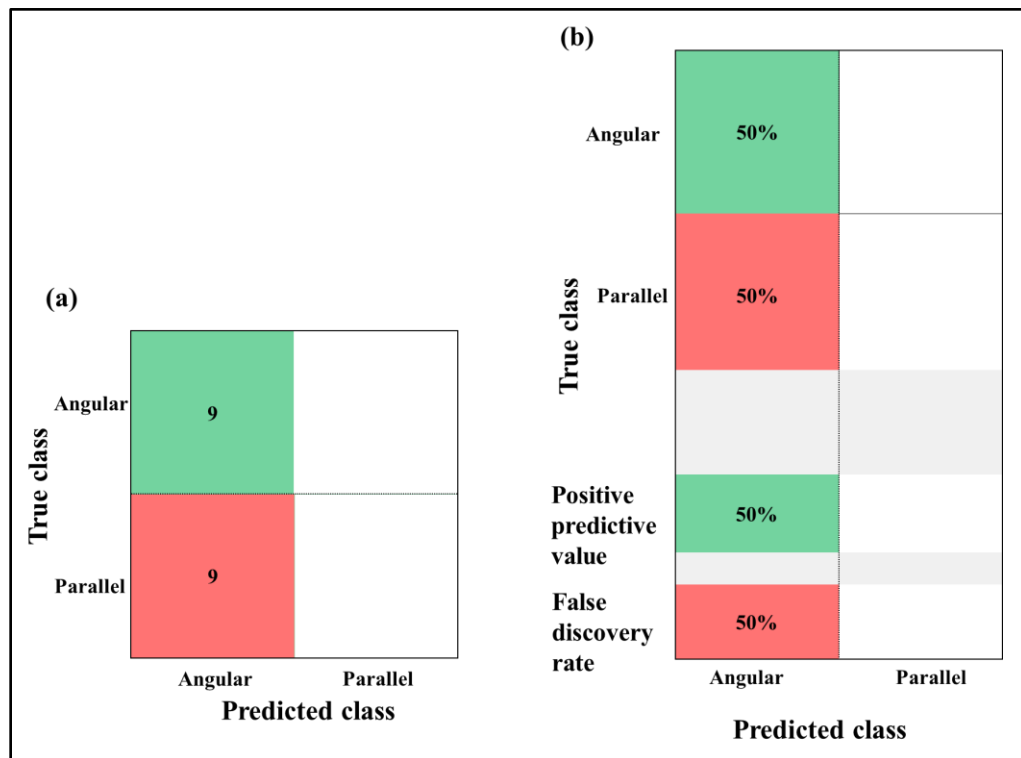


Figure 4.4. Result of Ensemble boosted trees (a) confusion matrix (b) positive predictive value & false discovery rate plot.

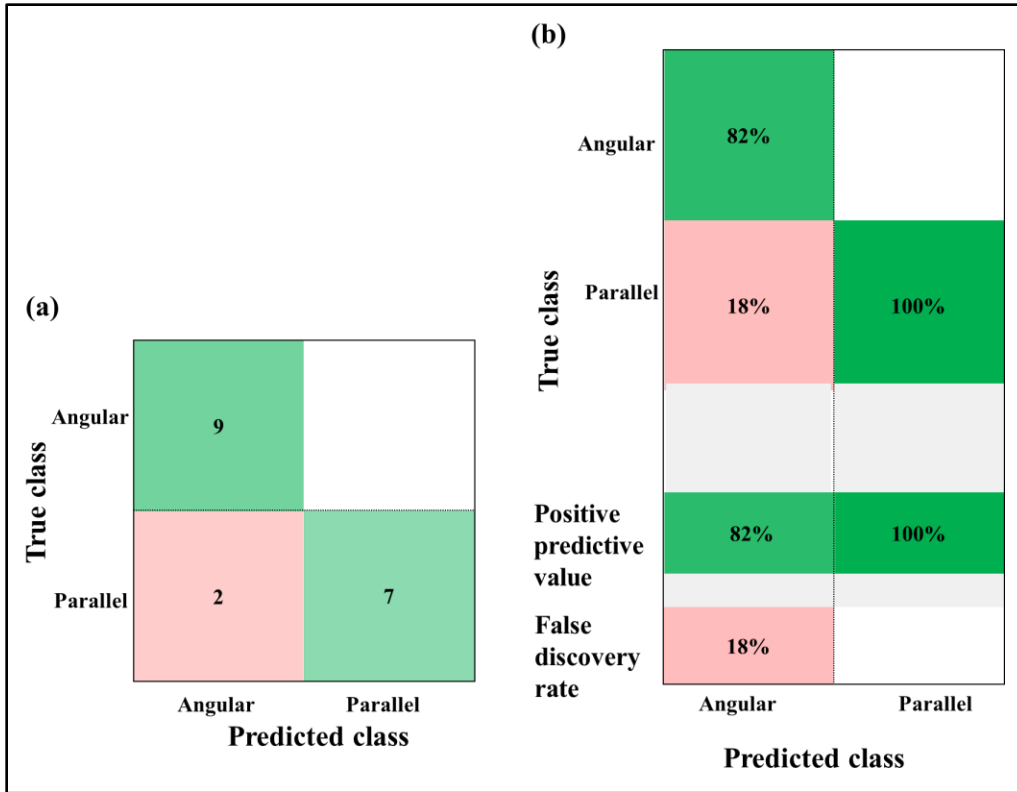


Figure 4.5. Result of logistic regression (a) confusion matrix (b) positive predictive value & false discovery rate plot

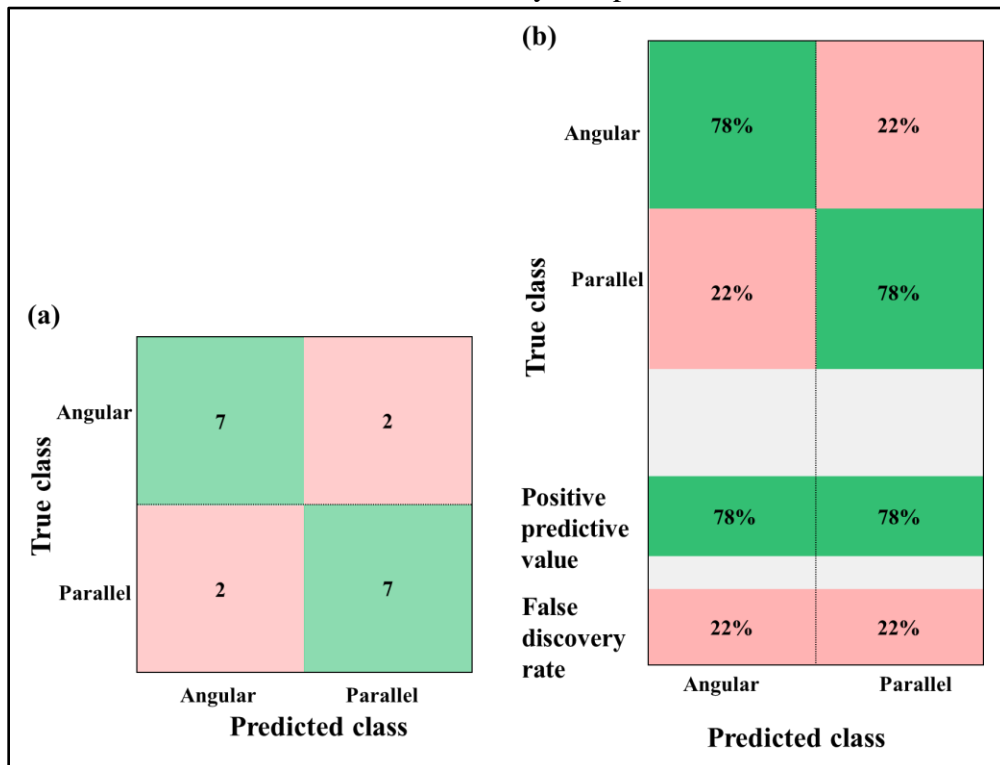


Figure 4.6. Result of KNN (a) confusion matrix (b) positive predictive value & false discovery rate plot

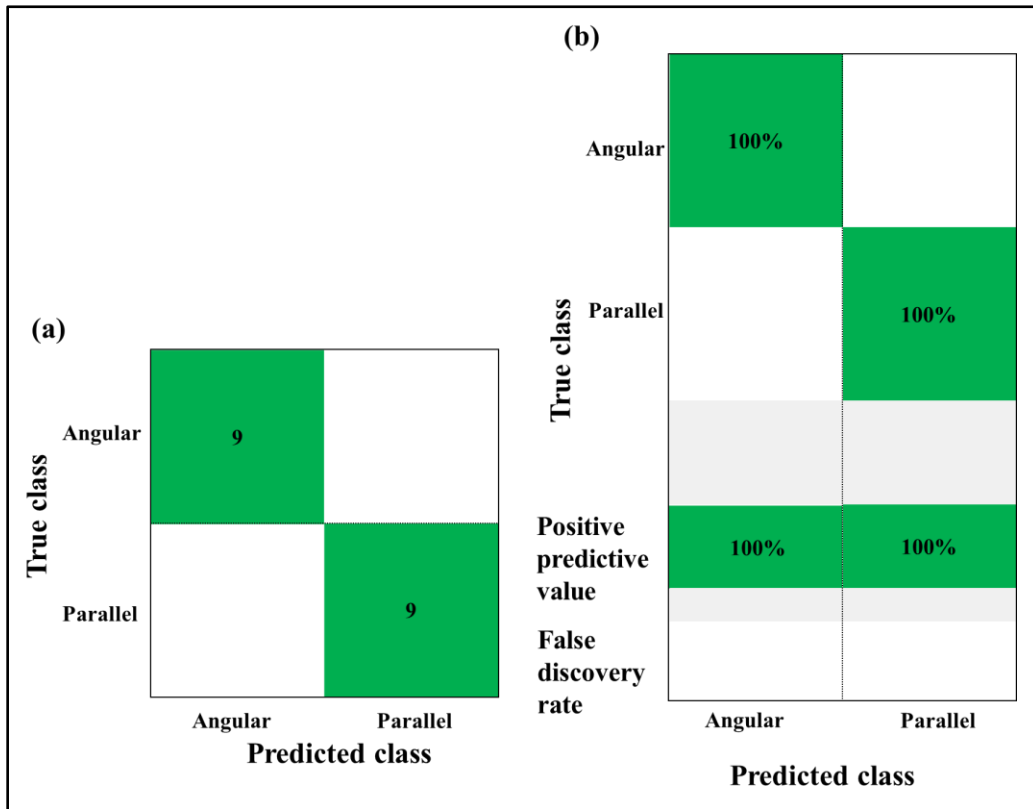


Figure 4.7. Result of SVM (a) confusion matrix (b) positive predictive value & false discovery rate plot

The classification accuracy summary table for case I, which shows the comparison between vibration, acoustic and vibro-acoustic sensor data fusion is given in Table 4.2,

Table 4.2 Summary Table for case I: No Load Conditions

Machine Learning algorithm	Vibration data	Acoustic data	Vibro-acoustic data (Sensor fused data)
Naive Bayes	81.6%	72.4%	66.7%
Ensemble boosted tress	46.8%	56.4%	50%
Logistic regression	71.9%	76.6%	88.9%
KNN	66%	72%	77.8%
SVM	86.2%	76.2%	100%

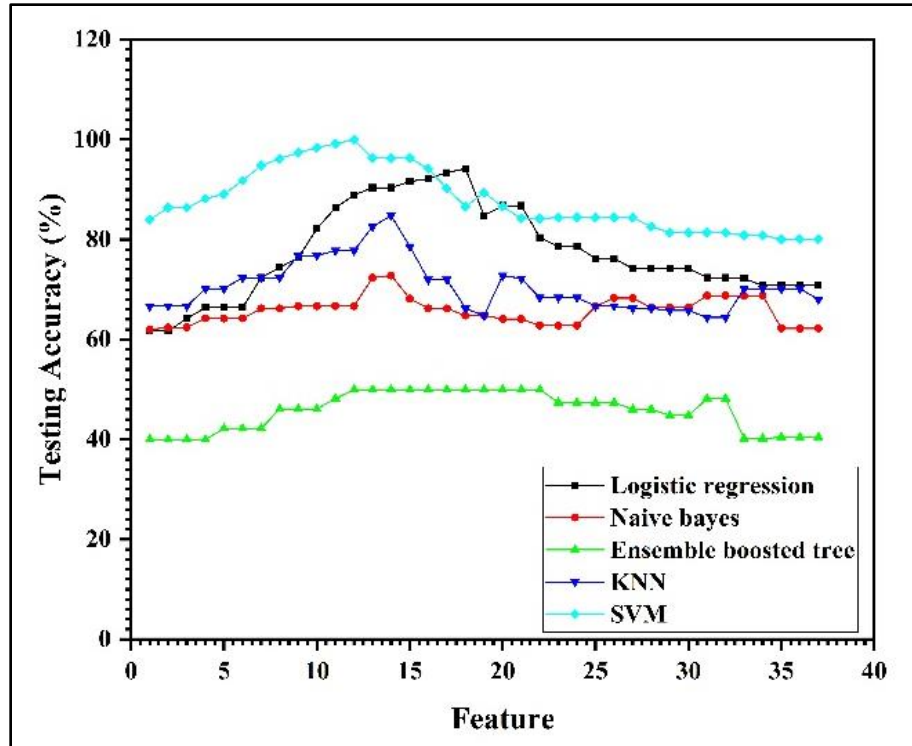


Figure 4.8. Feature vs Testing accuracy plot for No load conditions

Figure 4.8 shows the Feature vs Testing accuracy plot for No load condition, it depicts that SVM can achieve 100% accuracy in the scenarios explored only when considering twelve number of features as ranked using a one-way ANOVA. It does not perform at the stated 100% accuracy, 100% of the time and other classifiers do outperform the SVM. Logistic regression outperforms SVM in some selected feature combinations. Ensemble boosted trees plot shows that there is not much effect on classification accuracy with number of feature addition. Naive bayes algorithm also gave result in the range of 60-70%.

4.3.3.2 Case 2: With Load Condition (13.4 N)

In case 2, the shaft is loaded with 13.4N of load at its centre. The readings are recorded for three different shaft frequencies. Total 20 features (refer Table 4.1) are used to train the algorithms based on their sensitivity towards fault classification, 4 features from radial direction vibrational data, 4 from axial direction and 12 features are selected from acoustic data, which are contributing towards fault classification. The same method of feature selection is followed for both cases. Figures 4.9, 4.10 and 4.11 indicate the fault classification result of Naïve Bayes, ensemble boosted trees and logistic regression. The accuracy achieved is 61.1%, 50% and 94.4% respectively. Naive bayes algorithm classified angular fault correctly but 5 of the parallel faults were misclassified as angular,

so positive prediction value is 58% in case of parallel and only 2 of angular faults are misclassified as parallel so its positive prediction value is 67%. In case of ensemble boosted trees, the algorithm failed to segregate between angular and parallel faults. It grouped all faults into angular case. so, the accuracy is 50% and false discovery rate is also 50%. In case of logistic regression, only one misclassification noted. all angular faults are correctly classified but one of the parallel faults is classified as angular. The accuracy achieved using KNN is 83.3%.

Figure 4.12 shows result for fault classification using KNN. It is observed that one angular and 2 parallel faults are incorrectly classified. so, the positive prediction value in case of angular is 80% and in case of parallel it is 88%. Figure 4.13 indicates the result of SVM, the accuracy obtained is 100%. All green entries indicates that each of the faults grouped into accurate class and this algorithm performed excellently compared to other.

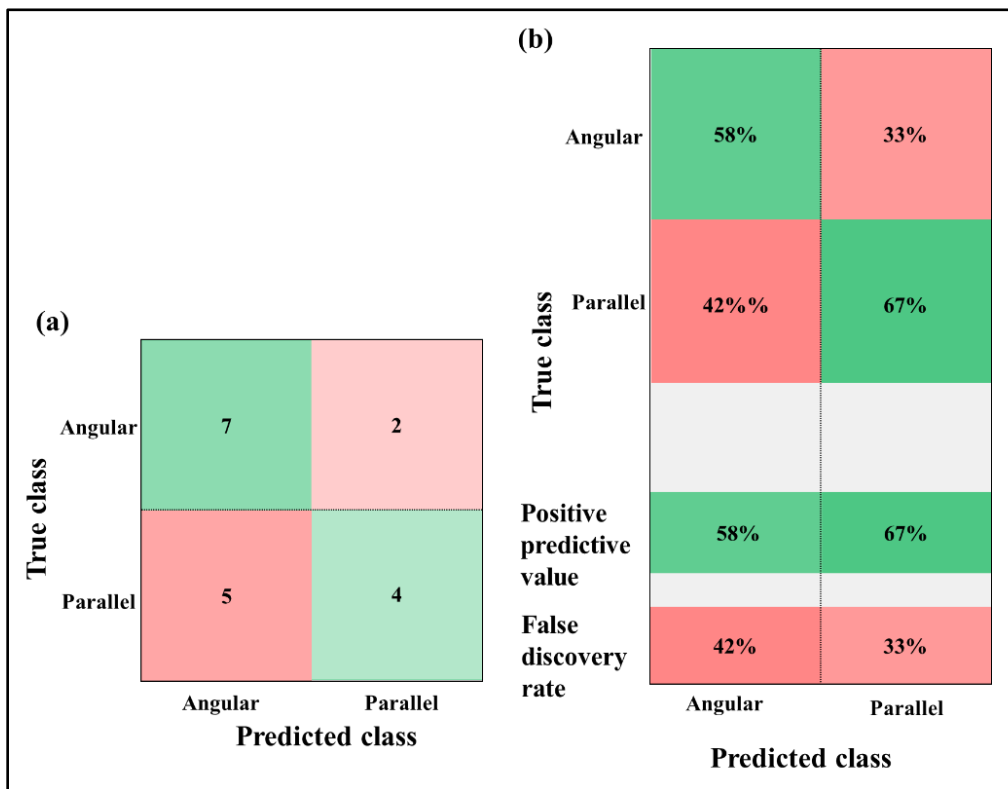


Figure 4.9. Result of Naive Bayes (a) confusion matrix (b) positive predictive value & false discovery rate plot

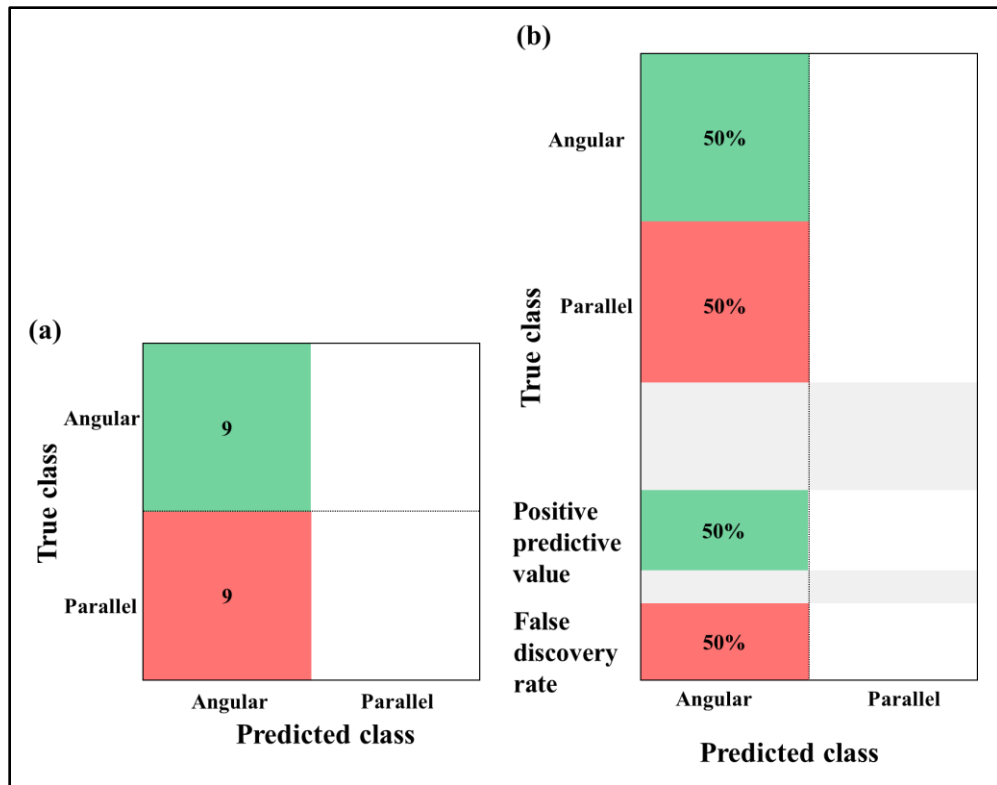


Figure 4.10. Result of Ensemble boosted trees (a) confusion matrix (b) positive predictive value & false discovery rate plot.

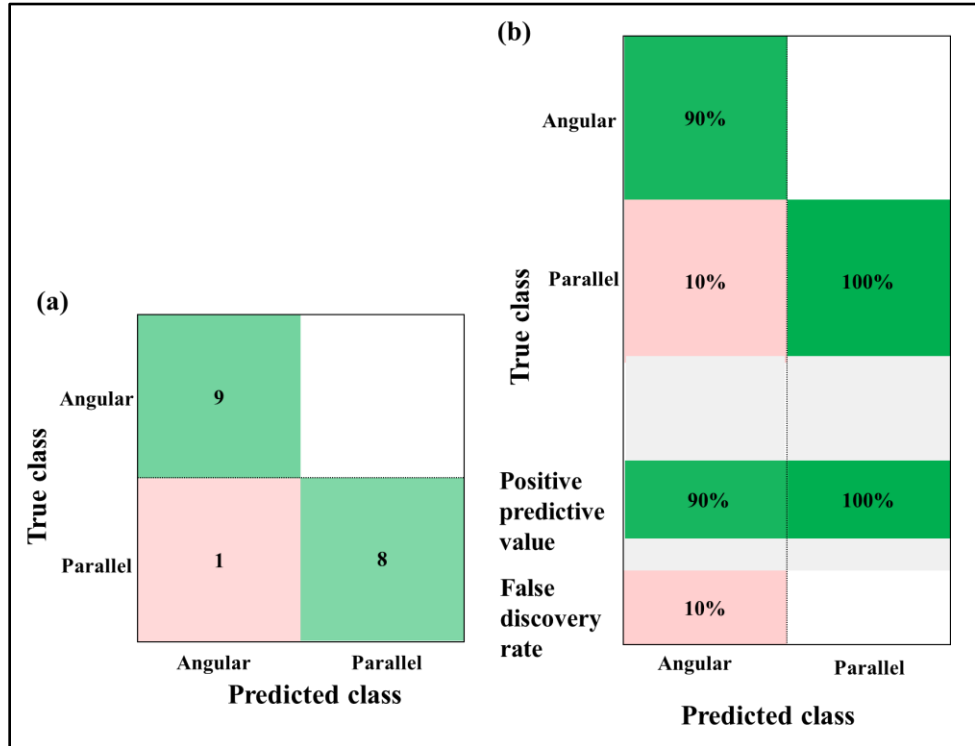


Figure 4.11. Result of Logistic regression (a) confusion matrix (b) positive predictive value & false discovery rate plot.

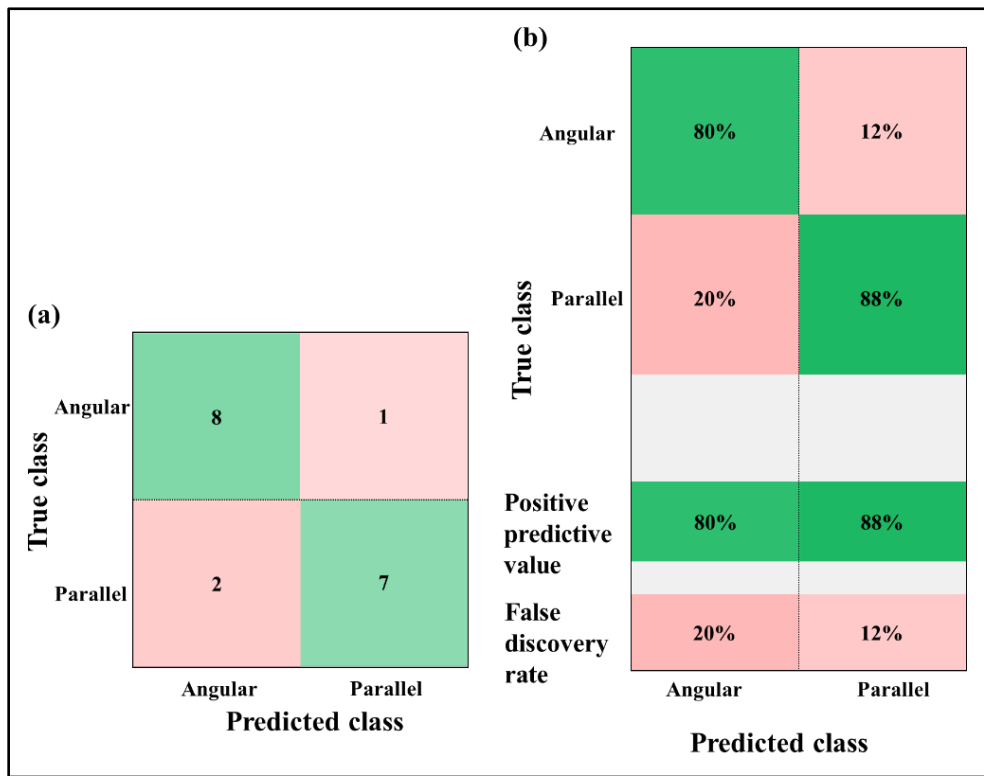


Figure 4.12. Result of KNN (a) confusion matrix (b) positive predictive value & false discovery rate plot

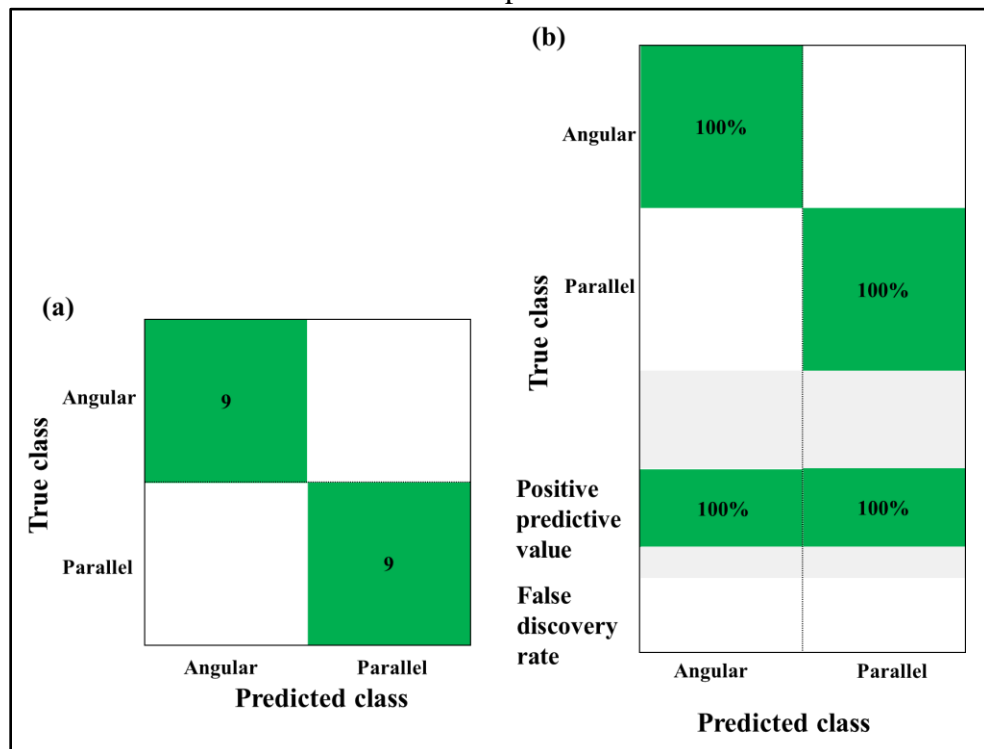


Figure 4.13. Result of SVM (a) confusion matrix (b) positive predictive value & false discovery rate plot

Umbrajkaar et al. [23] carried out misalignment fault classification by employing vibration data alone. They used machine learning algorithms like SVM and ANN for segregation of faults. They extracted features from time-frequency domain and features ranking was done by using ReliefF algorithm. The accuracy of fault classification using ANN was 94.17% and using SVM was 97.72%. The proposed method outperforms the results obtained employing SVM, ANN by using vibration data alone. It is also found that generally the diagnosis of misalignment is carried out through vibration measurements. Especially, the presence of a strong 2x peak is usually accepted. But both angular and parallel misalignment fault shows the peak at 2x, so, it will be difficult to identify the correct form of misalignment. Apart from this, there are some other rotor-bearing faults, which lead to major 2x vibrations. Therefore, distinguishing misalignment by using vibration signals alone is a difficult activity [15, 24]. The proposed method of sensor data fusion of vibro-acoustic type outperforms the fault classification using only vibrational data. From the results obtained above, it is confirmed that the sensor fusion enhances the accuracy of fault classification.

To check the efficacy of the proposed method, it is compared with fault classification using vibrational data and acoustic data separately for the same dataset. The results obtained using sensor data fusion are superior to the fault classification using individual sensor data. A below table shows the comparison among these methods with accuracy of fault classification.

Table 4.3 Summary Table for Case II

Machine Learning algorithm	Vibration data	Acoustic data	Vibro-acoustic data (Sensor fused data)
Naive Bayes	88.9%	66.7%	61.1%
Ensemble boosted tress	50%	50%	50%
Logistic regression	61.1%	55.6%	94.4%
KNN	50%	50%	83.3%
SVM	88.9%	72.2%	100%

Figure 4.14 shows the accuracy per feature addition in order of ANOVA's ranking for case 2. It is found that SVM results are most consistent among all algorithms. From Figure 4.14, it is observed that in some cases for some selected features logistic regression outperform SVM. SVM does not perform at the stated 100% accuracy, 100% of the time. 500+ repetitions are common in machine learning; it is likely the other ML Algorithms explored had lower performance due to limited data samples. SVM performed excellently with few data samples. The accuracy of other algorithms is less compared to SVM.

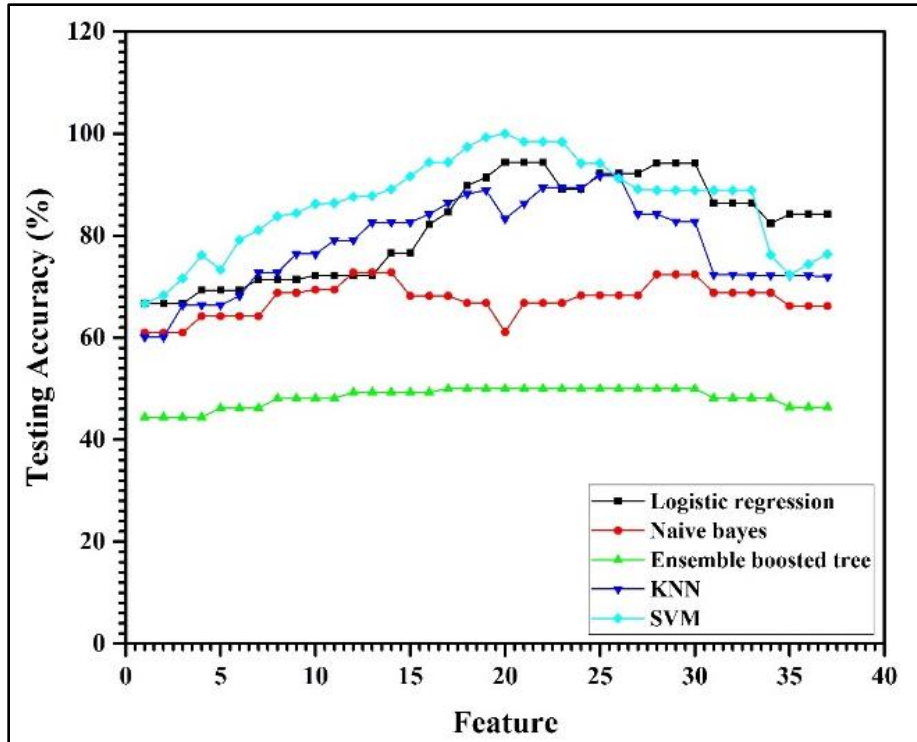


Figure 4.14. Feature Vs Testing accuracy plot for case II

In KNN, During the learning phase, the algorithm does not learn anything, the training data is not used to construct any discriminative features. So, it is sensitive to the scale of the data and irrelevant features. Ensemble boosted tree is prone to overfitting the data. There was no significant improvement in it, the classification accuracy was almost unaltered. While in case of Naive bayes the features offered are self-contained and have no effect on one another, which is not the case in reality. The features are dependent on the presence or quantity of another, which the Naive Bayes classifier simply ignores. The assumption of linearity between the dependent and independent variables is a key flaw in Logistic Regression.

Figure 4.15 is a scatter plot, shows the prediction accuracy of SVM, kurtosis from acoustic signal is used to plot the graph. The saffron colour dot indicates it is grouped into parallel fault and blue dot indicates the angular fault. The misclassification indicated by crossed sign. From figure 4.15 it is observed that, all faults are grouped accurately in to parallel and angular classes. It depicts that SVM gives 100% accurate results. It indicates the parabolic plot for SVM, and all faults are grouped into respective class.

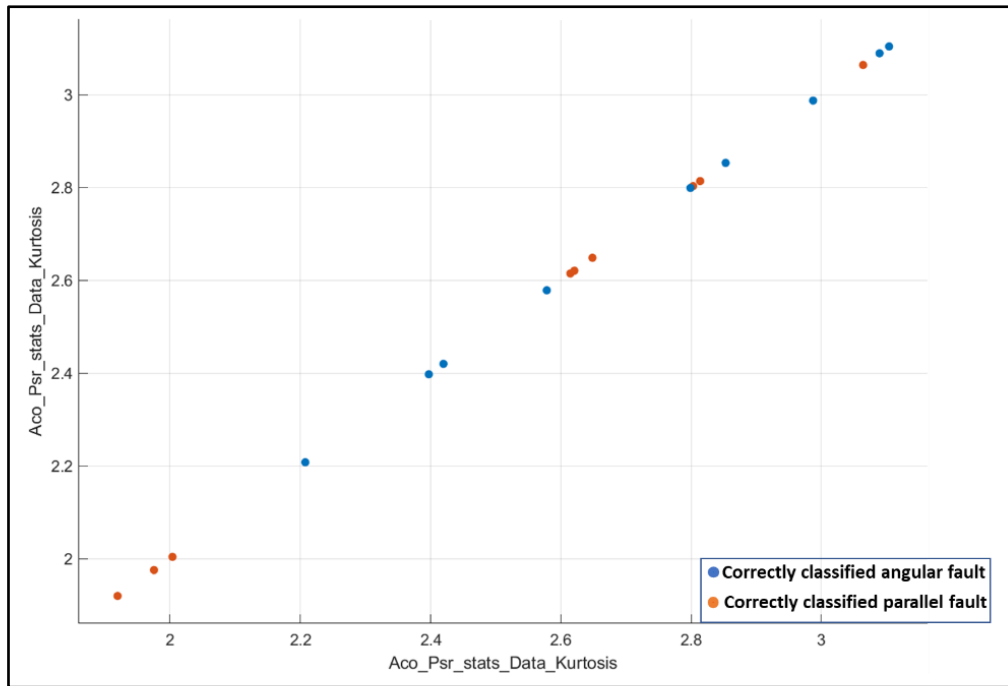


Figure 4.15. Predictions model for SVM

4.3.3.3 Case 3: With Load Condition (6.7N)

Figure 4.16 shows confusion matrix result for case 3 with the load of 6.7N with same speed and defect severity conditions used in case 1 and case 2. The classification accuracy for this loading condition is given in Table 4.4. It is found that results are consistent with previous case results and SVM gave 100% accurate results with the fifteen features out of total thirty-seven features. Logistic regression also able to segregate the fault with 94.4% accuracy while ensemble boosted trees performed poor for binary fault classification. Ensemble boosted trees algorithm failed to identify parallel type fault (refer figure 4.16).

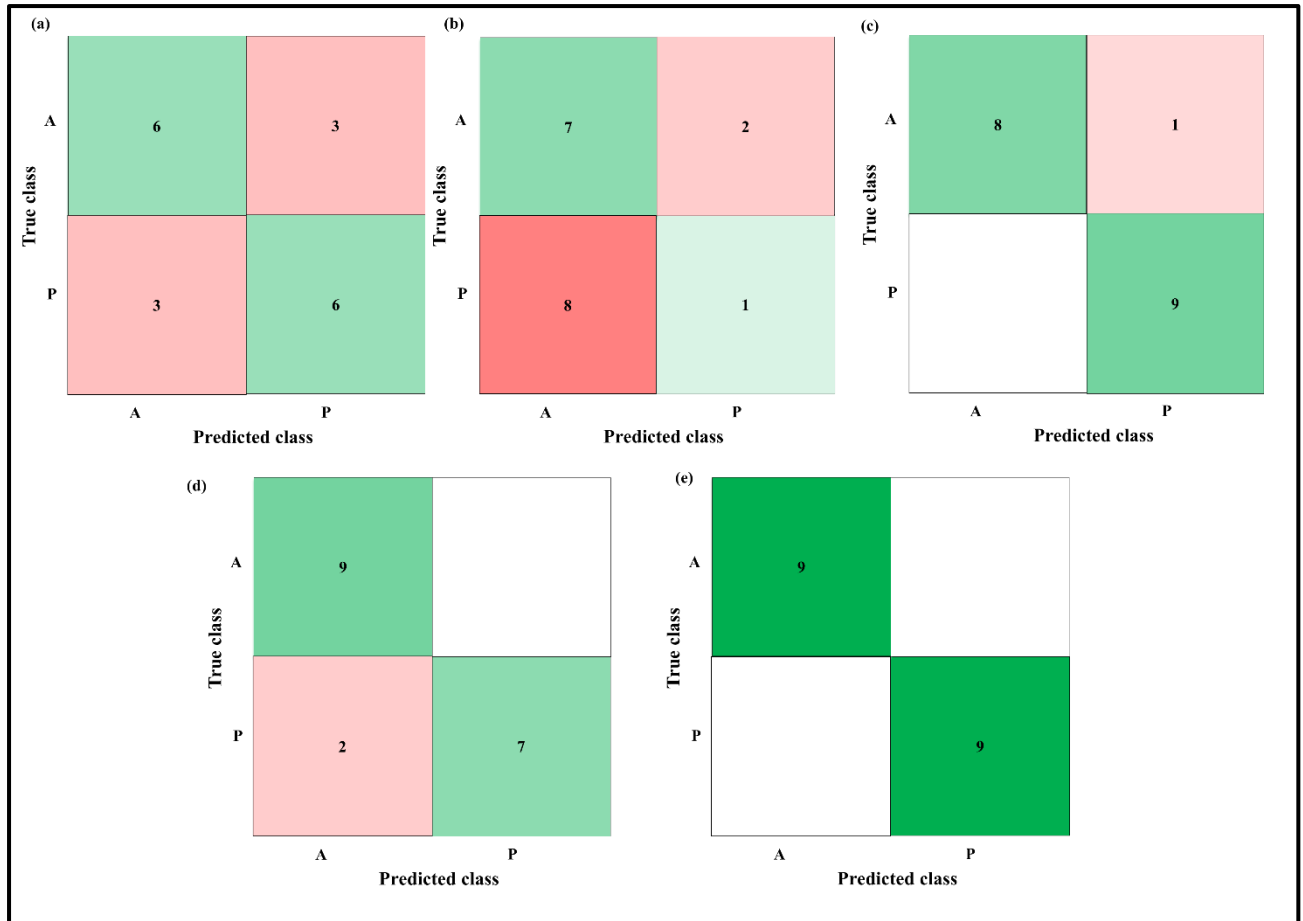


Figure 4.16. Confusion matrix result with a load of 6.7N for a) Naive Bayes b) Ensemble boosted trees c) Logistic regression d) KNN e) SVM

Table 4.4 Result Summary with a load of 6.7N

Machine Learning algorithm	Vibration data	Acoustic data	Vibro-acoustic data (Sensor fused data)
Naive Bayes	71.4%	66%	66.7
Ensemble boosted tress	50%	46.4%	44.4
Logistic regression	88.9%	74.6%	94.4
KNN	76.4%	72%	89.4
SVM	89.4%	74.2%	100%

4.4 Parallel, Angular, and Combined Misalignment Fault Classification

This is the first attempt to use vibro-acoustic sensor data fusion to segregate all 3 modes of misalignment fault under different operating conditions. 27 tests are performed, 9 tests for each failure mode. One of the innovative aspects of this experimental investigation is the use of the acoustic sensor in the parallel and combined misalignment classification. This study attempts to establish an even higher accuracy than the 98% percent accuracy reported by considering

combined misaligned case as well. Figure 3.1 shows the experimental set up used to perform the experiments. Initial alignment is done by using reverse dial indicator to remove previously existing misalignment if any. Figure 4.18 shows the reverse dial indicator.

Three defect conditions (Parallel, angular, and combined misalignment) are considered at three levels of severity. Three different speed levels: 1020, 1860 and 2580 rpm at constant loading (13.4N) condition is considered for this study. The amount of misalignment considered during investigation is presented in Table 4.5, these values are decided based on literature review.



Figure 4.17. Reverse Dial Indicator

Table 4.5 Defects Dimension.

Defect type	Unit	Levels		
		-1	0	1
Parallel	mm	0.3	0.5	0.7
Angular	degree	0.1	0.2	0.3
Combined		0.3 mm and 0.1 degree	0.5 mm and 0.2 degree	0.7 mm and 0.3 degree

4.4.1 Data Acquisition and Signal Processing

The eight channels multi-analyser (OROS-OR35, NVGATE software) is used to filter and analyse the recorded vibration and acoustic signals from MFS. While data was being collected from each signal, the sampling rate was 25.6KHz, and the sample durations were synchronized between the vibration and acoustic sensors. The signal acquisition is done for 10 seconds, and the acquired signals are passed through the analyser's built-in anti-aliasing filter. Time domain features namely skewness, crest factor, impulse factor, mean, clearance factor, shape factor, SINAD (signal to noise and distortion ratio), kurtosis, SNR (signal to noise ratio), standard deviation, RMS (root mean square), peak value, THD (Total harmonic distortion) are extracted from vibrational signal in X (radial), Z (axial) directions and acoustic signal data using matlab.

From vibrational and acoustic data, a total of 39-time domain features is extracted. After extraction of the features, feature level fusion is carried out and ranking of the features is performed using t test, 26 features out of 39 features are used based on their importance. Not all the features were sensitive towards the fault classification; hence manually varied the number of features and its effect on fault classification is observed. It is found that only 26 features were sensitive towards fault classification. It is also observed that addition of more features, resulted into decrease in fault classification accuracy. Table 4.6 shows the feature ranking using t test. In Table 4.6, Vib represents vibrational data and Aco represents acoustic data.

Table 4.6. Feature Ranking

Ranking	Features	t test score One-way ANOVA	Ranking	Features	t test score One-way ANOVA
1	X_Vib/Data_THD	4.5046	21	X_Vib/Data_ImpulseFactor	0.3261
2	Z_Vib /Data_ClearanceFactor	1.9230	22	X_Vib /Data_ClearanceFactor	0.3222
3	Z_Vib /Data_ImpulseFactor	1.8942	23	X_Vib /Data_Mean	0.2937
4	Z_Vib /Data_CrestFactor	1.8328	24	Aco_Vib /Data_RMS	0.2422
5	Aco_Vib /Data_Skewness	1.2597	25	Aco_Vib /Data_Std	0.2422
6	Z_Vib /Data_Kurtosis	1.2322	26	X_Vib /Data_ShapeFactor	0.2184
7	Aco_Vib /Data_CrestFactor	1.2080	27	Z_Vib /Data_PeakValue	0.1810
8	Aco_Vib /Data_ImpulseFactor	1.1108	28	X_Vib /Data_SINAD	0.1491
9	Aco_Vib /Data_ClearanceFactor	1.0632	29	X_Vib /Data_SNR	0.1485
10	Z_Vib /Data_Mean	1.0230	30	Z_Vib /Data_SNR	0.1171
11	Z_Vib /Data_ShapeFactor	1.0108	31	Z_Vib /Data_SINAD	0.1126
12	X_Vib /Data_Skewness	0.7895	32	X_Vib /Data_Kurtosis	0.0619
13	Aco_Vib /Data_SINAD	0.6792	33	Z_Vib /Data_RMS	0.0568
14	Aco_Vib /Data_ShapeFactor	0.6636	34	Z_Vib /Data_Std	0.0568
15	Aco_Vib /Data_SNR	0.6580	35	Aco_Vib /Data_PeakValue	0.0331
16	Aco_Vib /Data_Kurtosis	0.5996	36	Z_Vib /Data_Skewness	0.0152
17	Aco_Vib /Data_THD	0.4150	37	X_Vib /Data_Std	0.0031
18	Z_Vib/Data_THD	0.4036	38	X_Vib /Data_RMS	0.0031
19	Aco_Vib /Data_Mean	0.3365	39	X_Vib /Data_PeakValue	0.0031
20	X_Vib /Data_CrestFactor	0.3343			

First 26 Features are selected from total 39 features to train algorithms. Out of 26 features, seven features are from x directional vibration data, seven from z directional data and twelve from acoustic sensor data are selected. It is observed that the features derived from Z directional

vibrational data rank higher than other features, because axial vibration plays an important role in the detection of misalignment faults. The selected features are imported into classification learner platform of matlab. In classification learner app, the cross-validation model was selected. The complete data was split into 5 folds. Initially 4 folds (F1, F2, F3 and F4) were employed for training (80% of data) and 1-fold (F5) was used for testing (20% of data). Then in next step it takes F1, F2, F3 and F5 for training and then uses F4 for testing. This way, it uses all data for training. The results presented are of test set which includes nine parallel, nine angular and nine combined fault cases. This method suits best for small number of datasets.

4.4.2. Results and Discussion

In this section fault classification results of KNN, SVM and ensemble subspace classifier are discussed. To verify the accuracy of each algorithm for proper fault classification, confusion matrix, receiver operating characteristic (ROC) curve and the model prediction graphs are plotted.

Figure 4.18. shows the result of KNN. KNN classified the angular misalignment type perfectly, it is indicated in green colour but failed to classify the parallel and combined misalignment fault cases. Out of 9 combined fault cases, 8 classified accurately while 1 of the combined fault cases is classified as parallel, which is shown in pink colour in the column of parallel fault. This algorithm failed to identify parallel fault type, 3 of the 9 parallel faults misclassified as angular.

In confusion matrix, we can plot some subplots like True Positive and False Negative Rates plot and Positive Predictive Values and False Discovery Rates plot. Figure 4.18 (b) indicates the True Positive and False Negative Rates plot for KNN. In the last two columns on the right display summaries per true class. KNN classified the angular misalignment type perfectly so true positive rate is 100% and false negative rate is zero. While in case of parallel, 3 faults misclassified as angular, so true positive rate is 67% and false positive rate is 33%. In case of combined it is 89% true positive and 11% false negative.

Figure 4.18 (c) indicates the positive predictive values and false discovery rates plot. Below the table, the matrix displays summary rows. Positive predictive values for properly predicted points in each class are given in green, and false discovery rates for erroneously predicted points in each class are indicated in pink below. It is observed that none of the fault is misclassified as combined so positive prediction value is 100% and false discovery rate is 0. While the algorithm failed to segregate between parallel and angular, so false discovery rates are associated with angular and parallel fault cases and are 25% and 14% respectively.

Figure 4.18 (d) indicates the ROC curve which indicates true positive vs. false positive rate plot. The marker (dot in saffron color) on the plot indicates the output of the classifier currently selected. A right angle to the top left of the plot is a perfect outcome with no misclassified points. The region under the curve is an indicator of the classifier's overall efficiency. Larger area under curve values suggests better performance of the classifier. Here angular is positive class and other (parallel and combined) faults are negative classes. With a false positive rate of 0.17, the current classifier wrongly allocates 17% of observations to the positive class. A true positive rate of 1 show that the current classifier properly classifies 100% of the observations as positive. The accuracy of fault classification achieved using KNN is 85.2%.

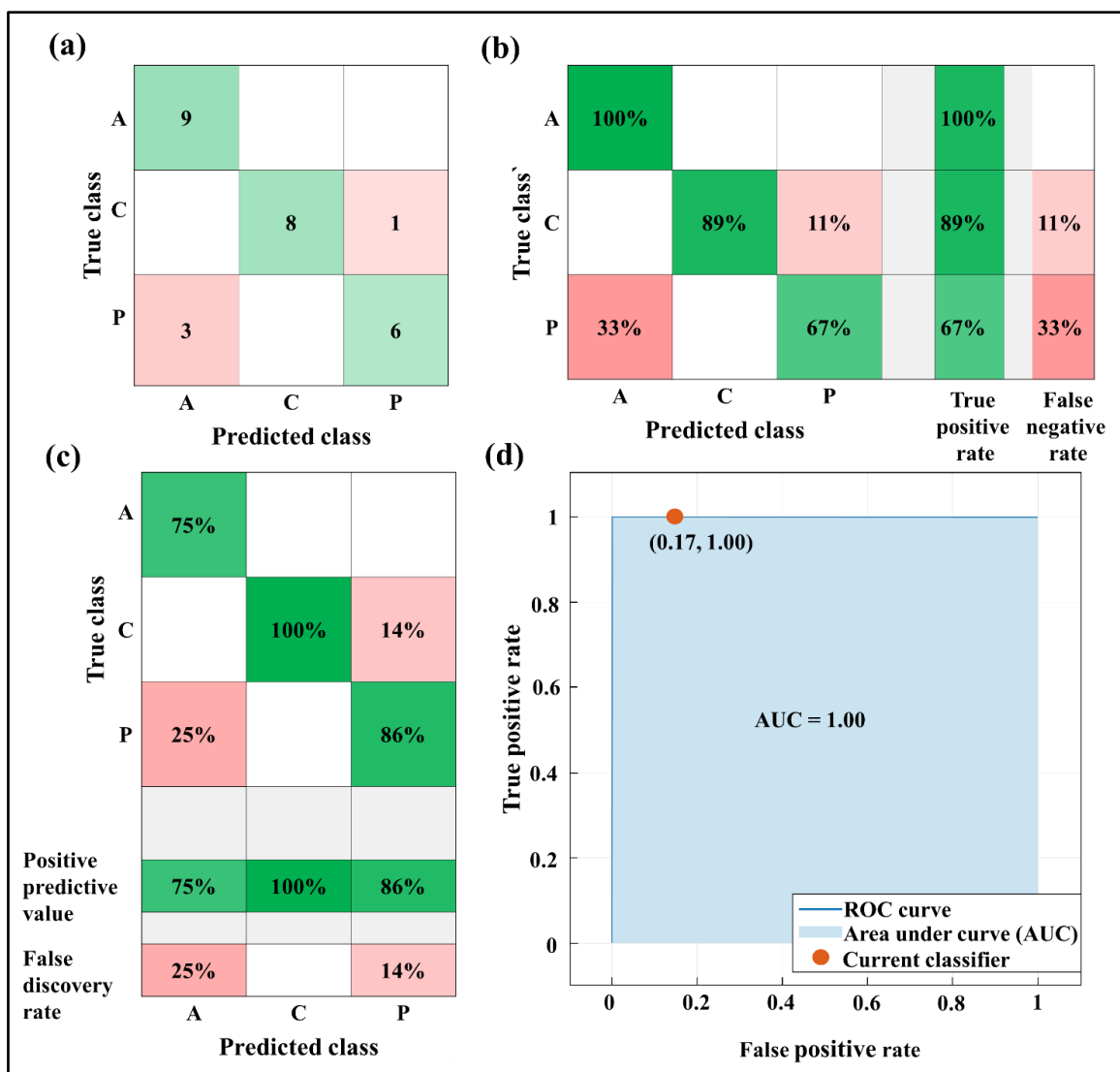


Figure 4.18. Result of KNN (a) Confusion matrix (b) True Positive Rates and False Negative Rates graph (c) Positive Predictive Values and False Discovery Rates graph (d) ROC curve.

Figure 4.19. shows the result of SVM, the fault classification accuracy achieved using SVM is 96.3%. SVM classified angular and parallel fault class accurately, only one of the combined

fault classes misclassified as angular. The algorithm was able to isolate the angular and parallel fault types. True positive rate for angular and parallel is 100%. None of class wrongly classified as combined or parallel so false discovery rate for combined and parallel is zero. Even though all angular faults classified accurately, the positive prediction value for angular is 90% and false discovery rate is 10%, because along with angular faults, one of the combined faults also identified as angular. The ROC plot shows the AUC is 1.0, it means, all angular faults are accurately categorized but there was false positive rate was 0.06 because of combined fault grouped into angular.

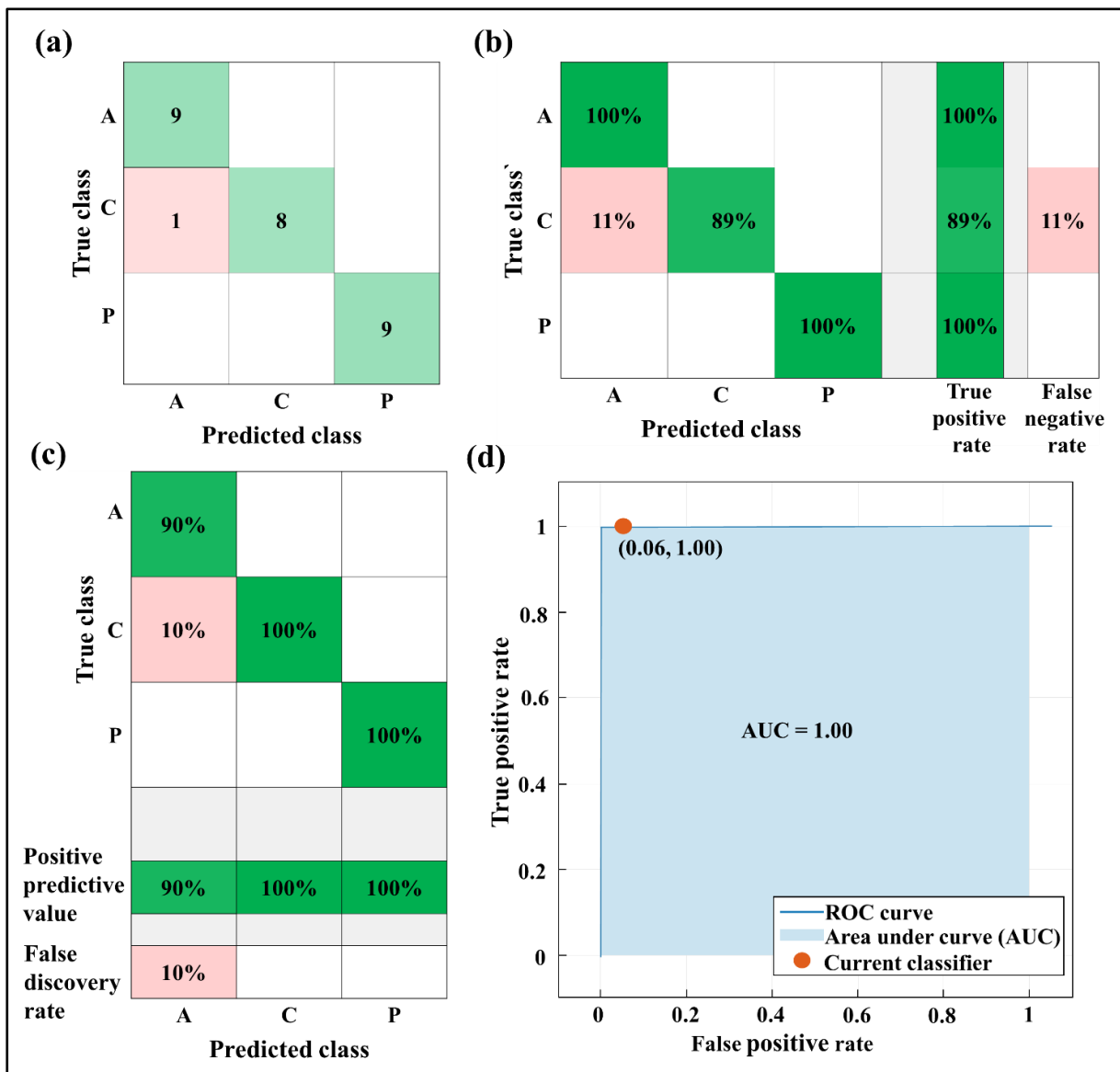


Figure 4.19. Result of SVM (a) confusion matrix (b) True Positive Rates and False Negative Rates graph (c) Positive Predictive Values and False Discovery Rates graph (d) ROC curve.

Figure 4.20. shows result for ensemble sub space discriminant algorithm. The correct fault classification accuracy is 100%. This algorithm classified the faults in parallel, angular, and

combined misalignment classes perfectly. In figure 4.20 (a) diagonal entries in green colour shows that each fault classified into accurate group. True positive rate (figure 4.20 b) is 100% for each case. False negative rate is zero. False discovery rate (figure 4.20 c) for predicted class is zero means none of the fault is misclassified, so positive prediction value is 100% for each class. The AUC is 100% and co-ordinates of predicted class is 0, 1. Which indicates that false positive rate is zero and predicted positive rate is 100% for each fault type.

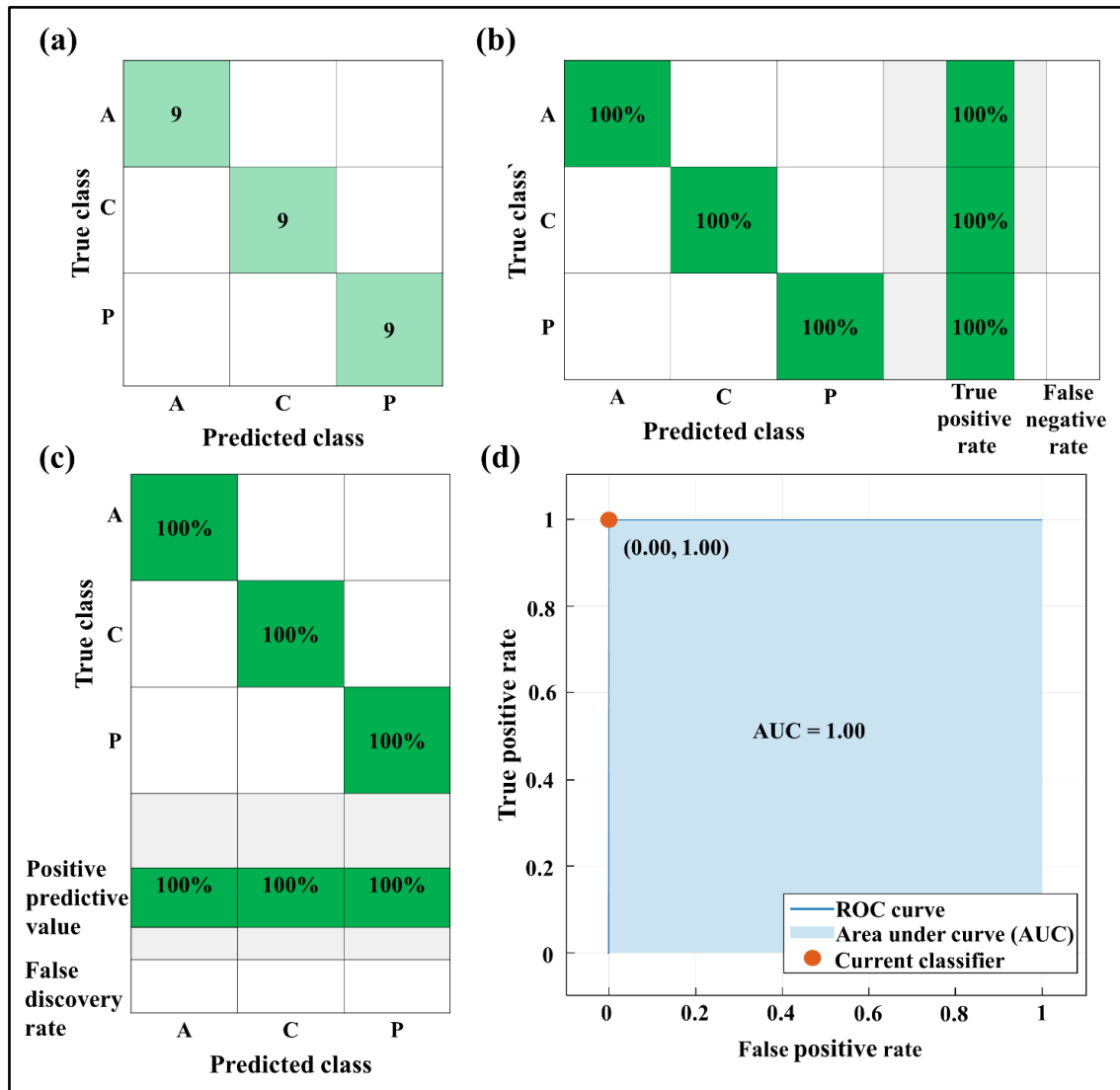


Figure 4.20. Result of Ensemble sub space discriminant (a) confusion matrix (b) True Positive Rates and False Negative Rates (c) Positive Predictive Values and False Discovery Rates graph (d) ROC curve.

The efficacy of the proposed method can be verified by the result summary table (Table 4.7), it shows the fault classification comparison between the individual vibrational data, acoustic data, and feature level sensor data fusion technique. The results indicate that the proposed method outperforms fault classification using vibration signal and acoustic signal separately.

Figure 9 depicts the accuracy per feature addition in order of ANOVA ranking. Ensemble subspace discriminant algorithm results are found to be the most consistent among all.

Table 4.7 Summary Table

Machine Learning algorithm	Vibration data	Acoustic data	Vibro-acoustic data (Sensor fused data)
KNN	76.6%	72.4%	85.2%
SVM	86.8%	78.4%	96.3%
Ensemble subspace discriminant	90.6%	80.4%	100%

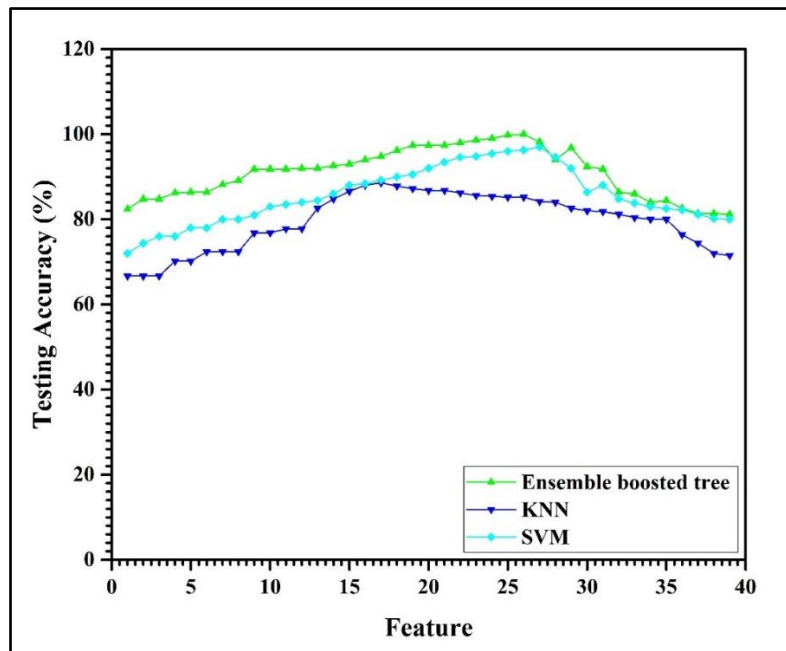


Figure 4.21. Feature Vs Testing accuracy plot

There could be several reasons why the load factor has no discernible impact on the accuracy of the SVM when using fused data:

- **Insensitivity to Load Variations:** The fault patterns or characteristics being analyzed through the fused data may be relatively insensitive to changes in the load factor.
- **Feature Independence:** The selected features for fault classification from the fused data may be inherently independent of the load factor. These features might capture fault-specific information that remains consistent across different load conditions.
- **Robust Fusion Technique:** The data fusion technique employed in this study may be robust in handling load variations and extracting fault-related information. The fusion process could effectively combine vibration and acoustic data, emphasizing fault-specific features while mitigating the impact of load-induced variations.

4.5. Conclusion

This study employs vibro-acoustic sensor data fusion method to detect various forms of misalignment under different operating conditions. Different load, speed and fault severity conditions are considered for the investigation, which may reproduce the actual conditions under which this fault occurs. The following conclusions can be drawn from the present investigation.

The following conclusions can be drawn from the binary fault classification.

- Results showed that fault classification accuracy is improved with sensor fusion technique compared to individual sensor data. The SVM outperforms the other algorithms towards the binary misalignment fault classification.
- As the study aims to check the performance of different algorithms with limited dataset, it is found that SVM gave accurate results. The results obtained from logistic regression and KNN for binary fault classification were 94.4% and 83.3% respectively. The other algorithm performance might have been affected by the dataset limitation, generally all ML algorithms uses 500+ repetitions.
- The accuracy obtained using SVM is 100%, the obtained results are better than the fault classification accuracy obtained by Umbrajkaar et al. They reported classification accuracy using SVM (97.72%) by employing the vibration data alone. So, the proposed method, vibro-acoustic sensor data fusion works best for misalignment fault classification.
- The addition of case 3 with load of 6.7N, supports the conclusion drawn and strongly encourages the application of the stated method in practical use scenario.
- The proposed methodology of fault classification works effectively for varying loading conditions.
- The results also proved the significance of acoustic signal data in misalignment fault classification. So, the acoustic sensor, which is non-contact type, can be used in the place where installing accelerometer is difficult.
- It is also observed that the axial vibrations which are generally ignored in bearing analysis play a remarkable role in misalignment fault classification. This outcome is well associated with the well-established conclusion about the role of axial vibration in the detection of misalignment faults.

- The application of acoustic signal in angular fault detection has been reported but the use of acoustic sensor in parallel misalignment classification is also one of the novel features of our experimental investigation.

A significant amount of work related to misalignment fault diagnosis has been reported till now; but limited research is reported on the parallel, angular, and combined fault classification in case of misalignment. From the present study, the following conclusions can be drawn.

- Ensemble sub space discriminant algorithm gives 100% accurate results when all three forms of misalignment are considered.
- One of the objectives of this work is comparing the performance of various algorithms with a limited dataset, it is observed that ensemble subspace discriminant produced the most accurate results when compared to the other algorithms presented in the article. KNN and SVM yielded results of 85.2 percent and 96.3 percent, respectively.
- It is observed from feature ranking table; axial vibration plays an vital role in misalignment fault classification.
- The 26 features are selected to train the different algorithms, out of 26, 12 features are from acoustic signal, which forms 46.15% of features used. This indicates that acoustic signal played a important role for fault classification. The results proved the significance of acoustic signal data in misalignment fault classification. So, the acoustic sensor, which is non-contact type, can be used in the places where installing accelerometer is difficult.
- The application of acoustic signal in angular fault detection has been reported [20] but the use of acoustic sensor in parallel and combined misalignment classification is also one of the novel features of our experimental investigation.

References

- [1] J. Ben Ali, N. Fnaiech, L. Saidi, B. Chebel-Morello, and F. Fnaiech, "Application of empirical mode decomposition and artificial neural network for automatic bearing fault diagnosis based on vibration signals," *Appl. Acoust.*, vol. 89, pp. 16–27, Mar. 2015.
- [2] M. Unal, M. Onat, M. Demetgul, and H. Kucuk, "Fault diagnosis of rolling bearings using a genetic algorithm optimized neural network," *Measurement*, vol. 58, pp. 187–196, Dec. 2014.
- [3] M. Delgado, A. Garcia, J. A. Ortega, J. J. Cardenas, and L. Romeral, "Multidimensional intelligent diagnosis system based on Support Vector Machine Classifier," in *2011 IEEE*

- International Symposium on Industrial Electronics*, 2011, pp. 2124–2131.
- [4] L. Saidi, J. Ben Ali, and F. Fnaiech, “Application of higher order spectral features and support vector machines for bearing faults classification,” *ISA Trans.*, vol. 54, pp. 193–206, Jan. 2015.
- [5] Vladimir N. Vapnik, *Statistical learning theory*. New York, New York, USA: Wiley, 1998.
- [6] B. Samanta, K. R. Al-Balushi, and S. A. Al-Araimi, “Artificial neural networks and support vector machines with genetic algorithm for bearing fault detection,” *Eng. Appl. Artif. Intell.*, vol. 16, no. 7–8, pp. 657–665, Oct. 2003.
- [7] V. Sugumaran and K. I. Ramachandran, “Automatic rule learning using decision tree for fuzzy classifier in fault diagnosis of roller bearing,” *Mech. Syst. Signal Process.*, vol. 21, no. 5, pp. 2237–2247, Jul. 2007.
- [8] R. S. Gunerkar and A. K. Jalan, “Classification of Ball Bearing Faults Using Vibro-Acoustic Sensor Data Fusion,” *Exp. Tech.*, vol. 43, no. 5, pp. 635–643, Oct. 2019.
- [9] H. S. Haroun S, Seghir AN, Touati S, “Misalignment fault detection and diagnosis using AR model of torque signal,” in *IEEE 10th International Symposium on Diagnostics for Electrical Machines Power Electronics and Drives (SDEMPED)*, 2015, pp. 322–326.
- [10] C. Kumar, G. Krishnan, and S. Sarangi, “Experimental investigation on misalignment fault detection in induction motors using current and vibration signature analysis,” in *2015 International Conference on Futuristic Trends on Computational Analysis and Knowledge Management (ABLAZE)*, 2015, pp. 61–66.
- [11] A. K. Verma, S. Sarangi, and M. Kolekar, “Misalignment Fault Prediction of Motor-Shaft Using Multiscale Entropy and Support Vector Machine,” 2015, pp. 359–370.
- [12] J.-L. Lin, J. Y.-C. Liu, C.-W. Li, L.-F. Tsai, and H.-Y. Chung, “Motor shaft misalignment detection using multiscale entropy with wavelet denoising,” *Expert Syst. Appl.*, vol. 37, no. 10, pp. 7200–7204, Oct. 2010.
- [13] M. Chandra Sekhar Reddy and A. S. Sekhar, “Detection and monitoring of coupling misalignment in rotors using torque measurements,” *Measurement*, vol. 61, pp. 111–122, Feb. 2015.

- [14] A. K. Verma, S. Sarangi, and M. H. Kolekar, “Experimental Investigation of Misalignment Effects on Rotor Shaft Vibration and on Stator Current Signature,” *J. Fail. Anal. Prev.*, vol. 14, no. 2, pp. 125–138, Apr. 2014.
- [15] J. L. Ferrando Chacon, E. Artigao Andicoberry, V. Kappatos, G. Asfis, T.-H. Gan, and W. Balachandran, “Shaft angular misalignment detection using acoustic emission,” *Appl. Acoust.*, vol. 85, pp. 12–22, Nov. 2014.
- [16] Y.-S. Lee and C.-W. Lee, “Modelling and Vibration Analysis of Misaligned Rotor-Ball Bearing Systems,” *J. Sound Vib.*, vol. 224, no. 1, pp. 17–32, Jul. 1999.
- [17] R. Isermann, “Fault diagnosis of machines via parameter estimation and knowledge processing—Tutorial paper,” *Automatica*, vol. 29, no. 4, pp. 815–835, Jul. 1993.
- [18] A. K. Jalan and A. R. Mohanty, “Model based fault diagnosis of a rotor–bearing system for misalignment and unbalance under steady-state condition,” *J. Sound Vib.*, vol. 327, no. 3–5, pp. 604–622, Nov. 2009.
- [19] M. Monte, F. Verbelen, and B. Vervisch, “Detection of Coupling Misalignment by Extended Orbits,” 2015, pp. 243–250.
- [20] A. Kumar Jalan, S. Patil, and G. Mittal, “A Review on Fault Diagnosis of Misaligned Rotor Systems,” *Int. J. Performability Eng.*, vol. 16, no. 4, p. 499, 2020.
- [21] T. W. Way, B. Sahiner, L. M. Hadjiiski, and H.-P. Chan, “Effect of finite sample size on feature selection and classification: A simulation study,” *Med. Phys.*, vol. 37, no. 2, pp. 907–920, Jan. 2010.
- [22] W. Liu, K. He, Q. Gao, and C. Liu, “Application of EMD-Based SVD and SVM to Coal-Gangue Interface Detection,” *J. Appl. Math.*, vol. 2014, pp. 1–6, 2014.
- [23] A. M. Umbrajkaar, A. Krishnamoorthy, and R. B. Dhumale, “Vibration Analysis of Shaft Misalignment Using Machine Learning Approach under Variable Load Conditions,” *Shock Vib.*, vol. 2020, pp. 1–12, Jul. 2020.
- [24] C. Junsheng, Y. Dejie, and Y. Yu, “The application of energy operator demodulation approach based on EMD in machinery fault diagnosis,” *Mech. Syst. Signal Process.*, vol. 21, no. 2, pp. 668–677, Feb. 2007.

RUL PREDICTION OF TAPER ROLLER BEARING UNDER INDUSTRIAL SETTINGS

5.1 Introduction

The requirements for system stability, efficacy, and security have been continuously growing in recent years as various systems continue to evolve in terms of complexity and integration. The identification of current health status according to the characteristics offered by monitoring big data is of major significance for the implementation of system health management in view of industrial big data trends. It is essential to efficiently monitor and assess a system's health condition and accurately anticipate its Remaining Useful Life (RUL) based on the monitoring data to reduce the probability of system failures and lower the cost of operation and maintenance.

A single sensor was used in most earlier investigations on system RUL prediction. However, in actual system operation, relying on a single sensor output is frequently insufficient to fully describe the system's probable degradation mechanism. Numerous stochastic elements, such as the system's complicated structure and the dynamic operating environment, contribute to the accuracy and unreliability of RUL prediction results[1]. It is frequently required to simultaneously monitor the system using several sensors to thoroughly evaluate the health state of the system and precisely anticipate its RUL[2]. From the perspective of fusion content, RUL prediction approaches based on multi-sensor information fusion are essentially divided into three categories: data fusion [3], decision fusion[4], and model fusion [5]. Multiple signals are combined using techniques that apply a data fusion approach to define the system's deteriorated properties for RUL predictions [6]. To assess the degradation performance of an engine, Ren first combined data from numerous sensors into a composite health indicator. Ren then used a linear Wiener process to simulate the degradation of the composite health indicator and estimated the lifetime of the engine[7]. However, it should be mentioned that the effectiveness of data-level fusion is highly related to the quality of the raw data [8], [9]. Multiple degraded data are used in decision fusion approaches to run RUL prediction modelling separately. Additionally, they use evidence reasoning and rule-based fusion methods to arrive at the final RUL[10]. They combined the translated data with the field data using the evidence reasoning algorithm, producing extremely reliable result. It should be noticed that the designed decision function impacts how well decision-level fusion performs [11] and that there is no exact

correlation between monitoring data and probable health states [12]. A multidimensional stochastic process degradation model or a Copula function stochastic correlation model is constructed using the model fusion approach using data from several sensors to forecast RUL [12]. Peng et al. [13] proposed a multivariate Wiener process to forecast the RUL of a multi-sensor fusion. A binary degradation model was developed by Fang et al. [14] based on the Wiener process and the Copula function; in this model, the Wiener process was used to describe the edge distribution of each degraded data and the Copula function was used to explain the correlations between degraded data. For the linear Wiener process, Wei et al. [5] suggested a centralized multi-sensor life prediction fusion model. They claimed that the accuracy of the projected results of the fusion model was higher than that of the results of a single sensor.

In the present chapter, the RUL estimation of a taper roller bearing is performed. The data is collected at NBC Bearing Jaipur, under actual industrial settings. The test setup allows 5 milliradians of misalignment to accommodate shaft deflection under severe accelerated tests. All the test bearings developed natural failure, and the data collection was run to failure. A total of 3 bearings data is used for the analysis. Two new approaches have been proposed in this chapter as two case studies. In both cases, data fusion is carried out to train the discussed algorithms. In Case I, features are extracted using wavelet scattering of time series data and prediction is done by employing xgboost regression. The results are also compared with wavelet scattering-LSTM approach. While in case II, time domain features are extracted, HI is selected based on feature ranking and nonlinear autoregressive network with exogenous inputs neural network (NARX-NN) is used for prediction.

5.2 Theoretical Background

5.2.1 Wavelet Scattering Transform (WST)

A popular technique for time-frequency analysis is the wavelet transform, which has the benefit of remaining stable and multi-scale in the presence of local deformation. It can efficiently extract local features from signals, but it is dynamic and is prone to leaving out important signal features. The wavelet scattering transform (WST), presented by Mallat [15], is a superior time-frequency analysis method based on the wavelet transform. The process is just an iterative combination of a deep convolution network made up of low-pass filter averaging, a complex wavelet transforms, and modulus operation [16]. It overcomes the disadvantage of changing over time with the added benefits of translation invariance, local deformation stability, and rich feature information representation. For any given time-domain signal, x , the operation of WST can be described as follows:

RUL prediction of taper roller bearing under industrial settings

1. At first, x is convolved with the dilated mother wavelet ψ , which has the center frequency of λ , to calculate the WST. This operation can be expressed as $X * \psi_\lambda$. Here, the average of the convolved signal, which oscillates at a scale of $2j$, is zero.
2. After that, a nonlinear operator, such as a modulus, is applied to the convolved signal to eliminate these oscillations (i.e., $|X * \psi_\lambda|$). This procedure is used to make up for the information lost due to down sampling by doubling the frequency of the given signal.
3. Finally, a low-pass filter ϕ is applied to the resultant absolute convolved signal, which is equivalent to $|X * \psi_\lambda| * \phi$.

Therefore, for any scale ($1 \leq j \leq J$), the first-order scattering coefficients are calculated as the average absolute amplitudes of wavelet coefficients over a half-overlapping time window having the size $2j$. This can be written as (5.1)

$$S_{1x}(t, \lambda_1) = |X * \psi_{\lambda_1}| * \phi \quad (5.1)$$

The invariance ability will undoubtedly decrease when the high-frequency components are restored as a result of the aforementioned approach. By repeating the discussed steps on $|X * \psi_\lambda|$, the scattering coefficients for the second order can be calculated as (5.2)

$$S_{1x}(t, \lambda_1, \lambda_2) = ||X * \psi_{\lambda_1}| * \psi_{\lambda_2}| * \phi \quad (5.2)$$

The wavelet scattering coefficients for higher orders, where $m \geq 2$, can be computed by iterating the mentioned process. This can be expressed as (5.3):

$$S_{1x}(t, \lambda_1, \lambda_2, \dots, \lambda_m) = |||X * \psi_{\lambda_1}| * \psi_{\lambda_2}| \dots \psi_{\lambda_m}| * \phi \quad (5.3)$$

The resultant scattering coefficients can be found by accumulating all of the coefficient sets of the scattering transform generated from the 0th to mth order, as shown in (5.4)

$$S_x = \{S_{0x}, S_{1x}, \dots, S_{mx}\} \quad (5.4)$$

The basic steps of computing the wavelet scattering coefficients up to level 2 are illustrated in Figure 5.1. Here, the final feature matrix will be found by accumulating all the features from levels S_{0x} , S_{1x} , and S_{2x} .

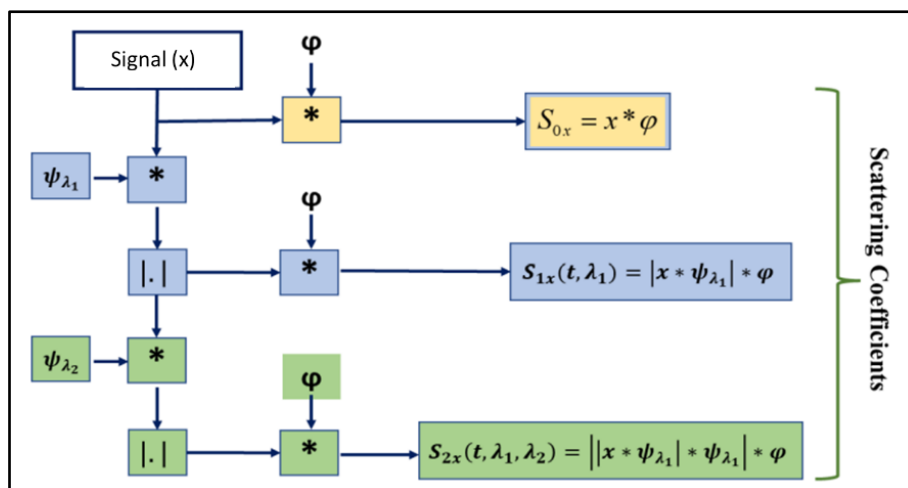


Figure 5.1 The schematic diagram of the feature extraction procedure with the second-order WST.

The zero-order scattering coefficients, denoted by the symbol S_{0x} , assess the local translation invariance of the input signal. Each stage's averaging operation results in the loss of the high-frequency components of the convolved signal, while the subsequent stage's convolution with the wavelet allows for their recovery. The WST approach is stable due to time warp deformation, energy conversion, and contraction, making it suitable for various classification and regression tasks and robust in noisy environments.

As a result of implementing the low-pass filter, ϕ , the network is invariant to translations up to a certain invariance scale. The resultant features from S_x inherit properties of wavelet transforms, which makes them stable against local deformations. This also allows the scattering decomposition to detect subtle changes in bearing signals' amplitudes under different conditions and makes the regression task easier. Therefore, the wavelet scattering network can be used as an effective way to create robust representations of different bearing conditions that minimize the differences under the same condition and maintain enough discriminability to distinguish among different bearing conditions and its predictions. Wavelet scattering networks and CNNs have a similar structural design, but there are two key differences: the filters are predetermined rather than learnt, and the features are not just the results of the final convolution layer but also the sum of all the layers. According to earlier studies, the first two levels of the scattering coefficient contain nearly 99% of the energy, with the energy rapidly decreasing as the layer levels increase.

5.2.2 Theory of NARX network

NARX neural network is another class of ANNs which are suitable to model nonlinear systems and time series[17]. The NARX network is a dynamic neural network that contains recurrent feedbacks to the input layer from a number of network layers[18]. Equation 5.5 can be used to represent NARX mathematically.

$$y(n + 1) = f[y(n), \dots, y(n - d_y); u(n), \dots, u(n - d_u)] \quad (5.5)$$

where $y(n), u(n) \in R$ are the input and output of the model at discrete time step n respectively, and $d_u \leq 1$ is the input and $d_y \leq 1, d_y \leq d_u$ is the output delay[19]. With one time series operating as both the input and the output for the NARX architecture depicted in Figure 5.2, the general NARX network equation is represented below (5.6).

$$y(n + 1) = f_0 \left[b_0 + \sum_{h=1}^{N_h} W_{ho} \cdot f_h \left(b_h + \sum_{i=0}^{d_u} W_{ih} \cdot u(n - i) + \sum_{j=0}^{d_y} W_{jh} \cdot y(n - j) \right) \right] \quad (5.6)$$

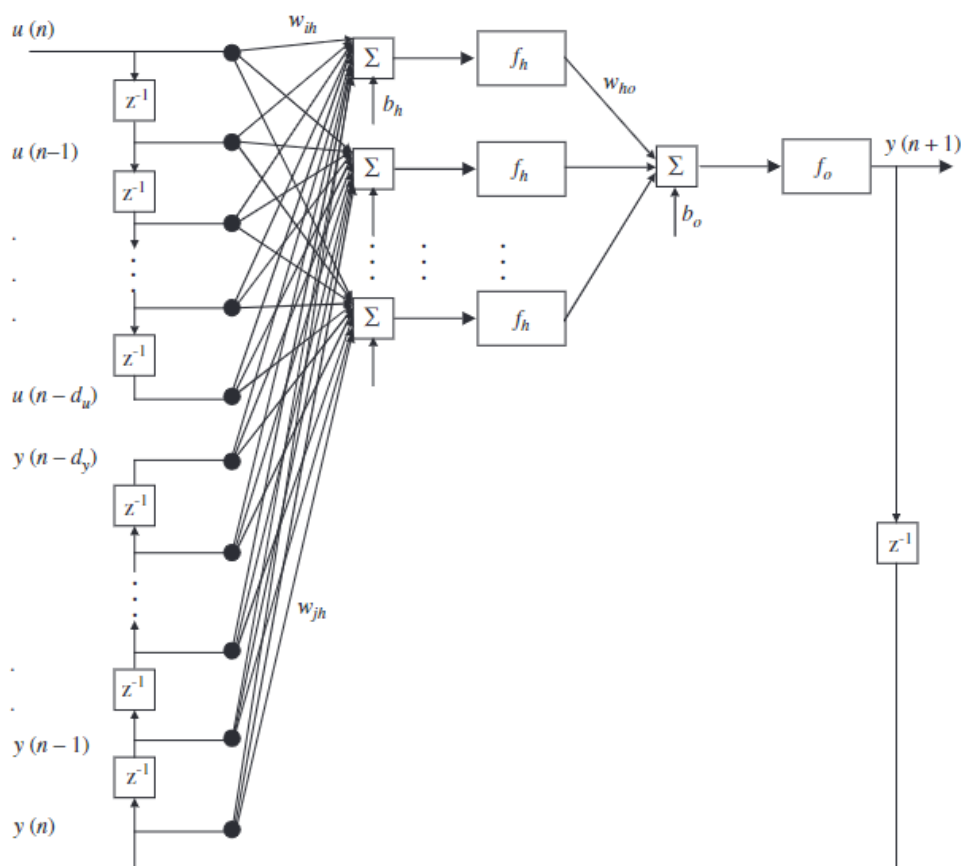


Figure 5.2 The architecture of NARX neural network[19].

W is the weight of the connections between the input units and the hidden units. NARX network can be used in multi-time series input and multi-time series output applications. NARX network is trained by Levenberg–Marquardt method. A NARX network's usual structure is made up of feedback connections from the output neuron. The NARX network is a feedforward

time delay neural network (TDNN) without delayed feedback loops when used for a univariate time-series prediction. In this case, the output memory order of the NARX neural network is reduced to zero.

5.3 Experimental Set up

Figure 5.3 indicates the experimental setup used in the investigation. Figure 5.4 shows the mounting of sensor on bearing housing. The test setup used is from NBC bearing testing premises, Jaipur. The taper roller bearing (model: 30205, NBC make) is used for the testing. From bearing model nomenclature, 3 indicates type of bearing i.e., taper, 02 is the diametric series which defines the thickness and 05*5 is the bore diameter. A tri-axial sensor is used to capture the vibrations. Figure 5.5 shows the schematic of the setup and loading condition for the test. F_a is the axial force and F_r is the radial force. As seen in figure 5.5, 2 support bearings and 2 test bearings are used in the study. Support bearings are designated as S1 and S2, while test bearings are designated as #1 and #2. Support bearings are used because the test conditions are high load severe accelerated test. ISO VG68 oil is used for lubrication. The lubrication oil supply was 1 litre/min. 1.8 tons of radial load is applied on each bearing and 0.58-ton load is applied in axial direction from both sides as depicted in figure 5.5. The speed was set to 4000 rpm. The oil temperature was recorded to be 70 degrees. The setup has 1 milli radians inherent misalignment to accommodate the deflection of shaft and to avoid unbalance issue.



Figure 5.3 Experimental Setup.



Figure 5.4 Sensor Mounting and Bearing Housing.

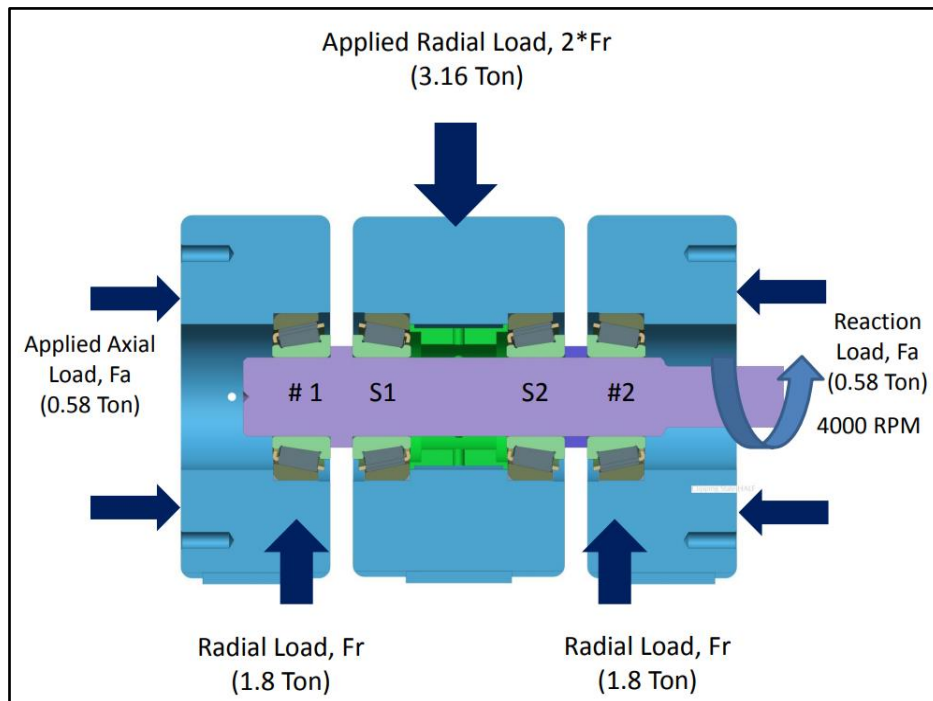


Figure 5.5 Set-up.



Figure 5.6 Test bearing: Taper roller bearing (NBC make).

Table 5.1 Specifications of the Test Bearing

Sr.no.	Parameter	Specification
1	Type of product	Taper Roller Bearing
2	Inside diameter (d) (mm)	25
3	Outside diameter (D) (mm)	52
4	Width (mm)	16.25
5	Bearing weight (kg)	0.148
6	Model no.	30205 (NBC Bearing)

5.4 Proposed Methodology

A framework for RUL prediction of taper roller bearing of NBC bearing, Jaipur with the vibrational signal is illustrated in Figure 5.7. The fault developed naturally in the bearing. The bearing data for three-axis is collected. The overall method is split into multiple phases, including data collection, processing of the vibrational signal data in time domain and frequency domain, and then resampling it, calculating the scattering coefficient using WST, training the ensemble ML classifiers (xgboost) and evaluating the model performance. The vibrations are captured and recorded using a tri-axial accelerometer and ONOSOKI data acquisition system. The data was captured from healthy to failure condition. With every regular interval of 10 mins, 1 second data was recorded with the sampling frequency of 20KHz. The vibrations are recorded in 2 radial and 1 axial direction. Taper roller bearing supports axial as well as radial forces. So, unlike ball bearing, we need axial vibrations captured as well. The captured signal is preprocessed, and then noise was removed using filters. The performance of the xgboost algorithm is tested using R^2 error.

RUL prediction of taper roller bearing under industrial settings

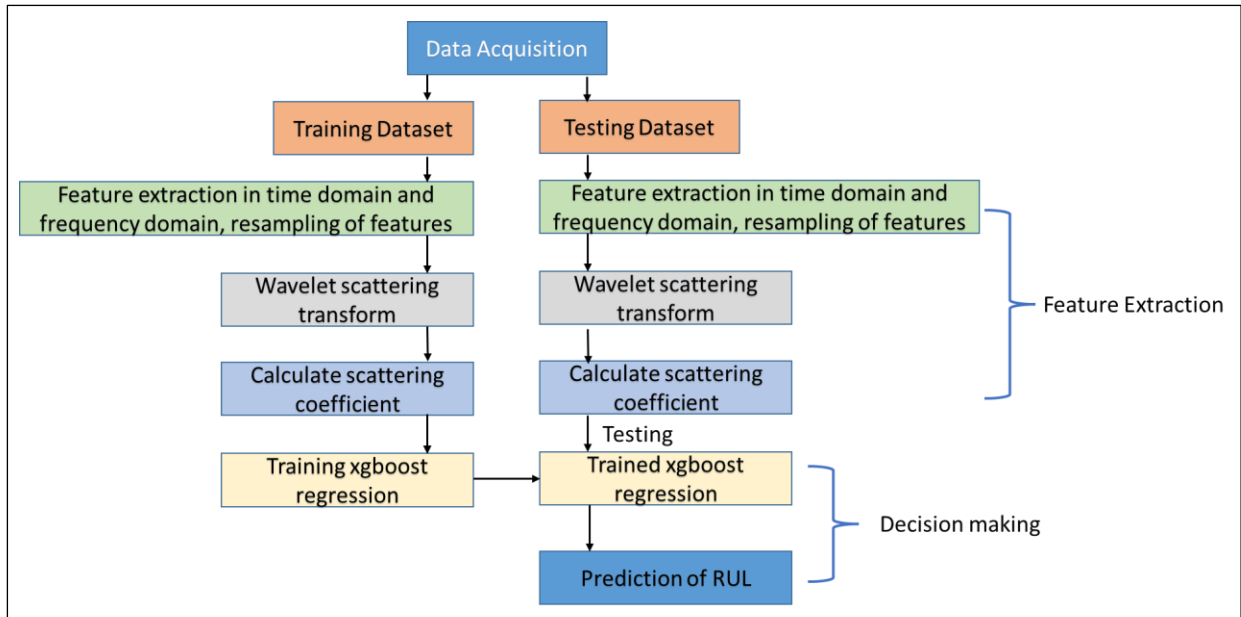


Figure 5.7 Flowchart of the proposed method for case I: wavelet scattering xgboost approach.

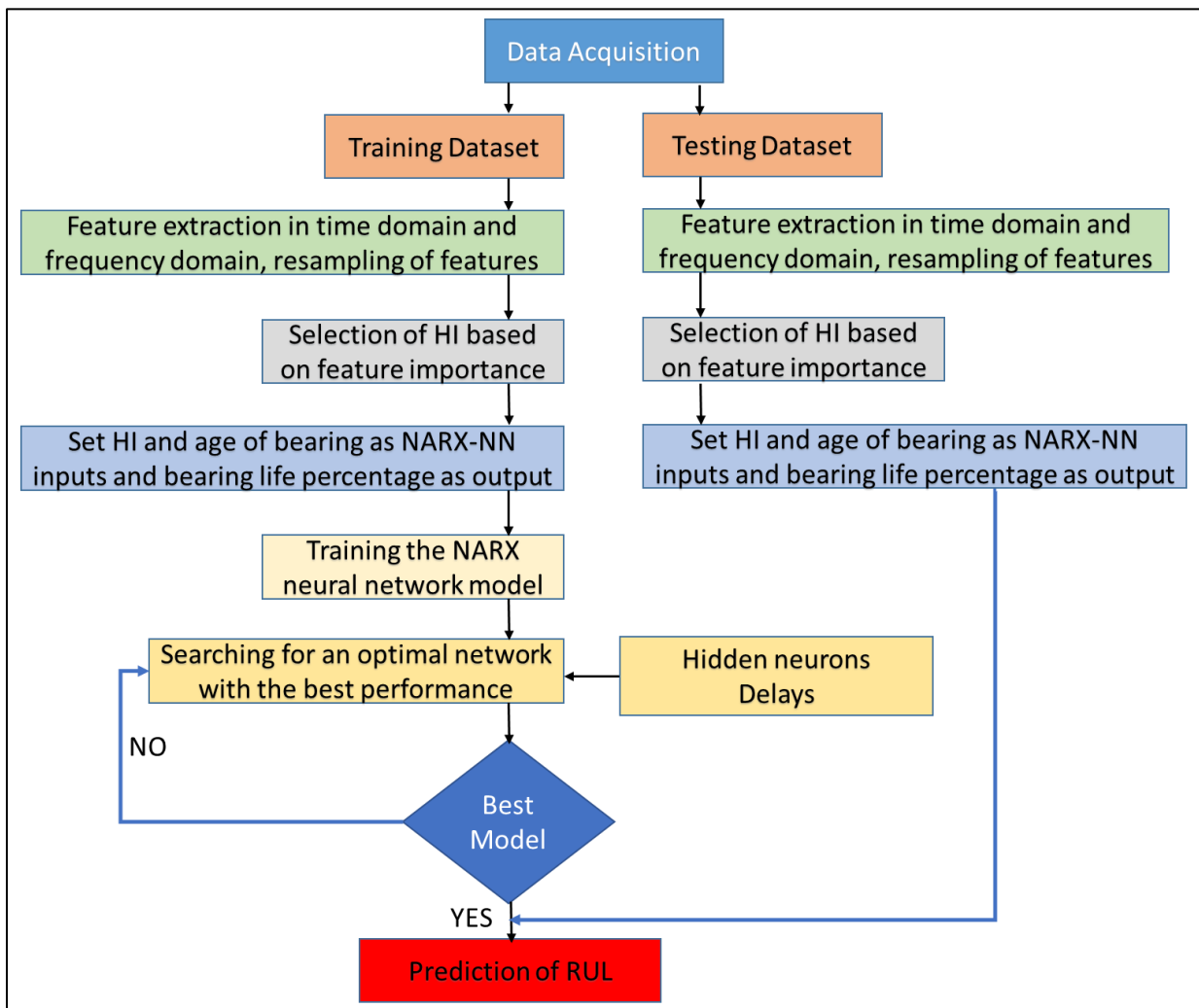


Figure 5.8 Flowchart of the proposed method for case II time domain-based HI and NARX.

In proposed case II, the time domain and feature domain features are extracted. The extracted features are ranked based on their monotonicity and Trendability. The best feature is selected as designated as HI. The HI and age of bearing is given as input to the NARX neural network and bearing life percentage as output. The algorithm is trained on given input and output vectors. The algorithm performs iterations until it gets an optimal network with the best performance of performance indicator. Then training validation accuracy is checked and the best model is selected. If the error is high, then more hidden layers will be added and the algorithm continues iterations until it gets best model. Once the model is selected then it is tested on a test dataset and prediction is made. Finally, a comparison is made between proposed methods. The data used for the present study is collected in industry and in actual industrial settings.

5.5 Results and Discussion

5.5.1 Wavelet Scattering-xgboost Approach

In the present investigation, data level fusion is carried out. The vibration signals in 2 radial and 1 axial direction are concatenated. 70% of the data is used for training and 30% of the data is used for testing. Signal processing is carried out and features in time domain and frequency domain are extracted. To increase the feature set, resampling of features is performed using windowing function. The window length is set as 10 for resampling. After features are resampled, wavelet scattering is performed. It is a knowledge-based method with a convolution neural network-like topology. It offers real-valued signal features with low variance, which are typically required for prediction applications. These signals maintain information at high frequencies and are resistant to signal deformation. To create low-variance representations of time series, wavelet scattering propagates data through several wavelet transforms, nonlinearities, and averaging. Without sacrificing class discriminability, wavelet time scattering produces signal representations insensitive to input signal shifts. Matlab 2020 version is used for the analysis. All three bearings had an outer race defect.

With a Q factor of [8 1], a two-layer scattering network ($m = 2$) is used. The 0th channel is the initial signal, while the subsequent channels produce the final scattering coefficients. The original signal is represented by the 0th channel, via which the wavelet scattering coefficients are obtained. In comparison to other scattering orders, the zeroth order wavelet scattering coefficients' modulus contains the majority of the signal energy and is the most accurate approximation of the original signal. Additionally, the amount of scattering has an impact on the signal's energy. Therefore, the energy of the high scattering coefficients will be smaller. It

RUL prediction of taper roller bearing under industrial settings

is possible to think of a wavelet as a band-pass filter, and its dilated version as a dilated band filter. In contrast to the wavelet, which catches high-frequency components and greater signal details, the scaling function or low-pass filter only records the lower signal details. Therefore, at each level, the signal's finer features are retrieved. The difference between the raw receiver signal strength indicator (RSSI) of a single measurement at a reference points (RP) and its zeroth order scalogram is depicted in Figure 5.12. AP stands for access points.

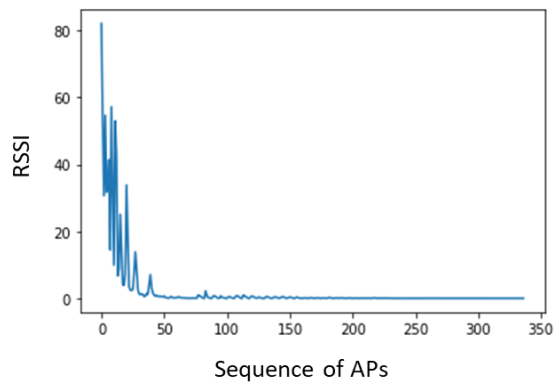


Figure 5.9 RSSI repartition.

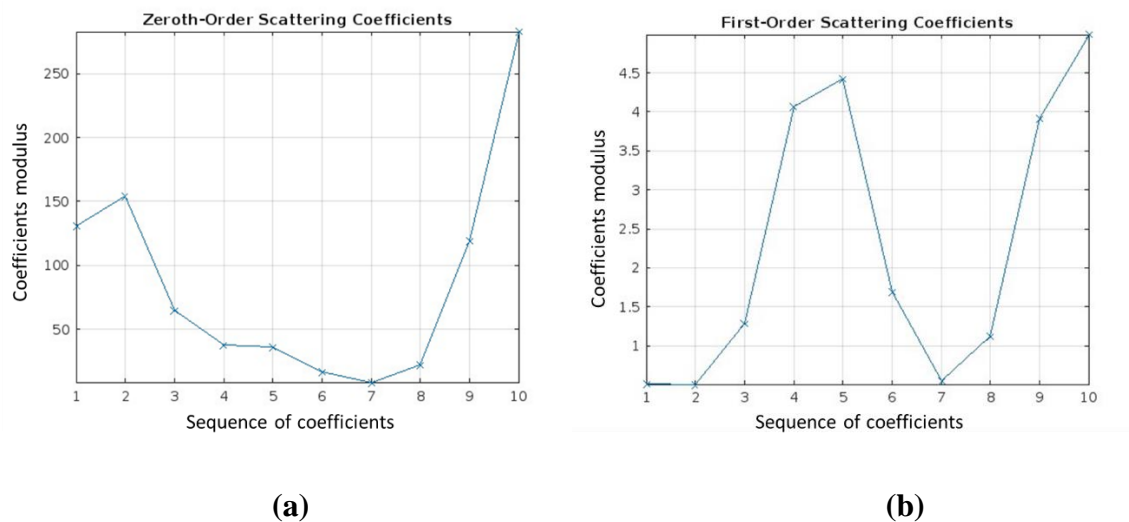


Figure 5.10 Time series bearing data, (a) 0th and (b) 1st order scattering coefficients of the outer race faulty conditions.

Figure 5.10 represents the 0th and 1st order scattering coefficients of an RSSI measurement. The result of the scattering transform is a vector of 10 elements. The entire scattering process begins with the input signal being convolved with a dilated wavelet as stated in Equation 5.1. The modulus of this wavelet is then convolved with the averaging function to produce the first scattering order. To generate the scattering coefficients modulus of first order, the modulus of this convolution result is computed, and the result is averaged using the low-pass filter.

RUL prediction of taper roller bearing under industrial settings

The morlet wavelet is utilized for wavelet decomposition, and the invariance scale value is set to 0.5 s. Figure 5.11 displays the fundamental wavelet and the generated two-layer wavelet scattering network with $Q1 = 8$ and $Q2 = 1$. In terms of the invariance scale and wavelet octave resolution, this architecture preserved the most signal information for prediction when compared to other configurations.

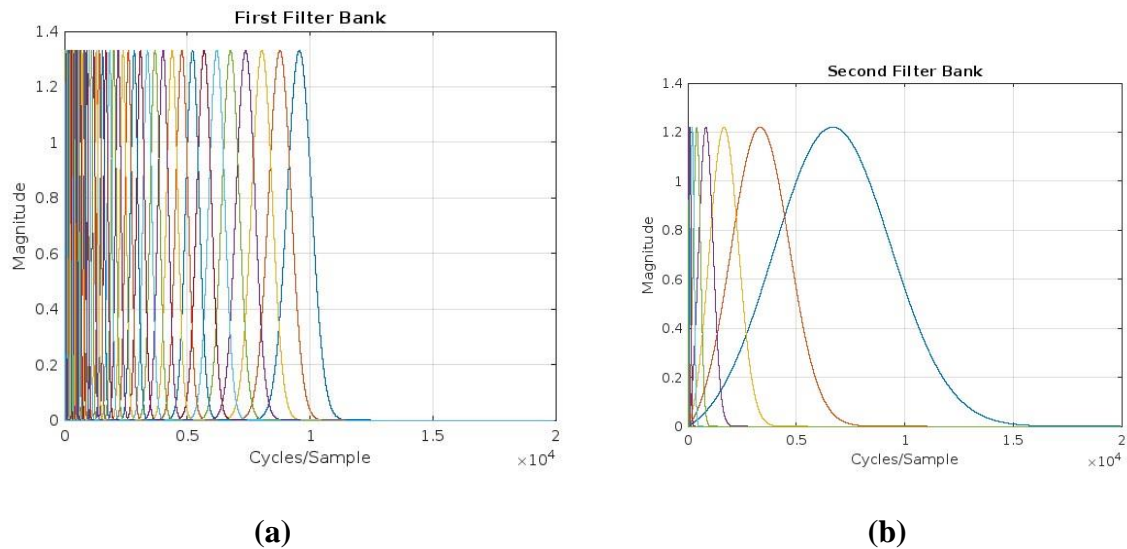


Figure 5.11 (a) (b) Frequency response of the first and second filter banks with eight and one wavelets per octave respectively.

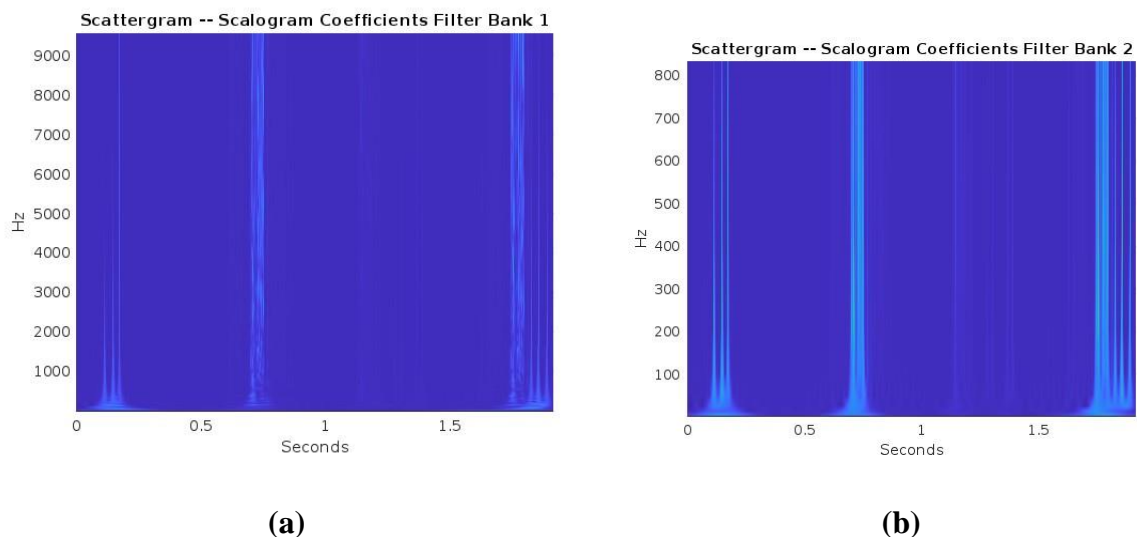


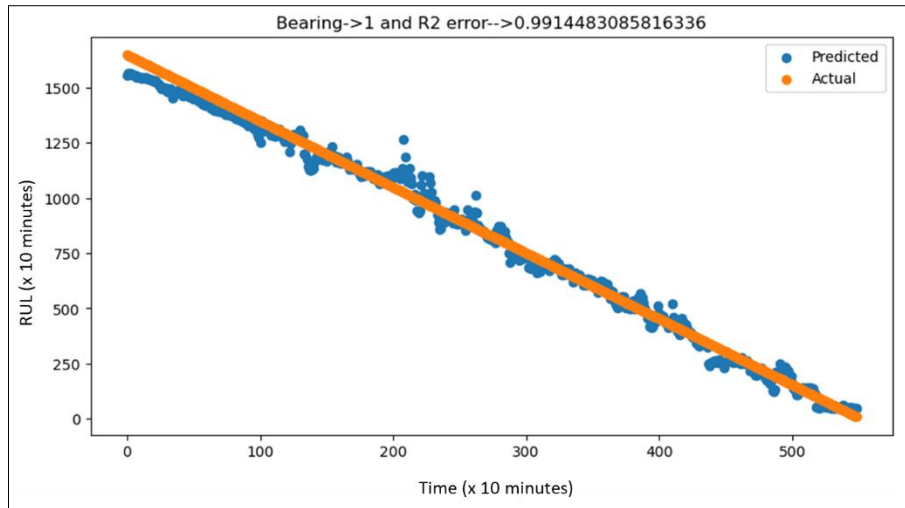
Figure 5.12 (a) Scattering coefficients scattergram for filter bank 1 (b) Scattering coefficients scattergram for filter bank 2.

Figure 5.12 (a), (b) indicates scattering coefficients scattergram for filter bank 1 and filter bank 2 respectively. It clearly depicts that the fault has occurred in the bearing. The input signal in the case of the scalogram coefficients and the lowpass filtering of the input signal using the scaling function in the case of the scattering coefficients, respectively, correspond to the zeroth

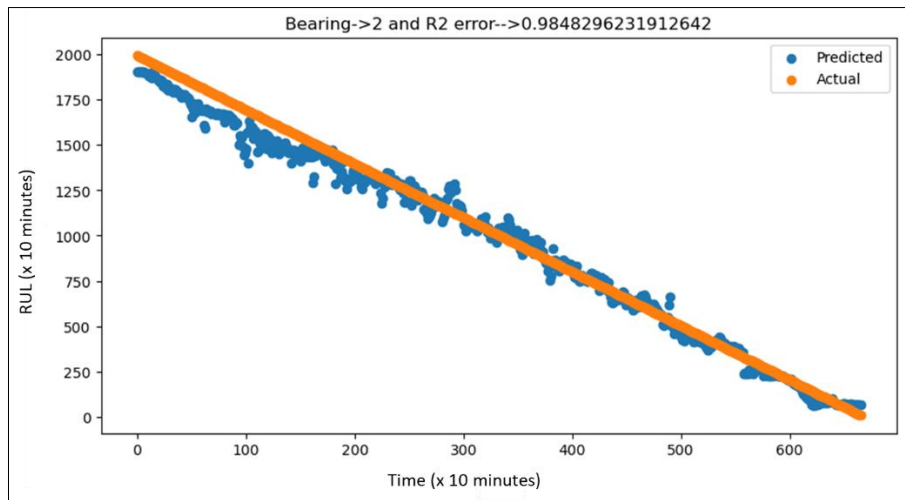
filter bank if filter bank is equal to 1. Figure 5.10 (b) shows the visualization of Equation 5.1 and represents the first order scattering coefficients. Figure 5.11 shows the analysing frequency interval of wavelet scattering, which is 2–10000 Hz, the half of maximum sampling rate, obvious features are seen in the plot.

These scattering coefficient matrix and age of bearing forms an input vector for the xgboost prediction and output vector is percentage of life, which is calculated in R^2 error. Finding a single health indicator that often varies monotonically over time to represent a bearing's health is typically challenging. Finding a failure threshold value for the indicator is quite difficult, even if we can discover such an indicator. However, it is true that the health of the bearing degrades over time, and we can assume that the genuine inherent health condition index rises monotonically over time without losing generality. We can try to find a measure that has a monotonic mapping connection with the genuine inherent health condition index since it is difficult to discern the true inherent health condition index based on the measurements of condition monitoring that have been obtained. Generally, the classical feature extraction techniques are sensitive to the noisy component of the signal and need more time for training. The present data is collected at actual industrial settings, where the number of machines surrounds and adds to the noise. For such challenging data, developing a single health indicator is difficult as the noise affects the performance of the health indicator. The proposed method gives very stable health indicator in time frequency domain. The R^2 error on the test data for bearing 1-3 is shown in figure 5.13. There is a good fit between actual and predicted values. Here actual values are plotted from the industrial experimental data (run to failure data). The proposed wavelet scattering in combination with xgboost regression tracks the degradation of bearings correctly with an accuracy of 99.14, 98.48 and 99.44% respectively for B1-B3. When test set was combined (B1-B3) then accuracy with xgboost is reported as 97%. The proposed method is also compared with time domain features in combination with xgboost. The R^2 error for time domain features-xgboost combination is found to be 0.78. LSTM is also employed for prediction of RUL by using wavelet scattering features and R^2 error reported is 0.98.

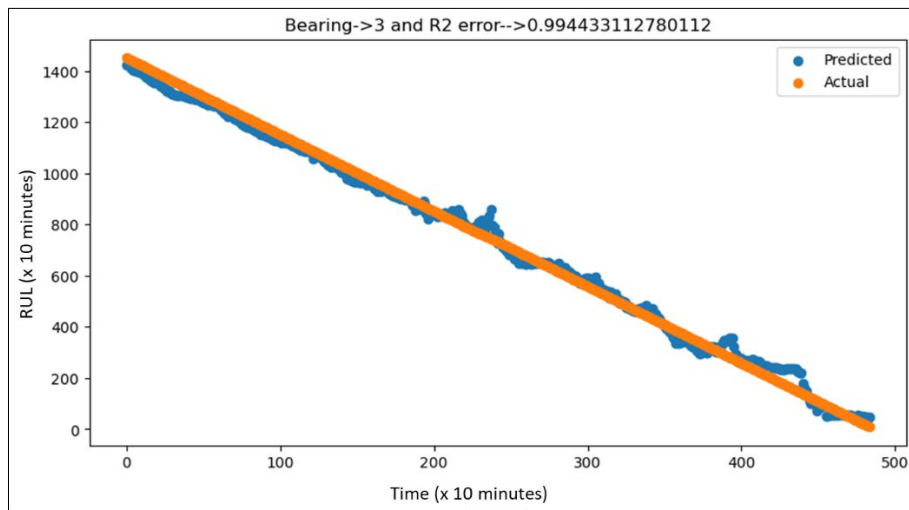
RUL prediction of taper roller bearing under industrial settings



(a)



(b)



(c)

Figure 5.13 Case I RUL prediction of NBC bearing (a) Bearing 1 (b) Bearing 2 (c) Bearing 3.

5.5.2 Time Domain Feature Based HI-NARX Approach

In the proposed case II, time domain and frequency domain features are extracted from the captured vibrational signal and features are ranked as per their importance on the basis of monotonicity and trendability. RMS is the top feature among all feature sets. Then RMS is set as HI for further analysis. HI along with the age of bearing is given as input to NARX network (shown in figure 5.14) for the prediction. A total of 3 nets are used for non-linear autoregressive neural networks. To estimate the future value of the life-percentage or RUL, NARX-NN uses the measurement results from previous inspection points as training data. The validation set is constructed using a data division approach. The best model is selected using an independent test set, which eliminates the chance of inaccuracies resulting from overfitting in the ANN. The training algorithm used for the NARX network is the well-known Levenberg–Marquardt (LM) algorithm. The network performance is assessed based on the mean square error (MSE).

This analysis is completed entirely in the MATLAB [21] software environment. The NARX-NN must first be trained before being put into use. The NARX-inputs NN's consist of the HI and age of the bearing, and its output is the life percentage of the bearing. The equipment's life % in relation to its lifetime is a good measure of the state of the bearings. The choice of output as the life percentage makes sense because a machine's health condition deteriorates with age. There is no need to establish a threshold for RUL assessment because the bearing will entirely fail when the life percentage hits 100%. Note that the network target will be set to $T/100$ if the life percentage of a bearing is $T\%$ [20]. The NARX-NN is trained using bearings B1–B3 and bearing B1 is used for testing in order to confirm the efficacy of the suggested strategy. The data is originally divided randomly into two sets of 70% each for training and validation, and 30% for the test set. Table 1 shows the MSEs between the actual and predicted life percentages across the whole lifetime of the bearings. The actual life from experiments is reported as 5640, 6810 and 4990 minutes for B1, B2 and B3 respectively.

Table 5.2 MSEs Between the Actual and Predicted Life Percentages

Details	Case I	Case II	Case III
Training bearings	B1, B2, B3	B1, B2, B3	B1, B2, B3
Testing bearings	B1	B2	B3
MSE	0.0182	0.0281	0.0217
Test Bearing actual life	5640 minutes	6810 minutes	4990 minutes

RUL prediction of taper roller bearing under industrial settings

If the hidden layer's hidden neurons are sufficient, two-layer (i.e., one-hidden-layer) feed-forward neural networks can fit any input-output relationship. The term "hidden layer" refers to layers that are not output layers. Here a single hidden layer with ten neurons has been used. More neurons and possibly more layers are often needed to solve more challenging issues. Because the network hasn't yet been set up to match our input and goal data, the input and output both have sizes of 0 (refer figure 5.14 a). When the network is taught, this value will change to 1 (figure 5.14 b, c).

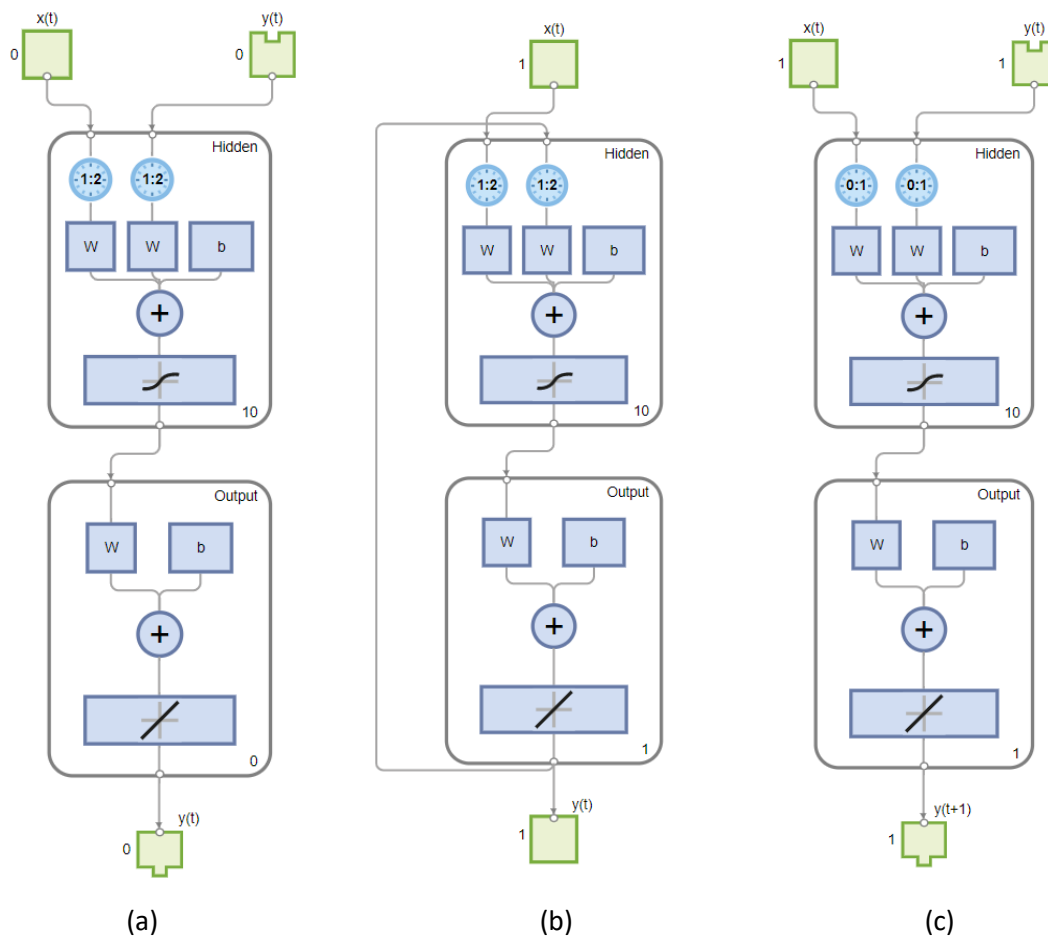


Figure 5.14 NARX net view

Figure 5.15 indicates the training summary; data division is performed randomly. As long as the network keeps getting better on the validation set, training continues. The test set offers a wholly impartial evaluation of network accuracy. The neural network is being trained, and the training algorithms are displayed by the neural network training tool. The criteria that ended training will be marked in green, and it also shows the training condition while training. A total of 6 validation checks are used. The gradient value decreases, initially it was $5.68e+06$ then after 258 epochs it reached to $1e-07$. This shows how the loss function is reduced over the training epochs. Performance value is the RMSE value, at beginning it is reported as $3.08e+06$

RUL prediction of taper roller bearing under industrial settings

then it approaches to zero. Levenberg-marquardt algorithm is used for training. Training state information is given in figure 5.16. We can see that gradient value is decreasing as the number of epochs are increasing. Val fail is close to 0.

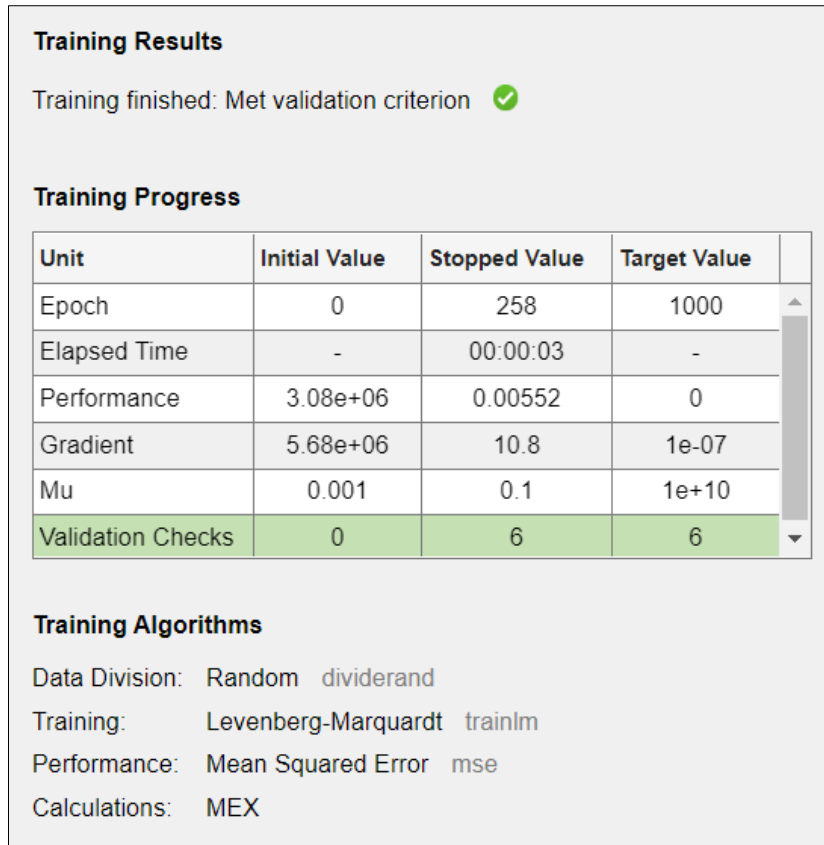


Figure 5.15 Training summary

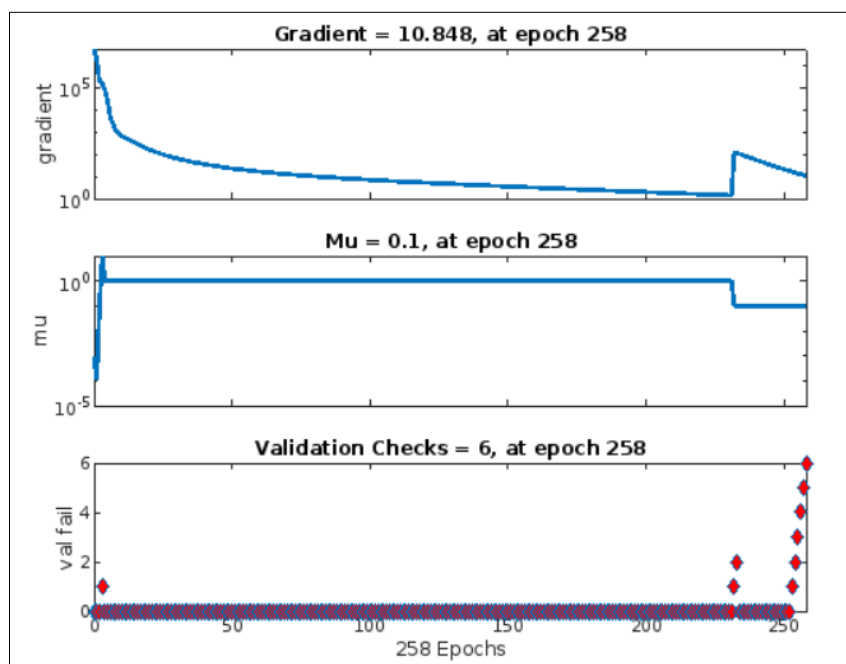


Figure 5.16 Training state information

RUL prediction of taper roller bearing under industrial settings

The training set, the validation set, and the test set are the three categories into which the feature vectors are split throughout the training phase. When network adaptation stops getting better, the training is stopped using the validation data and the weights and biases are adjusted. The training process is unaffected by the test data, which is used to measure network performance impartially. Both the MSE for the training set and the validation set decrease in the early stages of the training process, but after a certain point, the MSE for the validation set begins to rise. This suggests that training should end since the network has begun to overfit the training data. Early stopping is the term used to describe this generalization process. The overfitting issue causes the network to perform well with the validation dataset but poorly with the test data set. The network that yields the lowest test MSE is, therefore, the best network in this study. Performance for every training, validation, and test set is displayed in figure 5.17. The network that performed the best on the validation set is the final network.

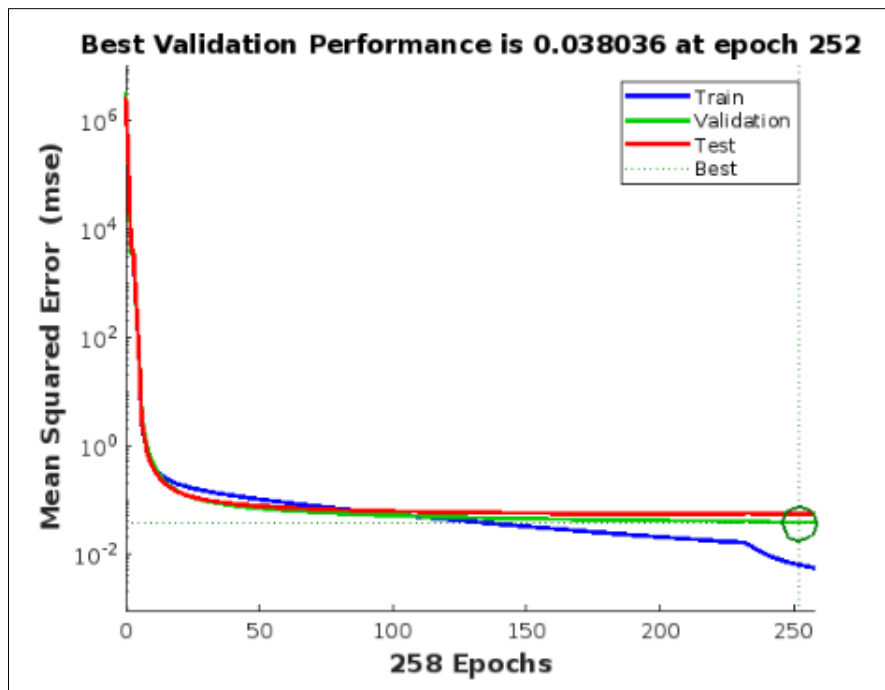


Figure 5.17 Performance of the network.

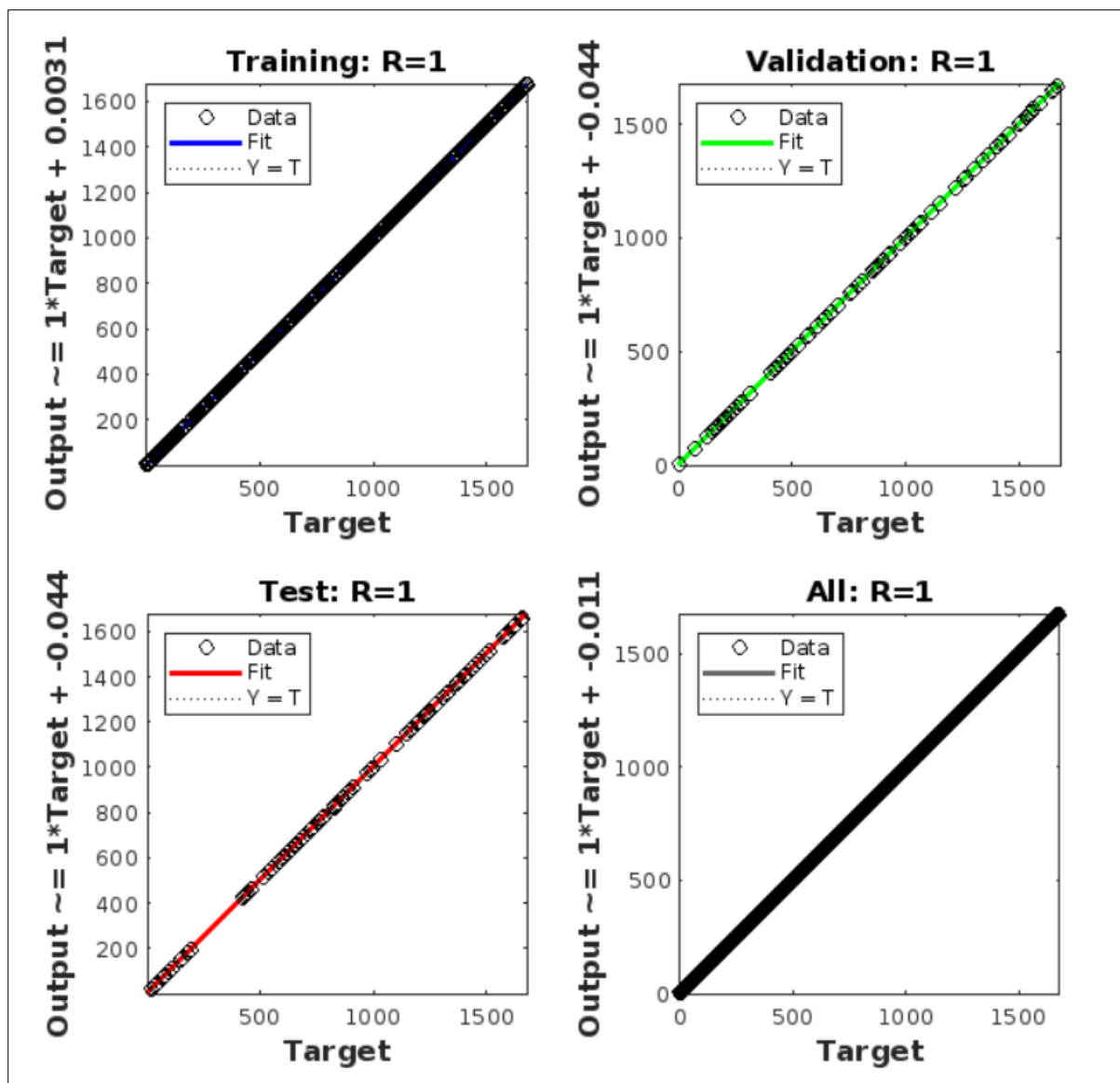


Figure 5.18 NARX performance for vibrational data

Figure 5.18 shows the optimal network's learning curves. For each of the training, validation, and independent test datasets. Figure 5.18 further shows that a higher value of regression i.e $R=1$ is reached. The actual network outputs are presented in relation to the corresponding target values in the regression plot. The linear fit to this output-target relationship should nearly intersect the bottom-left and top-right corners of the plot if the network has successfully learned to fit the data. If this is not the case, it would be advisable to continue training or to train a network with more hidden neurons.

A precise calculation of RUL throughout the end phases becomes increasingly important to prevent the unexpected failure of bearings because it is obvious that damage during the later stages of bearing life accumulates at a much faster pace than it does during the early ones. It can be observed from Figure 5.19 that the predicted RUL and the actual RUL has the best

RUL prediction of taper roller bearing under industrial settings

agreement. The predicted RUL does, however, become very closer to the actual RUL as the bearing ages, improving prediction accuracy. An underestimated RUL value enables sufficient time to carry out the necessary maintenance procedures by giving an early warning of the bearing failure.

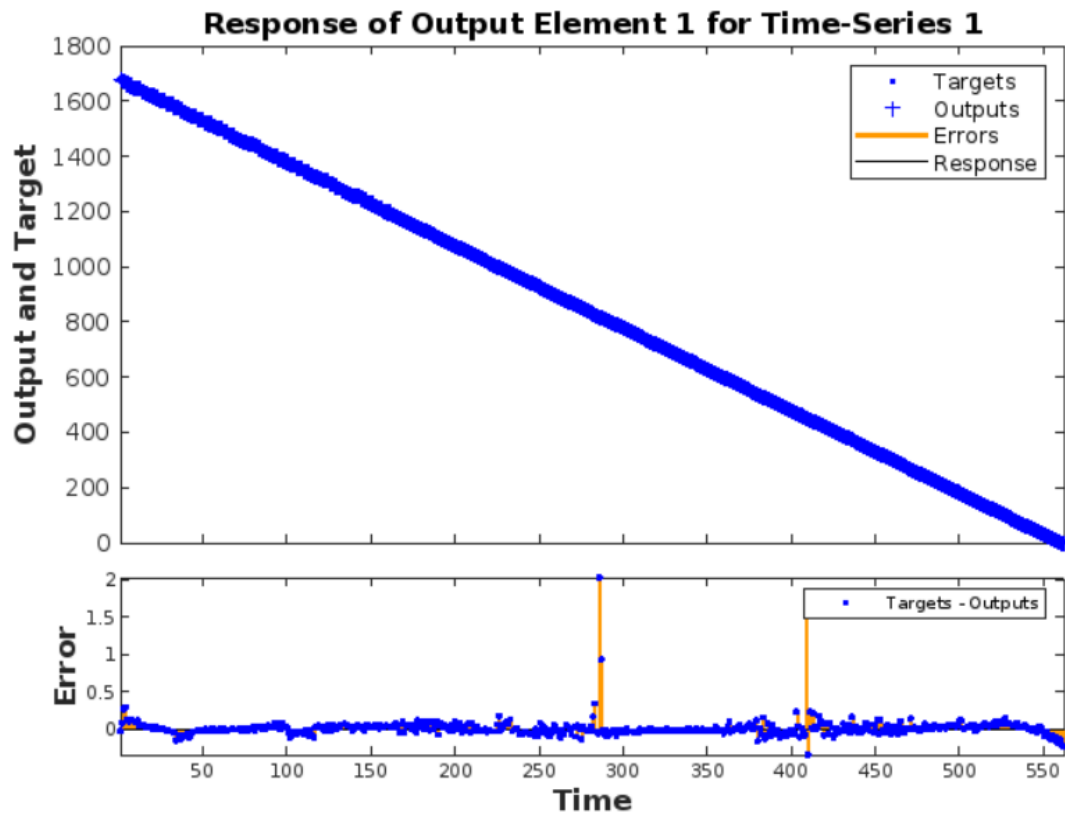


Figure 5.19 RUL prediction result

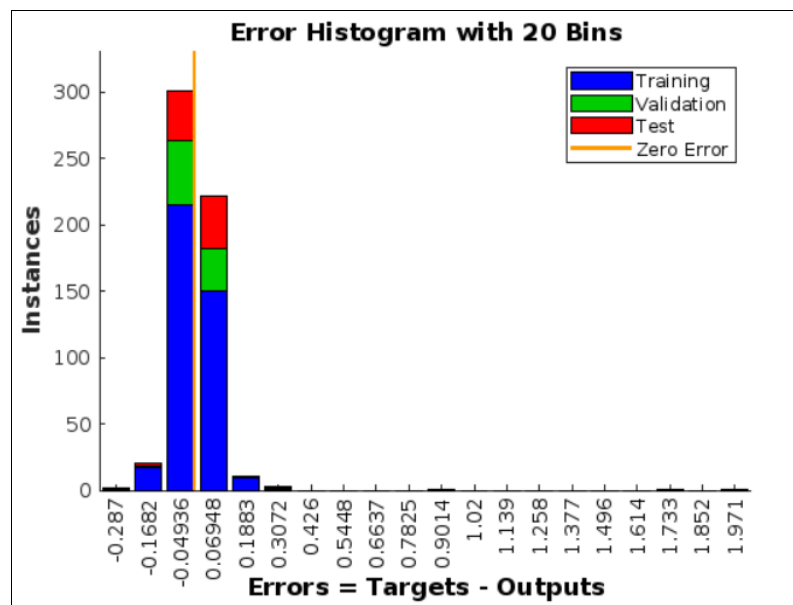


Figure 5.20 Error histogram

RUL prediction of taper roller bearing under industrial settings

Another measure of how well the neural network has fit data is the error histogram. Figure 5.20 shows how the error sizes are distributed. Typically, most errors are near zero, this indicates the data fit is good.

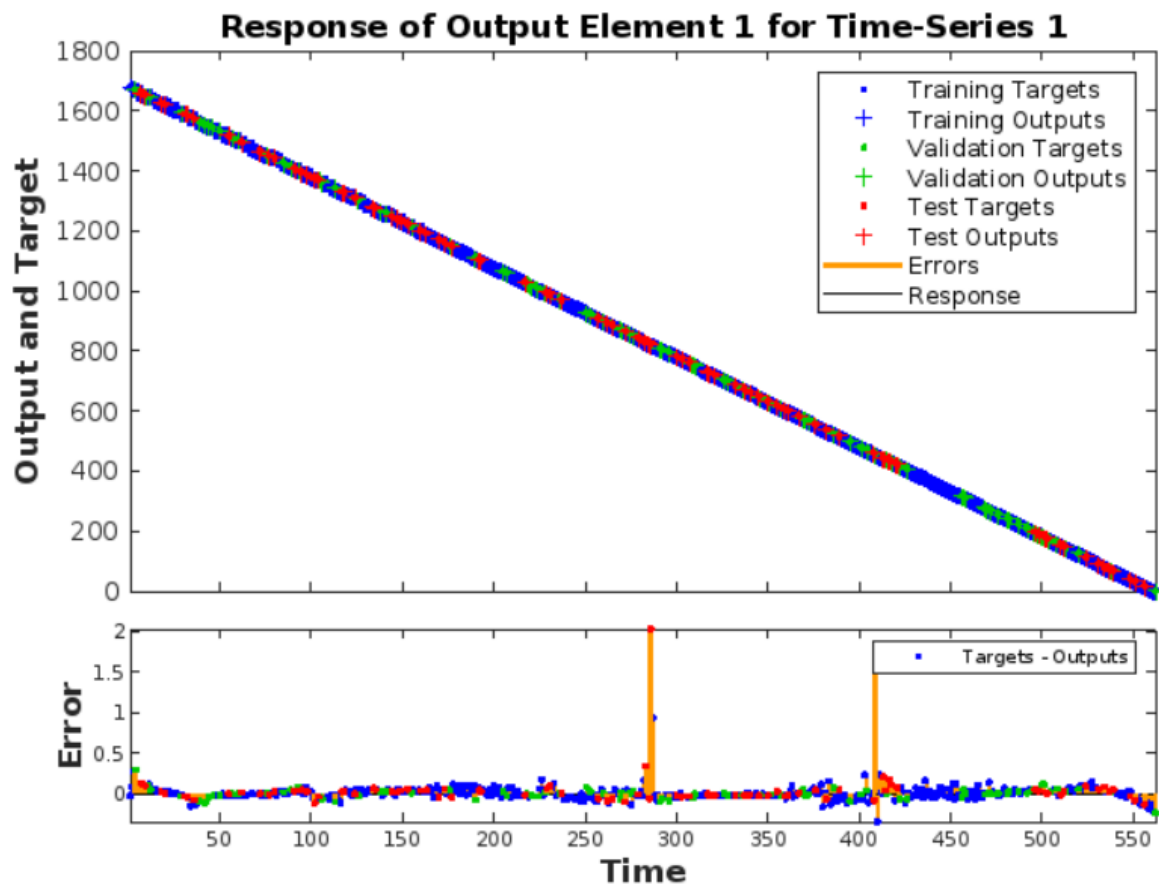


Figure 5.21 Combined performance plot for training, validation, and testing set

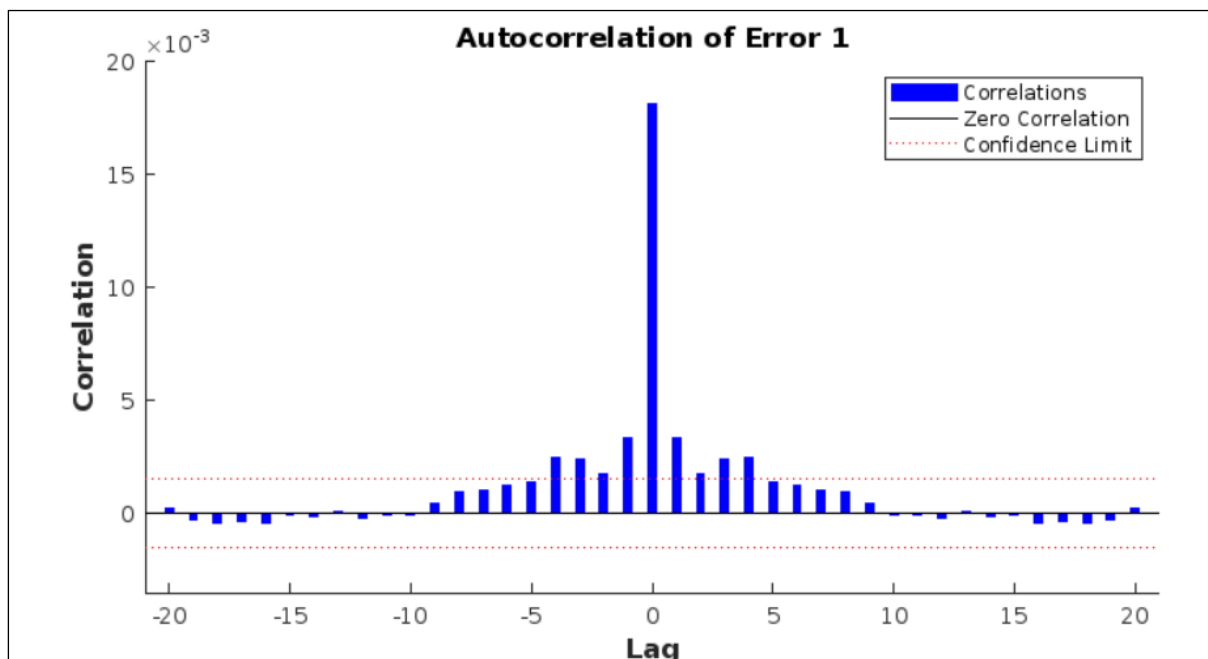


Figure 5.22 Autocorrelation error plot

RUL prediction of taper roller bearing under industrial settings

combined performance plot for training, validation, and testing set is shown in figure 5.21. The NARX has performed excellently with all training, validation and testing sets. From figure 5.22, it is seen that the autocorrelation of error is close to zero. This depicts the algorithm has performed well with the data. Testing results for bearing 2 and bearing 3 is given in figure 5.23. It is observed that NARX has performed well with bearing 2 and bearing 3 as well with the MSE of 0.0281 and 0.0217 respectively.

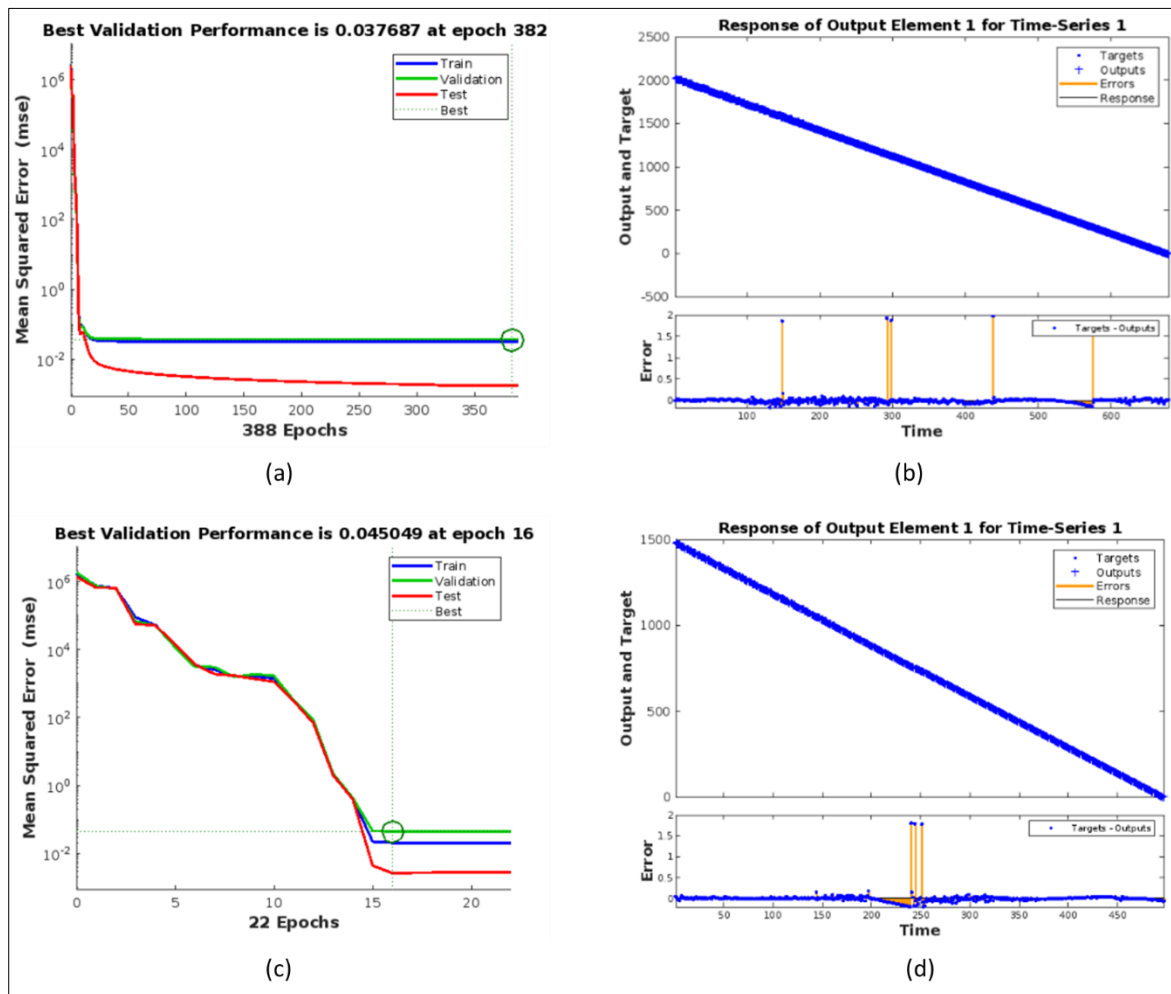


Figure 5.23 (a, b) Validation and testing results for bearing 2 (c, d) validation and testing results for bearing 3.

5.6 Conclusion

The following conclusions can be drawn from the present investigation.

1. The experimental outcomes indicate that the predictions achieved by the proposed methods become accurate in all stages of bearing life.

RUL prediction of taper roller bearing under industrial settings

2. The data used in the present investigation is own, generated in the NBC bearing Jaipur, India in actual industrial settings.
3. The experimental results demonstrate that WST-based features, when used with xgboost regression, achieve 99.14% prediction accuracy.
4. The efficiency and the accuracy of the proposed HI-NARX model with a group of bearings working under high load and speed combinations is better than WST-xgboost regression results. The reported RMSE is 0.0182 with R=1.
5. In the present study inherent misalignment of 1 milli radians is considered for the RUL prediction under accelerated testing conditions.
6. It is challenging to develop a single health indicator and set up the threshold value for industrial data. For which again testing against noise is tedious. So, the suggested approach is more reliable as the data acquisition is carried out in actual industrial settings under noisy environment.
7. Resampling of features using windowing helps to improve the results.

References

- [1] E. Skordilis and R. Moghaddass, "A Double Hybrid State-Space Model for Real-Time Sensor-Driven Monitoring of Deteriorating Systems," *IEEE Trans. Autom. Sci. Eng.*, vol. 17, no. 1, pp. 72–87, Jan. 2020.
- [2] M. Kim and K. Liu, "A Bayesian deep learning framework for interval estimation of remaining useful life in complex systems by incorporating general degradation characteristics," *IJSE Trans.*, vol. 53, no. 3, pp. 326–340, Mar. 2021.
- [3] M. Wei, M. Chen, and D. Zhou, "Multi-Sensor Information Based Remaining Useful Life Prediction With Anticipated Performance," *IEEE Trans. Reliab.*, vol. 62, no. 1, pp. 183–198, Mar. 2013.
- [4] T. Wang, Z. Liu, M. Liao, and N. Mrad, "Life prediction for aircraft structure based on Bayesian inference: towards a digital twin ecosystem," *Annu. Conf. PHM Soc.*, vol. 12, no. 1, p. 8, Nov. 2020.
- [5] Muheng Wei, Maoyin Chen, D. Zhou, and W. Wang, "Remaining useful life prediction using a stochastic filtering model with multi-sensor information fusion," in *2011 Prognostics and System Health Management Conference*, 2011, pp. 1–6.
- [6] P. Wen, S. Zhao, S. Chen, and Y. Li, "A generalized remaining useful life prediction

- method for complex systems based on composite health indicator,” *Reliab. Eng. Syst. Saf.*, vol. 205, p. 107241, Jan. 2021.
- [7] A. Saxena, K. Goebel, D. Simon, and N. Eklund, “Damage propagation modeling for aircraft engine run-to-failure simulation,” in *2008 International Conference on Prognostics and Health Management*, 2008, pp. 1–9.
- [8] P. Wen, Y. Li, S. Chen, and S. Zhao, “Remaining Useful Life Prediction of IIoT-Enabled Complex Industrial Systems With Hybrid Fusion of Multiple Information Sources,” *IEEE Internet Things J.*, vol. 8, no. 11, pp. 9045–9058, Jun. 2021.
- [9] H. Li, H.-Z. Huang, Y.-F. Li, J. Zhou, and J. Mi, “Physics of failure-based reliability prediction of turbine blades using multi-source information fusion,” *Appl. Soft Comput.*, vol. 72, pp. 624–635, Nov. 2018.
- [10] D. Liu and S. Wang, “Reliability estimation from lifetime testing data and degradation testing data with measurement error based on evidential variable and Wiener process,” *Reliab. Eng. Syst. Saf.*, vol. 205, p. 107231, Jan. 2021.
- [11] K. Liu, A. Chehade, and C. Song, “Optimize the Signal Quality of the Composite Health Index via Data Fusion for Degradation Modeling and Prognostic Analysis,” *IEEE Trans. Autom. Sci. Eng.*, vol. 14, no. 3, pp. 1504–1514, Jul. 2017.
- [12] Z. Pan, N. Balakrishnan, Q. Sun, and J. Zhou, “Bivariate degradation analysis of products based on Wiener processes and copulas,” *J. Stat. Comput. Simul.*, vol. 83, no. 7, pp. 1316–1329, Jul. 2013.
- [13] W. Peng, Z.-S. Ye, and N. Chen, “Joint Online RUL Prediction for Multivariate Deteriorating Systems,” *IEEE Trans. Ind. Informatics*, vol. 15, no. 5, pp. 2870–2878, May 2019.
- [14] G. Fang, R. Pan, and Y. Hong, “Copula-based reliability analysis of degrading systems with dependent failures,” *Reliab. Eng. Syst. Saf.*, vol. 193, p. 106618, Jan. 2020.
- [15] S. Mallat, “Group Invariant Scattering,” *Commun. Pure Appl. Math.*, vol. 65, no. 10, pp. 1331–1398, Oct. 2012.
- [16] J. Anden and S. Mallat, “Deep Scattering Spectrum,” *IEEE Trans. Signal Process.*, vol. 62, no. 16, pp. 4114–4128, Aug. 2014.

- [17] K. L. Du and M. N. S. Swamy, “Neural networks in a softcomputing framework,” *Neural Networks a Softcomputing Framew.*, pp. 1–566, 2006.
- [18] I. J. LEONTARITIS and S. A. BILLINGS, “Input-output parametric models for non-linear systems Part I: deterministic non-linear systems,” *Int. J. Control*, vol. 41, no. 2, pp. 303–328, Feb. 1985.
- [19] M. Ardalani-Farsa and S. Zolfaghari, “Chaotic time series prediction with residual analysis method using hybrid Elman–NARX neural networks,” *Neurocomputing*, vol. 73, no. 13–15, pp. 2540–2553, Aug. 2010.
- [20] A. Rai and S. H. Upadhyay, “The use of MD-CUMSUM and NARX neural network for anticipating the remaining useful life of bearings,” *Measurement*, vol. 111, pp. 397–410, Dec. 2017.
- [21] Mathworks.com

OVERALL CONCLUSIONS AND FUTURE PERSPECTIVES

6.1 Overall Conclusions

The overall thesis conclusion is presented as a methodology for fault diagnosis of a misaligned rotor system and prediction of the remaining useful life of rolling element bearing. The scheme is developed based on the work carried out in individual chapters of this thesis. The fault-diagnosis approach incorporates statistical analysis employing response surface methodology, classification of various misalignment defects using sensor fusion (Vibro-Acoustic), and evaluation of the remaining useful life of the taper roller bearing of the NBC bearing dataset.

The following conclusions are drawn from individual chapters presented in the thesis.

1. The conditions considered in the present investigation mimic the actual conditions under which such type of fault is generated. So, it helps to understand the important parameters for system vibrations in a misaligned rotor system. Response surface study showed that the change in load value does not affect vibration amplitude significantly in the case of horizontal and vertical directions, while significant variation in RMS value is observed in the axial direction in both parallel and angular misalignment. This observation can play a vital role in identifying misalignment when there are multiple faults simultaneously present in the system. Axial vibrations, which are often overlooked in bearing analysis, play a significant role in locating misalignment faults. This result is consistent with previous research on the function of axial vibration in the detection of misalignment defects. In the same experiment variation in load and its effect on RMS value in horizontal and vertical directions are also recorded but it is observed that there is no significant change in RMS value. These results differentiate the misalignment from other defects.
2. Defect size variation has NO significant impact on the vibration response in horizontal and vertical directions; the change in RMS value is very small, while in the case of axial direction, a slight increase in RMS value with respect to defect severity is observed. It is observed that a significant increase in RMS value with an increase in speed in both types of misalignments.
3. Results obtained using an acoustic sensor are well aligned with the RSM finding using vibrational data. So, an acoustic sensor which is a non-contact type can be effectively used at the places where installation of the accelerometer is not possible.

4. One of the objectives of this research work is to carry out misalignment fault classification using the limited dataset by comparing the performance of various algorithms. It is observed that the ensemble subspace discriminant algorithm gave 100% accurate results when compared to the other algorithms presented in the article. KNN and SVM yielded results of 85.2% and 96.3%, respectively. Acoustic signal features played an important role in fault classification. The results proved the significance of acoustic signal data in misalignment fault classification.
5. From the present analysis it is found that vibroacoustic sensor data fusion is one of the promising techniques for developing a suitable diagnosis scheme and correct identification of misalignment fault type. The results were compared with vibration analysis and acoustic analysis separately. The vibroacoustic sensor data fusion overperformed the vibration analysis and acoustic analysis which gives an accuracy of 89.4% and 74.2% respectively.
6. The wavelet scattering-xgboost regression method and time domain features-based HI with NARX neural network as a predictor are proposed in this study for RUL prediction of taper roller bearing. The data used in the present investigation is own, generated in the NBC bearing Jaipur India under actual industrial settings.
7. The experimental results demonstrate that wavelet scattering-based features when used with xgboost regression, have a prediction accuracy of 99.14%. The efficiency and the accuracy of another proposed approach of the time domain feature-based HI-NARX model are also better. The reported RMSE is 0.0182 with R=1.
8. In the present study, inherent misalignment of 1 milli radians is considered for the RUL prediction under accelerated testing conditions.

6.2 Novelty of Work

- The application of acoustic signals in angular fault detection has been reported but the use of acoustic sensors in parallel and combined misalignment classification is one of the novel features of our experimental investigation.
- This is one of the primary research reports on the RSM study of misaligned rotor systems using vibrational data and acoustic data.
- This is the first attempt to carry out the investigation on remaining useful life estimation for rolling element bearing under actual industrial data.
- Use of vibroacoustic feature level fusion for misalignment fault classification.

- Sensor data fusion for the prediction of remaining useful life prediction of taper roller bearings. The proposed methods give good results in RUL prediction. The data also includes the random noise, while capturing it in actual industrial settings.

6.3 Future scope

- To address the issue of reliable fault diagnosis of specific faults, the multiple sensor fusion approach should be improved with more sophisticated machine learning, deep learning algorithms, and signal processing techniques. There must be sufficient testing with various types of sensors (vibration, acoustic, temperature, motor current signature analysis) in this area. This enables researchers to comprehend a sensor's prediction ability and select the best sensor for a given diagnosis.
- Misalignment fault quantification needs to be performed. The present study can be able to segregate different types of misalignment faults but cannot quantify the amount of misalignment present in the system.
- No attempt has been reported on the single rotor system with multiple misalignment faults at multiple locations. There is no literature found on the modeling and experimental work of such a system. Model-based analysis has enormous potential for fault presence detection and accurate measurement of faults in the system. However, it is time-consuming and complex. The combination of a technique with others can help improve the diagnosis of faults. Therefore, a combined approach may better achieve the correct diagnosis and prognosis of rotor system faults.
- Sensor data fusion needs to be explored for the prediction of the remaining useful life of bearings. It might help to develop a more reliable prediction scheme. More research needs to be performed on transfer learning techniques.
- Digital twin-driven degradation assessment and RUL prediction of bearings.
- Explainable AI (XAI) should be explored to understand the feature selection by deep neural networks.

❖ International Journal Publications

- [1] S. Patil, A. K. Jalan, and A. Marathe, "Condition Monitoring of Misaligned Rotor System Using Acoustic Sensor by Response Surface Methodology," *J. Nondestruct. Eval. Diagnostics Progn. Eng. Syst.*, vol. 6, no. 1, Feb. 2023 (<https://doi.org/10.1115/1.4054975>)
- [2] S. Patil and A. K. Jalan, "Ensemble Subspace Discriminant Classifiers for Misalignment Fault Classification Using Vibro-acoustic Sensor Data Fusion," *J. Vib. Eng. Technol.*, May 2022. (<https://doi.org/10.1007/s42417-022-00548-2>)
- [3] S. Patil, A. K. Jalan, and A. M. Marathe, "Support Vector Machine for Misalignment Fault Classification Under Different Loading Conditions Using Vibro-Acoustic Sensor Data Fusion," *Exp. Tech.*, Jan. 2022. (<https://doi.org/10.1007/s40799-021-00533-6>)
- [4] A. K. Jalan, S. Patil, and G. Mittal, "A Review on Fault Diagnosis of Misaligned Rotor Systems," *Int. J. Performability Eng.*, vol. 16, no. 4, p. 499, 2020. (doi: 10.23940/ijpe.20.04.p1.499509)
- [5] S. Patil, A. K. Jalan, and A. M. Marathe, "Experimental Investigation Using Response Surface Methodology for Condition Monitoring of Misaligned Rotor System," *J. Nondestruct. Eval. Diagnostics Progn. Eng. Syst.*, vol. 5, no. 2, May 2022. (<https://doi.org/10.1115/1.4051771>)
- [6] S. Patil, A.M. Marathe, A.K.Jalan, B.M.Dash, L.Agrawal, A.Singh, " Assessment of Remaining Useful Life of Rolling Element Bearing Under Noisy Environment", *International Journal of prognostics and health management (Under Review)*
- [7] S. Patil, A.M.Marathe, A.K.Jalan, L.Agrawal, A.Singh "Estimation Of Remaining Useful Life Of Taper Roller Bearing Using Sensor Data Fusion Technique", *Expert systems with applications (Under review)*

❖ International/national Conference

- [1] Shital Patil, Arun Kumar Jalan, Amol Marathe, Balyogi Mohan Dash, Lokesh Agrawal, Arendra Singh, "The Noise Resilient Algorithm for the Prediction of Remaining Useful Life of Rolling Element Bearing", PHM conference, November 2022, Nashville USA (Accepted).
- [2] S. Patil, A. K. Jalan, "Experimental Investigation Using Response Surface Methodology for Condition Monitoring of Combined Misaligned rotor system, International Conference on Vibration Engineering, Science, and Technology (INVEST 23) (Under review).

Biography



Mr. Shital Patil is pursuing PhD in department of mechanical engineering of Birla Institute of Technology and Science Pilani. His area of expertise is condition monitoring, vibration analysis, misalignment, bearing fault diagnosis and prognosis. He is recipient of prestigious prime minister fellowship. He has completed his BE in mechanical engineering from VTU Belgaum and ME from BITS Pilani Goa campus. During his masters he has done internship with Hindustan aeronautics limited and Skoda auto India Aurangabad. He has worked as assistant professor in department of mechanical engineering of SITCOE Yadrav for 2 years then he worked for BIT Mesra offshore campus in Dubai for three years. He has publications in international journal of well repute. Currently he is working as an Artificial Intelligence Specialist at Bosch Global Software Technologies, Bangalore.



Dr. Amol M. Marathe is assistant professor in department of mechanical engineering of Birla Institute of Technology and Science Pilani. His research interests include perturbation methods, Immune system modeling, predictive maintenance, and non- smooth dynamical systems.



Dr. Arun Kumar Jalan is associate professor in department of mechanical engineering of Birla Institute of Technology and Science Pilani. He is working in Vibration analysis, machinery fault diagnosis and prognosis, signal processing, condition monitoring, and tribology.

Appendix

Table 1. Statistical features in the time domain

Sr. no.	Time domain feature	Equation
1	Mean	$X_m = \frac{1}{N} \sum_{n=1}^N x_n$
2	Standard deviation	$X_{sd} = \sqrt{\frac{\sum_{n=1}^N (X(n) - X_m)^2}{N - 1}}$
3	Root Mean Square (RMS)	$X_{rms} = \sqrt{\frac{\sum_{n=1}^N (X(n))^2}{N}}$
4	Root amplitude	$X_{root} = \left(\sqrt{\frac{\sum_{n=1}^N \sqrt{ X(n) }}{N}} \right)^2$
5	Peak	$X_{peak} = \max X(n) $
6	Skewness	$X_{skewness} = \frac{\sum_{n=1}^N (X(n) - X_m)^3}{(N - 1)X_{sd}^3}$
7	Kurtosis	$X_{kurtosis} = \frac{\sum_{n=1}^N (X(n) - X_m)^4}{(N - 1)X_{sd}^4}$
8	Crest factor	$X_{crest} = \frac{X_{peak}}{X_{rms}}$
9	Clearance factor	$X_{clearance} = \frac{X_{peak}}{X_{root}}$
10	Shape factor	$X_{shape} = \frac{X_{rms}}{\frac{1}{N} \sum_{n=1}^N X(n) }$
11	Impulse factor	$X_{impulse} = \frac{X_{peak}}{\frac{1}{N} \sum_{n=1}^N X(n) }$

Table 2. Coefficients Estimate and Standard Error Matrix for Parallel Misalignment.

Factor	Coefficient Estimate			Standard Error		
	Horizontal Direction	Vertical Direction	Axial Direction	Horizontal Direction	Vertical Direction	Axial Direction
Intercept	2.49	0.5057	10.15	0.0102	0.0103	0.3658
Speed (A)	0.6809	-0.2227	3.78	0.0047	0.0048	0.1693
Load (B)	-0.0863	-0.0033	0.8617	0.0047	0.0048	0.1693
Defect (C)	0.0232	-0.0029	-0.1953	0.0047	0.0048	0.1693
AB	-0.0334	-0.0033	-0.2528	0.0058	0.0058	0.2074
AC	0.0054	-0.0023	-0.1307	0.0058	0.0058	0.2074
BC	-0.0076	0.0004	0.0418	0.0058	0.0058	0.2074
A ²	-0.2931	0.0730	0.2948	0.0082	0.0083	0.2933
B ²	-0.0757	-0.0087	2.85	0.0082	0.0083	0.2933
C ²	0.0032	0.0047	-0.2696	0.0082	0.0083	0.2933